BAJECE

e-mail: editor@bajece.com

Balkan Journal of Electrical & Computer Engineering

An International Peer Reviewed, Refereed, Indexed and Open Access Journal

www.bajece.com

Vol : 1
No : 2
Year : 2013
ISSN : 2147-284X

Sponsored by the

- Kirklareli University,
- Klaipeda University
- Inonu University
- Istanbul Technical University
- City University London

This journal is accredited by the Kirklareli University subsidy purposes. It is abstracted and indexed in Copernicus, Index Google Scholarship, the PSCR, DOAJ, Research Bible, Indian Open Access Journals (OAJ), Institutional Repositories (IR), Journal TOCs, J-Gate (Informatics India), Ulrich's, ResearchGate, International Society of Universal Research in Sciences, DRJI, EyeSource.

Aim & Scope

The journal publishes original papers in the extensive field of Electrical-Electronics and Computer engineering. It accepts contributions which are fundamental for the development of electrical engineering, computer engineering and its applications, including overlaps to physics. Manuscripts on both theoretical and experimental work are welcome. Review articles and letters to the editors are also included.
Application areas include (but are not limited to): Electrical & Electronics Engineering, Computer Engineering, Software Engineering, Biomedical Engineering, Electrical Power Engineering, Control Engineering, Signal and Image Processing, Communications & Networking, Sensors, Actuators, Remote Sensing, Consumer Electronics, Fiber-Optics, Radar and Sonar Systems, Artificial Intelligence and its applications, Expert Systems, Medical Imaging, Biomedical Analysis and its applications, Computer Vision, Pattern Recognition, Robotics, Industrial Automation.

BAJECE

Balkan Journal of Electrical & Computer Engineering

An International Peer Reviewed Refereed indexed and Open Access Journal

ISSN: 2147- 284X
Vol: 1
No: 2
Year: September 2013

CONTENTS

G. Gricius, D. Drungilas, J. Guseinovaitė, K. Grigaitis, A.A. Bielskis; Modeling of the Cloud Interconnected Human Friendly Multi-Agent Based Sustainable Power Controller,…….**49-55**

T. Slavov, L. Mollov, J. Kralev, P. Petkov; Real-time Robust Control Using Digital Signal Processor,…….**56-63**

S. Shojaeian, H. Akrami; Estimating Optimal Wind and Storage Capacity to Avoid Conventional Power Plants Expansion Using Monte Carlo Method;…….**64-70**

G. Yanik, E. Isen; Quasi-Resonant Full-Wave Zero-Current Switching Buck Converter Design, Simulation and Application, ……..……..….**71-77**

E. Nechadi, M.N. Harmas; Power System Stabilizer Based on Global Fuzzy Sliding Mode Control, **..78-84**

D. Dzhonova-Atanasova, A. Georgiev, R. Popov; Challenges of Marine Power in the Balkan Region, ……..…….**85-92**

B. Belabbas, T. Allaoui, M. Tadjine; Hybrid Fuzzy sliding mode performance control applied to a DFIG system for the production and integrated wind energy into a power grid based three-level converters, ……..…….**93-101**

BALKAN JOURNAL OF ELECTRICAL & COMPUTER ENGINEERING
(An International Peer Reviewed, Refereed, indexed and Open Access Journal**)**

Contact
https://www.bajece.com

e-mail: editor@bajece.com
bajece@bajece.com

Phone: +90 288 214 05 14
Fax: +90 288 214 05 16

Kirklareli University, Department of Electrical & Electronics Engineering, 39060, Kirklareli-Turkey.

Modeling of the Cloud Interconnected Human Friendly Multi-Agent Based Sustainable Power Controller

G. Gricius, D. Drungilas, J. Guseinovaitė, K. Grigaitis and A. A. Bielskis

***Abstract*-- The paper presents model of the cloud interconnected multi-agent human friendly sustainable power controller (Controller). The Controller is based on the human ambient comfort affect reward index (ACAR index). The ACAR index depends on human physiological parameters: the temperature, the ECG- electrocardiogram and the EDA-electro-dermal activity. These physiological parameters are used for sustainable power control by multi-agent system developed as the cloud interconnected, instrumented, and intelligent environment. The Environment Sense Agent, the Environment Adaptation Agent, the Raw Data Processing and EDA Parameters Extraction Agent, and the Neural Network Training Agent are proposed and implemented into the multi-agent based emotion recognition and environment control system. The modeling results show that proposed system can find such the environmental state characteristics that may improve comfort for people affected by this environment.**

Index Terms—**Multi-agent power controller, cloud computing, emotion recognition, smart environment**

I. Introduction

THE investigation of dynamic interrelation between mind and body dates back to the beginning of 20th century. However, the connection between specific somatic states and different emotions is still a very promising field for investigations. Emotion recognition is achieved by multiple methods. One of the ways is through use of biosensors, which are claimed to be more advantageous than other methods by being unobtrusive and resistant to different environmental conditions [1]. There were attempts to value emotion-induced physiological state by measuring cardiorespiratory (ECG and respiratory) activity. However, the study indicated the need to better define all the factors involved in cardio-respiratory regulation during emotion [2]. Another way is based on measuring human skin resistance. There is constructed an ESI (emotional stress indicator) kit, which captures the changes in human skin resistance and based on that measures the person's stress level [3]. According to galvanic skin response theory, resistance varies inversely proportional to the stress. The lowering of skin resistance during stress is caused by an increased blood flow and permeability, which increases the electrical conductivity of the skin. The same principle is used in a lie detector or psychogalvanometer. It is worth mentioning that there are certain diseases which can affect the skin resistance pattern and that should be considered while interpreting the data [4]. The third major criteria are the change in body temperature. Literature presents some data claiming that anger causes a sharp increase in body temperature, and fear is marked by an opposite response. [5]

The European Union has actively promoted political campaigns toward energy efficiency and renewable energy [6]. The model of Home/Building Automation system [7] to control rolling shutters, heat pump and lighting system finalized to users comfort and energy saving, maximizing the exploitation of solar energy [8]. Multi-Agent Based E-Social Care Support System for Inhabitancies of a Smart Eco-Social Apartment is proposed in [9].This system was developed as an Ambient Comfort Affect Reward Based Multi-Agent Lighting Controller in [11]. The variable air volume (VAV) type of heating, ventilating, and/or air-conditioning (HVAC) systems can be controlled by using simple ON-OFF, intelligent ON-OFF and optimal Controllers [12]. Reinforcement Learning [13] for Building Environmental Control[14] helps to creating of users thermal and lighting comfort in the sustainable home. LED lighting can also increase comfort and save energy in the sustainable home. Nevertheless, according to Directive 2006/25/EC [8], the artificial optical radiation (AOR) exposure leads to health effects for specific wavelength and energy absorbed by different anatomical structures such as skin and eyes. The evaluation of exposure to AOR involves the wavelength classification in ranges between: 180 nm and 400 nm, due to photochemical retinal damage, skin rash, elastosis and skin cancer; 300 nm and 600 nm (blue light), due to photochemical retinal damage; 380 nm and 1400 nm (visible light and infrared), due to thermal retinal damage [10]. Our eyes need light to work, but too much of the wrong kind of light can lead to diseases like age-related macular degeneration, and there is more evidence that blue light (400 –

This work was partly supported by project "Promotion of Student Scientific Activities" (VP1-3.1-ŠMM-01-V-02-003) from the Research Council of Lithuania (K. G.). This project is funded by the Republic of Lithuania and European Social Fund under the 2007-2013 Human Resources Development Operational Programme's priority 3.

G. Gricius is with the Department of Electrical Engineering of Klaipeda University, Klaipeda, 92294 Lithuania (e-mail: gediminas@ik.ku.lt).

D. Drungilas is with the Department of Electrical Engineering of Klaipeda University, Klaipeda, 92294 Lithuania (e-mail: dorition@gmail.com).

J.Guseinovaitė is with Faculty of Medicine of Vilnius University, Vilnius, 03101 Lithuania (e-mail: jurgita.guseinovaite@gmail.com)

K. Grigaitis is with Faculty of Medicine of Vilnius University, Vilnius, 03101 Lithuania (e-mail: grigaitis.kazimieras@yahoo.com)

A.A.Bielskis is with the Department of Electrical Engineering of Klaipeda University, Klaipeda, 92294 Lithuania (e-mail: andrius.bielskis@ik.ku.lt).

500nm) can damage our eyes, with people who have had cataracts removed being particularly vulnerable [7]. Infrared and ultraviolet LEDs can also be hazardous [15]. Principles of development of the model of the Cloud Interconnected Human Friendly Multi-Agent Based Sustainable Power Controller are described in this paper.

II. The Ambient Comfort Affect Reward Based Sustainable Power CONTROLLER MODEL

The model of multi-agent ambient comfort affect reward based sustainable power controller system of Fig. 1 consists of the following parts: the *Environment Evaluation Intelligent Service*, the radial basis neural network, *the RBF Intelligent Service*, and the *Learning Algorithm* service. The *Environment Evaluation Intelligent Service* is used to evaluate the ambient human comfort by sensing the affect of the following environment parameters: the temperature, the lighting, and the air conditioning.

The human comfort is expressed as an Ambient Comfort Affect Reward, the *ACAR*, index function:

$$ACAR = f\{a(l_{ci}, t_a, a_{ci}, t_b, c, d), v(l_{ci}, t_a, a_{ci}, t_b, c, d)\},$$
$$ACAR = [-3,3], \quad (1)$$

where a and v are arousal and valence functions respectively dependent on the following ambient comfort and human physiological parameters: l_{ci} – the modified color lighting index from [2] for local dimmable RGBY LEDs in the laboratory, $T_z = t_a$ – ambient temperature of the zone, $Wz = a_{ci}$ – air conditioning index of specific humidity in the zone, t_b – human body temperature, c – *ECG*, electrocardiogram and d – *EDA*, electro-dermal activity. The (1) type function can be approximated by neural networks, fuzzy logic or other regression methods. In this case, we use fuzzy logic to approximate (1) by defining two fuzzy inference systems: the *Arousal-Valence System*, and the *Ambient Comfort Affect Reward (ACAR) System*. (See Fig.2)

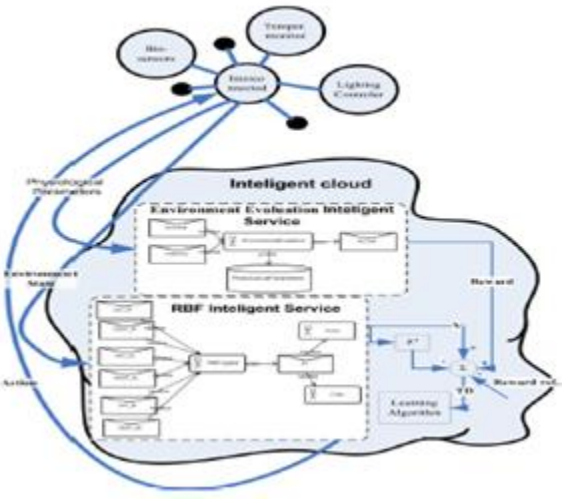

Fig.1. Block diagram of the Ambient Comfort Affect Reward Based Sustainable Power Controller system

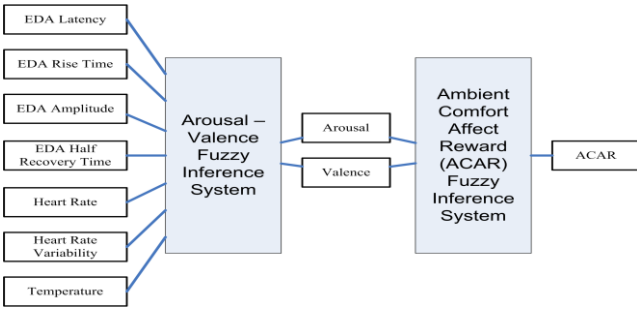

Fig.2. Ambient Comfort Affect Reward (ACAR) System

III. Scenario Monitoring Agents

The *Environment Evaluation Intelligent Service* of Fig.1 is implemented by introducing the following scenario monitoring agents: the Environment Sence Agent and the Environment adaptation agent.

A. Environment Sense Agent

The *Environment Sence Agent* is discribed by pseudo-code of Fig.3. It uses the measured *Temperature raw data*, *Lighting raw data*, and *Air quality raw data* as the input parameters. The agent's output is the following ambient environment parameters: *temperature*, *temperature change*, *lighting*, *lighting change*, *air quality*, and *air quality change*.

Input: *Temperature raw data*
Lighting raw data
Air quality raw data
Output: *Environment = {temperature, temperature change, lighting, lighting change, air quality, air quality change}*
// ambient environment parameters
Initialize: *sampling time T*
WHILE *not end of signal* **DO**
t = sample Temperature raw data at time τ
l = sample Lighting raw data at time τ
a = sample Air quality raw data at time τ
$\Delta t = t_k - t_{k-1}$ *//temperature change*
$\Delta l = l_k - l_{k-1}$ *//lighting change*
$\Delta a = a_k - a_{k-1}$ *//air quality change*
Environment={t, l, a, Δt, Δl, Δa}
ENDWHILE

Fig.3. Pseudo-code fragment for describing of the *Environment Sense Agent*

B. Environment Adaptation Agent

Fig.4 depicts a pseudo-code fragment of the *Environment Adaptation Agent.* The Agent takes the *initial environment state* as an input and gives the following output parameters: *State trace*, *Action trace*, *Temporal difference trace*, and *Value trace*.

IV. Measured Emotional Data Preprocessing Agents

The *RBF Intelligent Service* of Fig.1 is implemented by introducing the following measured emotional data preprocessing agents: the *Raw Data Preprocessing and EDA Parameters Extraction Agen*t and the *Neural Network Training Agent.*

A. Raw Data Processing and EDA Parameters Extraction Agent

Fig.5 depicts a pseudo-code fragment of the *Environment Adaptation Agent.* The Agent takes the following input parameters: *raw data of EDA measurements, X, sampling time of X, class indicator of emotional state, S,* and *sampling time of S.* The output of the Agent predicts the EDA parameters: *latency, EDA rise time, EDA ampliude*, and *EDA half recoveery time*.

Input: $state_{t=0}$ // *the initial environment state*
Output: state trace
Action trace
Temporal difference trace
Value trace
Initialize: $\Delta reward$ // *the change of the reward*
$ARVA_{t=0}$ // *the initial arousal-valence value vector*
$ACAR_{t=0}$ // *the Ambient Comfort Affect Reward*
center // *the centers of basis functions*
σ // *the width of basis functions*
γ // *the discount factor*
λ // *the decay factor*
$e_{t=0}=0$ // *the eligibility trace*
α // *the learning rate*
v // *the RBF neural network weights of actor*
w // *the RBF neural network weights of critic*
FOR *each* t^{th} *observation* **DO**
FOR *each action* **DO**
Initialize: $V_j=0$
FOR *each* j^{th} *basis function center* **DO**

$$\phi_j^{critic} = \exp\left(-\frac{\left\|state_t - center_j\right\|^2}{2\sigma_j^2}\right)$$

$V_j=V_j+ \Phi_j^{\text{critic}} \cdot w_j$
ENDFOR
$e_{t+1}=\gamma \cdot \lambda \cdot e_t+ \Phi_j^{\text{critic}}$
$\delta_t= ACAR_t + V_{j-1} - \gamma \cdot V_j$ // *the temporal difference*
FOR *each basis function center j* **DO**
$w_j = w_j + \alpha \cdot \delta_t \cdot e_{t+1} \cdot \Delta reward$
ENDFOR
Initialize: $action_t=0$
FOR *each basis function center j* **DO**
$v_j= v_j + \alpha \cdot \delta_t \cdot e_{t+1} \cdot \Delta reward$

$$\phi_j^{actor} = \exp\left(-\frac{\left\|state_t - center_j\right\|^2}{2\sigma_j^2}\right)$$

$action_t= action_t + \Phi_j^{\text{actor}} \cdot v_j;$
ENDFOR
get new state: $state_{t+1} = state_t + action_t$
simulate Arousal Valence: $ARVA_{t+1} = FIS(state_{t+1})$
// *FIS – Fuzzy Inference System*
$ACAR_{t+1} = FIS(ARVA_{t+1});$
$\Delta Reward = ACAR_{t+1} - ACAR_t$
ENDFOR
ENDFOR

Fig.4. Pseudo-code fragment of the *Environment Adaptation Agent*

Input: $X = x_1, x_2, \ldots, x_n$ // *raw data of EDA measurements, X*
$Tx = tx_1, tx_2, \ldots, tx_n$ // *sampling time of X*
$S = s_1, s_2, \ldots, s_i$// *class indicator of emotional state, S*
$Ts = ts_1, ts_2, \ldots, ts_i$ //*sampling time of S*
Output: EDA parameters
Initialize: $L = l_1, l_2, \ldots, l_i$ // *latency*
$RT = rt_1, rt_2, \ldots, rt_i$ // *EDA rise time*
$A = a_1, a_2, \ldots, a_i$ // *EDA amplitude*
$HRT = hrt_1, hrt_2, \ldots, hrt_i$// *EDA half recovery time*
X=**ksmooth(**X**)** //*kernel regression smoothing*
$j=1$
FOR *each* s_k **DO**
WHILE $tx_j<ts_k$ **DO** //*looking for beginning of stimulus*
$j=j+1$
ENDWHILE
$Xstart= tx_j$
$Ystart= x_j$
WHILE $x_j>= x_{j+1}$ **DO** //*looking for beginning of EDA rising*
$j=j+1$
ENDWHILE
$l_k= tx_j - Xstart$ //*calculating the latency*
$Xstart= tx_j$
WHILE $x_j<x_{j+1}$ **DO** //*looking for EDA peak*
$j=j+1$
ENDWHILE
$rt_k = tx_j - Xstart$ //*calculating the rise time*
$Xstart= tx_j$
$a_k = x_j - Ystart$ //*calculating the amplitude*
$Ystart= x_j$
WHILE Ystart - $x_j< a_k/2$ **DO**//*looking for EDA half recovery*
$j=j+1$
ENDWHILE
$hrt_k = tx_j - Xstart$// *calculating the half recovery time*
ENDFOR

Fig.5. Pseudo-code fragment of the *Raw Data Preprocessing and EDA Parameters Extraction Agen*t.

B. Neural Network Training Agent

Fig.6 presents a pseudo-code fragment of the *Neural Network Training Agent.* The Agent takes the following as an Input: *Pattern= {L, RT, A, HRT}* and *Class={S}.*The output of this agent is the *trained neural network, NN.*

Input: *Pattern={L, RT, A, HRT}*
Class={S}
Output: *NN // trained neural network*
Initialize: *NN //initial neural network with 4 inputs 8 outputs*
W //initial random neural network weights
FOR *each iteration t* **DO**
FOR *each example n* **DO**
run Patern forward through network, computing all o_i *(outputs of NN nodes) and* in_i *(inputs for hidden layers) for all weights (j,i)*
$\Delta_i= (Class_i-a_i)\cdot g'(in_i)$ // *weight correction if i is output node*
$\Delta_i= g'(in_i)\Sigma_k w_{ik}\Delta_k$ // *weight correction if i is not output node*
$w_{ji} = w_{ji}+\alpha\cdot a_j\cdot\Delta_i$ // *update NN weights*
ENDFOR
ENDFOR

Fig.6. Pseudo-code fragment of the *Neural Network Training Agen*t.

V. PRACTICAL IMPLEMENTATION OF ELEMENTS OF SUSTAINABLE POWER CONTROLLER FOR THE SINGLE ROOM LABORATORY

Fig. 7 represents the following wireless communication elements of prototype of the ACAR-Controller for the single room laboratory: The block diagram of the sustainable electric power distribution subsystem for measuring, sustainable control and delivering power to electric heater and fans by

using triac type AC power controllers DIM1 and DIM2 driven by MEGA32 type boards of Fig. 7a; The block diagram of the intelligent RGBY lighting subsystem, the IRGBY Light, with dimmable current stabilizers for each RGBY power LED to predicting limits of exposure to broad-band incoherent optical radiation by [15] of Fig.7b; The schematic diagram of the Mega128RFA1 transceiver board of Fig.7c. Fig.8 shows the noninvasive measuring subsystem of human reaction to comfort conditions in the laboratory. The ATMEGA128RFA1-ZU transceivers of Fig.7c are used to creating of the wireless communication subsystem between MEGA32 type boards and central computer connected to the Internet. It uses the 802.15.4 ZigBee low-power, short-distance wireless ISM standard for the 2.4GHz license-free radio bands.

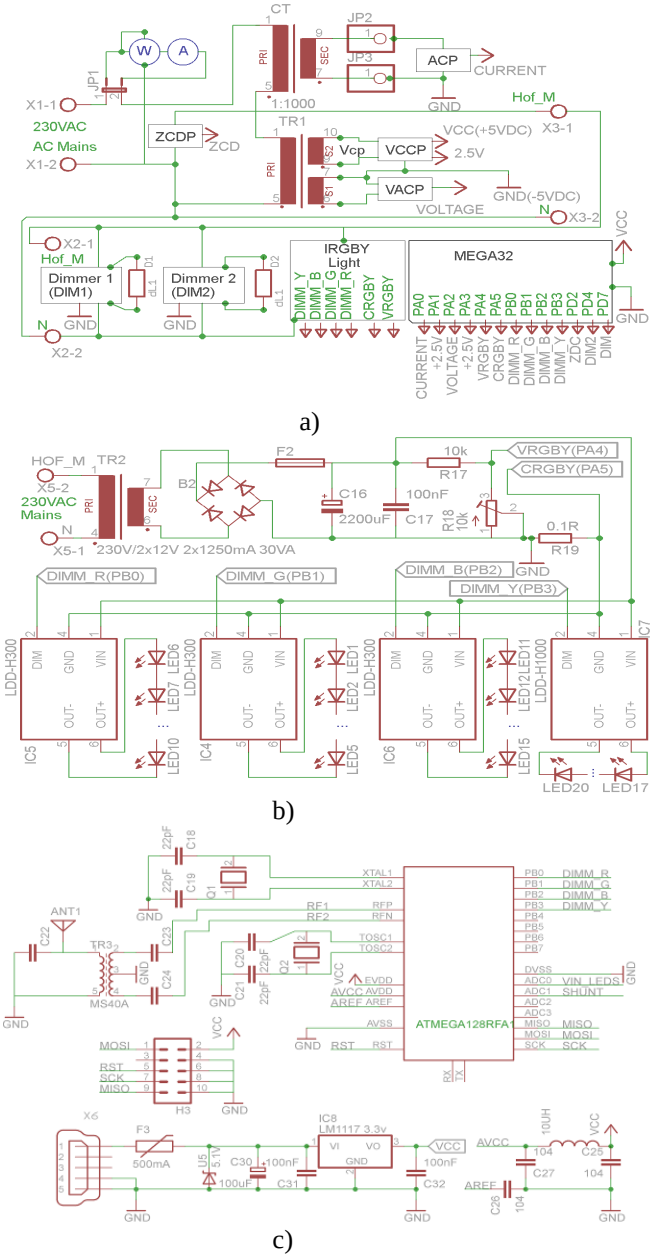

Fig.7. The sustainable electric power distribution subsystem for measuring, sustainable control and delivering power to electric heater and fans by using triac type AC power controllers driven by MEGA32 type boards: a) block diagram; b) IRGBY Light - the intelligent RGBY lighting subsystem with dimmable current stabilizers for each RGBY power LED; c) Mega128RFA1 transceiver board.

The subsystem for non-invasive measurements of human physiological parameters: the body temperature, the ECG-electrocardiogram and the EDA-electro-dermal activity to predicting human reaction to comfort conditions in the laboratory is presented in Fig.8. Fig.9 represents C program block for implementation of digital measurements of output signals of *VOLTAGE* (*VACP* block of Fig. 7a) and *CURRENT* (*ACP* block of Fig. 7a) by MEGA32 type board.

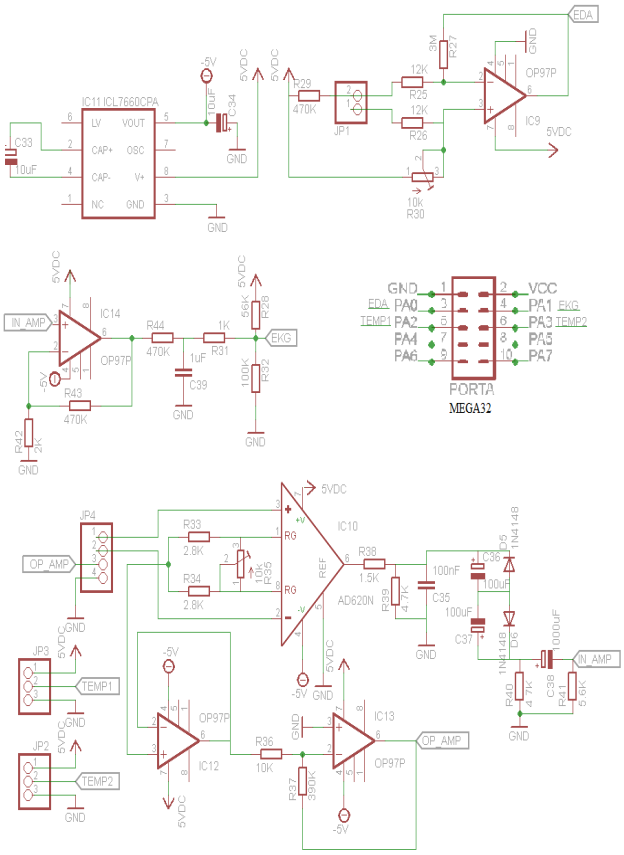

Fig.8. Schematic diagram of experimental subsystem for non-invasive measurements of human physiological parameters: the body temperature, the ECG-electrocardiogram and the EDA-electro-dermal activity to predicting human reaction to comfort conditions in the laboratory.

```
msr_info.v_rms_sum        +=        (int32_t)msr_info.
raw_inst_voltage *  msr_info.raw_inst_voltage;
msr_info.i_rms_sum        +=        (uint32_t)msr_info.
raw_inst_current * msr_info.raw_inst_current;
msr_info.vi_sum     +=     (int32_t)msr_info.raw_inst_
voltage*msr_info.raw_inst_current
double   v_rms   =   sqrt((double)msr_info.v_rms_sum   /
NUM_SAMPLES * v_coef * v_coef);
double   i_rms   =   sqrt(((double)msr_info.i_rms_sum   *
pow(i_coef/gain, 2)) / NUM_SAMPLES);
double p = (int32_t)msr_info.vi_sum / NUM_SAMPLES *
(i_coef/gain) * v_coef;
```

Fig.9. C program block for implementation of digital measurements of output signals of *VOLTAGE* (*VACP* block of Fig. 7a) and *CURRENT* (*ACP* block of Fig. 7a) by MEGA32 type board

VI. Results and Discussion

Fig. 10 represents digital measurement results of instantaneous values of 50 Hz mains voltage, *u* (V), taken as the output signals, *VOLTAGE*, of the *VACP* block of Fig. 7a and the mains instantaneous current, *i* (mA), taken as the output signals, *CURRENT*, of the *ACP* block of Fig. 7a versus time (sec*10^{-3}) measured by MEGA32 type board and calculated by the program of *Atmega Oscilloscope* respectively: for voltage, *u* (V), a) and current *i* (mA), b) of 0,7 kW heater, for voltage, *u* (V), c) and current *i* (mA), d) of the computer monitor, and for voltage, *u* (V), e) and current *i* (mA), f) of an refrigerator. Fig.11 depicts the screen shots of *Atmega Oscilloscope* program of instantaneous mains current, *i* (mA), versus time in sec*10^{-3} for: a) Unregulated 100W bulb; b) 100W bulb, regulated angle, α= 45°; c) 100W bulb, regulated angle, α= 45°, filtering: choke; d) 100W bulb, regulated angle, α= 45°, filtering: capacitor; e) 100W bulb , regulated angle, α= 45°, filtering: choke and capacitor. The current, *i* (mA), trough the 100W bulb type load was dimmed by triac type dimmer, *DIM1*, and measured by using the *CURRET* as an output signal of *ACP* block of Fig.7a.

The calculations of RMS values of current, $I_{RMS} = SQRT((\Sigma(v_iC_i/G)^2/n)$ = 2825.6 mA , voltage, $V_{RMS} = SQRT((\Sigma(v_vC_v)^2/n) = 230.0\ V$, apparent power, $S_{appparent} = V_{RMS}*I_{RMS}$ = 649.9 VA, active power, $P = \Sigma(v_iC_iv_vC_v/nG)$ = 628.119 W, power factor, $PF = P/S_{appparent}$ = 0.9665, C_i = 0.1206, C_v = 0.75, G = 1|10|200, and n = 3000 for the 0,7 kW heater are performed by system software every 0.7 sec. The constants C_v and C_i were calculated by using values of voltmeter, *V*, amp meter, *A*, and watt meter, *W*, of Fig.7a. The values of power factor of monitor and refrigerator are as follows: $PF_{monitor}$ = 0.3437 and $PF_{refrigarator}$ = 0.2598.

Digital measurements of instantaneous values of *k* sample of the mains voltage $(v_k + v_{k+2})/2$ and current i_{k+1} taken by the load from the mains have been performed every 0.8 sec*10^{-3} at 25 samples per 20 sec*10^{-3} period or 14.4°. Instantaneous active power value $p_k = ((v_k + v_{k+2})/2)* i_{k+1}$ was calculated after 3 first type differential convertions of every adjasent sample that takes 25 ADC clock cycles at a maximum speed of convertion of 200 KHz each, and 25/200.10^3 = 0.125 sec*10^{-3} or 6.28*0.125/20=0.03925 radians/2.25 degrees.

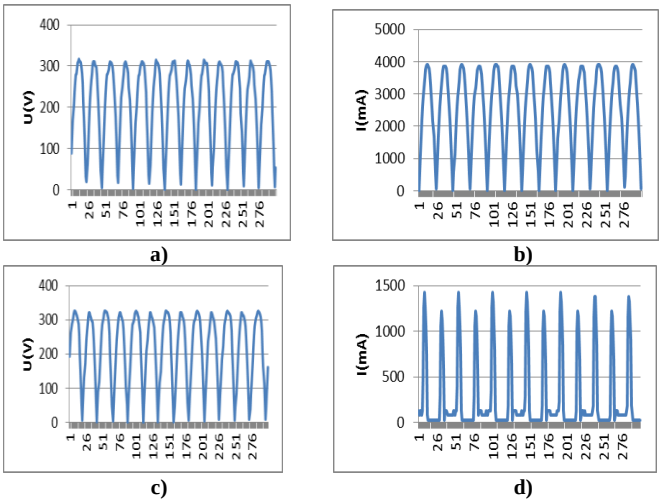

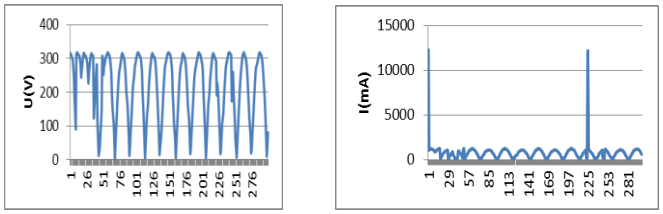

Fig.10. Screen shots of the program *Atmega Oscilloscope* of instantaneous values of output signals of *VOLTAGE* and *CURRENT* versus time in sec*10^{-3} measured by MEGA32 type board of Fig.2a respectively: for voltage, a) and current, b) of 0,7 kW heater; for voltage, c) and current, d) of computer monitor; for voltage, e) and current, f) of refrigerator.

The sample error can be: between the values of Err_{max}=512*(*sin*(0.03925)=20,09 (3.92%) and Err_{min}=512* *sin*(3.14/2) - (3.14/2-0.03925))=0.461(0.09%) which is acceptable.

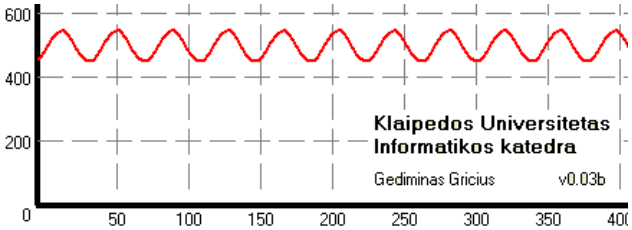

a) Unregulated 100W bulb, U_{RMS}=232 V, I_{RMS}=443 mA, Apparent power: 102,09 VA, Active power: 100,68 W, Power factor: 0,986

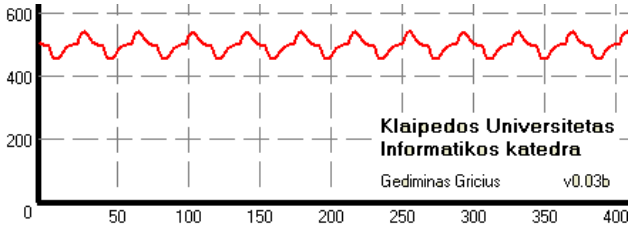

b) 100W bulb, α= 45°, U_{RMS}=232 V, I_{RMS}=318 mA, Apparent power: 73,79 VA, Active power: 36,60 W, Power factor: 0,496;

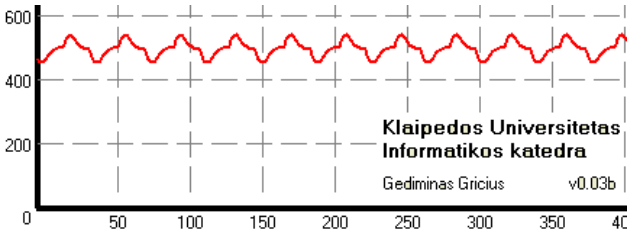

c) 100W bulb, α= 45°, filtering: choke, U_{RMS}=232 V, I_{RMS}=319 mA Apparent power: 73,18 VA Active power: 36,72 W Power factor: 0.502;

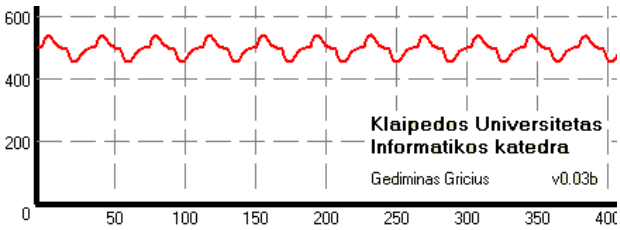

d) 100W bulb, α= 45°, filtering: capacitor, U_{RMS}=231 V, I_{RMS}=314 mA, Apparent power: 72,63 VA, Active power: 35,53 W, Power factor: 0,489;

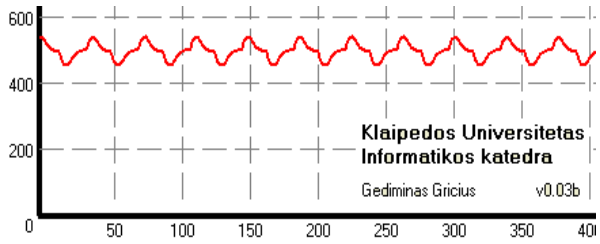

e) 100W bulb , α= 45°, filtering: choke and capacitor, U_{RMS}=231 V, I_{RMS}=314 mA, Apparent power: 72,94 VA, Active power: 35,88 W, Power factor: 0,492

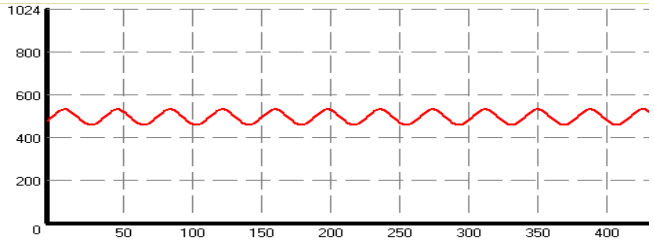

f) **Fan,** U_{RMS}=230 V, I_{RMS}=330 mA, Apparent power: 75.90 VA, Active power: 51.87 W, Power factor: 0.68

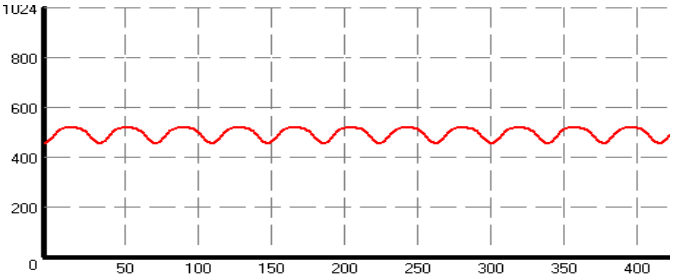

g) **Fan, , α= 5°,** U_{RMS}=230 V, I_{RMS}=288 mA, Apparent power: 66.24 VA, Active power: 46.43 W, Power factor: 0.70

Fig.11. Screen shots of *Atmega Oscilloscope* program of instantaneous current in mA versus time in 10^{-3}*sec for: a) Unregulated 100W bulb; b) 100W bulb, α= 45°; c) 100W bulb, α= 45°, filtering: choke; d) 100W bulb, α= 45°, filtering: capacitor; e) 100W bulb , α= 45°, filtering: choke and capacitor; f) Unregulated fan; g) Dimmable fan, α= 5°.

The measurement results of Fig.6 illustrate how dimming and filtering influence the parameters of power distributed to feeding the incandescent lamp of 100 W. For the case of Fig.11a of unregulated 100 W bulb**,** we have U_{RMS}=232 V, I_{RMS}=443 mA, apparent power, $S_{appparent}$ = 102,09 VA, active power, P = 100,68 W, power factor= 0,986. For Fig.11b of 100 W bulb with regulated angle, α=45°, we have U_{RMS}=232 V, I_{RMS}=318 mA, apparent power, $S_{appparent}$ = 73,79 VA, active power, P = 73,68 W, power factor= 0,496. For Fig.11c of 100 W bulb with regulated angle, α=45°, and filtering in series with 100 μH choke**,** we have U_{RMS}=232 V, I_{RMS}=319 mA, apparent power, $S_{appparent}$ = 73,18 VA, active power, P = 36,72 W, power factor= 0,502. For Fig.11d of 100 W bulb with regulated angle, α=45°, and filtering in parallel to the load with 470 nF capacitor**,** we have U_{RMS}=231 V, I_{RMS}=314 mA, apparent power, $S_{appparent}$ = 72,63 VA, active power, P = 35,53 W, power factor= 0,489. For Fig.11e of 100 W bulb with regulated angle, α=45°, filtering in series with 100 μH choke and in parallel to the load with 470 nF capacitor**,** we have U_{RMS}=231 V, I_{RMS}=314 mA, apparent power, $S_{appparent}$ = 72,94 VA, active power, P = 35,88 W, power factor= 0,492.

The dimming process introduces reactive power even in that case when there is an active load. It is seen from the results of Fig.6b where feeding the 100 W bulb with regulated angle, α=45°, we obtain the power factor= 0,496.

The simistor (triac) type dimmer introduces feature of capacitor type load and its influence may be minimized by introducing inductance type filter connected in series with the load. This statement can be proved by Fig.11c where 100 W bulb with regulated angle, α=45°, and filtering in series with 100 μH choke has the power factor= 0,502. The statement also can be proved by using Fig.11d where the power factor= 0,489 decreased when the 100 W bulb is fed from the 50 Hz mains with regulated angle, α=45°, and filtering in parallel to the load with 470 nF capacitor. The Fig. 11e demonstrates that filtering the load of 100 W bulb with regulated angle, α=45°, by using 2nd order filter in series with 100 μH choke and in parallel to the load with 470 nF capacitor does not make sense because in this case the power factor= 0,492, and it is less then in the case of Fig.11c when only filtering in series with 100 μH choke was used.

If the current, *i* (mA), trough the 75 VA single phase motor of the fan was dimmed by triac type dimmer, *DIM2*, and measured by using the *CURRENT* as an output signal of *ACP* block of Fig.7a, the dimming process increases the power factor. It is proved by using screen shots of *Atmega Oscilloscope* program shown in Fig.11f and 6g. Fig.11f gives data for fan fed by single phase 50 Hz mains with U_{RMS}=230 V, $I_{RM\,S}$=330 mA, apparent power=75.90 VA, active power= 51.87 W, power factor=0.68. Fig.11g gives data for dimmable fan with regulated angle, α= 5°, fed by single phase 50 Hz mains with U_{RMS} =230 V, I_{RMS}=288 mA, apparent power = 66.24 VA, active power = 46.43 W, and power factor=0.70.

VII. Conclusions

The model of the Cloud Interconnected Human Friendly Sustainable Power Controller is proposed based on describing of the Environment Evaluation Service, the Radial Basis Neural Network Service, and the Learning Algorithm Service in the multi-agent approach.

The Controller is based on the human ambient comfort affect reward index (ACAR index) which depends both on human physiological parameters: the temperature, the ECG-electrocardiogram and the EDA-electro-dermal activity as well as on the parameters of the sustainable electric power distribution subsystems for measuring, control and delivering power to electric heater, fans, and the intelligent RGBY LED lighting in a single room laboratory by using triac type AC power controllers driven by MEGA32 type boards.

The ATMEGA128RFA1-ZU transceivers are used to creating the cloud interconnected, instrumented, and intelligent environment by using MEGA32 type boards and central computer connected to the Internet.

The pseudo-codes of the Environment Sense Agent, the Environment Adaptation Agent, the Raw Data Processing

and EDA Parameters Extraction Agent, and the Neural Network Training Agent are proposed and implemented into the multi-agent based emotion recognition and environment control subsystem.

The modeling results show that the proposed system is able to automatically find such the environmental state characteristics that can improve both the power characteristics as well as the comfort conditions for people affected by this environment in the single room laboratory.

VIII. Acknowledgment

The authors gratefully acknowledge Lithuania Research Council for support of Project „Promotion of Students' Scientific Activities": http://studentai.lmt.lt/DOKUMENTAI/REZULTATAI/smp_2012_fbtz_finansuojamipt.pdf and the contributions of prof. E. Guseinovienė for her work on the original version of this document.

References

[1] A. Haag, S. Goronzy, P. Schaich, J. Williams, "Emotion Recognition Using Bio-sensors: First Steps towards an Automatic System", *Affective Dialogue Systems Lecture Notes in Computer Science*, Vol. 3068, 2004, pp.36-48.

[2] P. Rainville, A. Bechara, N. Naqvi, A.R. Damasio, "Basic emotions are associated with distinct patterns of cardiorespiratory activity", *International Journal of Psychophysiology*, Vol.61, No.1, July 2006, pp.5-18.

[3] A.A. Abdullah, U.H. Hassan, "Design and development of an emotional stress indicator (ESI) kit", *Sustainable Utilization and Development in Engineering and Technology (STUDENT)*, 2012 IEEE Conference, 6-9 October 2012, pp.253-257.

[4] P. Mika, Anu S. Tarvainen, Koistinen, Minna Valkonen-Korhonen, Juhani Partanen and Pasi A. Karjalainen, "Analysis of Galvanic Skin Responses With Principal Components and Clustering Techniques", *IEEE Transactions on Biomedical Engineering*, Vol.48, No.10, October 2001, pp.1071-1079.

[5] Philippot, P., Rimé, B., The perception of bodily sensations during emotion: A cross-cultural perspective", *Polish Psychological Bulletin*, 1997, 28, pp.175-188.

[6] G. Zheng, Y. Jing, H. Huang, P. Ma,"Thermal Comfort and Indoor Air Quality of Task Ambient Air Conditioning in Modern Office Buildings," *International Conference on Information Management, Innovation Management and Industrial Engineering, ICIII '09 Proc. 2009*, Vol.2, pp.533-536.

[7] S.M. Zanoli, D. Barchiesi, "Thermal and Lighting Control System with Energy Saving and Users Comfort Features", *Proc. 2012 IEEE 20th Mediterranean Conference on Control & Automation (MED)* Barcelona, pp.1322-1327.

[8] DIRECTIVE 2006/25/EC of the European Parliament and of the Council of 5 April 2006 on the minimum health and safety requirements regarding the exposure of workers to risks arising from physical agents (artificial optical radiation), 19th individual Directive within the meaning of Article 16(1) of Directive 89/391/EEC.

[9] Quarto, A., Di Lecce, V., Dario, R., Uva, J.**,** "Personal dosimeter for the measurement of artificial optical radiation (AOR) exposure", *Proc. IEEE International Conference on Computational Intelligence for Measurement Systems and Applications (CIMSA)*,2011, pp.1-6.

[10] A.A. Bielskis, A. Andziulis, O. Ramašauskas, E. Guseinovienė, D. Dzemydienė, G. Gricius, **"**Multi-Agent Based E-Social Care Support System for Inhabitancies of a Smart Eco-Social Apartment", *Electronics and Electrical Engineering*, 2011, Vol.1-(107), pp.11–14.

[11] A.A. Bielskis, E. Guseinovienė, D. Dzemydienė, D. Drungilas, G. Gricius, "Ambient Lighting Controller Based on Reinforcement Learning Components of Multi-Agents", *Electronics and Electrical Engineering*, Vol.5-(121), 2012, pp.79-84.

[12] K. Chinnakani, A. Krishnamurthy, J. Moyne, A. Arbor, and F. Gu, "Comparison of Energy Consumption in HVAC Systems Using Simple ON-OFF, Intelligent ON-OFF and Optimal Controllers", *Proc. IEEE Power and Energy Society General Meeting*, 2011, pp.1-6.

[13] R.S. Sutton, A.G. Barto, Reinforcement learning: An Introduction. Cambridge, MA: MIT Press**,** 2011.

[14] K. Dalamagkidis, D. Kolokotsa, Reinforcement Learning for Building Environmental Control", *Reinforcement Learning: Theory and Applications*, Book edited by Cornelius Weber, Mark Elshaw and Norbert Michael Mayer ISBN 978-3-902613-14-1, I-Tech Education and Publishing, Vienna, Austria, January 2008, pp.424.

[15] *ICNIRP Guidelines on limits of exposure to broad-band incoherent optical radiation (0.38 to 3 microM)*, ICNRP Statement @, 2011

Biographies

Gediminas Gricius is a Ph.D. student at the Department of Software Engineering of Vilnius University Institute of Mathematics and Informatics (Lithuania) and works as an lecturer at the Klaipeda University. He graduated MSc degree in computer science, Klaipeda University in 2010. Research interests include embedded systems, automated control and agent-based modeling.

Darius Drungilas is a PhD student at Institute of Mathematics and Informatics, Vilnius University (Lithuania). He graduated MSc degree in computer science, Klaipeda University in 2009. He is lecturer at the Department of Informatics engineering and Electrical Engineering of the Faculty of Marine Engineering of the Klaipeda University (Lithuania). His research interests include methods of artificial intelligence, agent-based modeling, digital adaptive control, machine learning and data mining.

Jurgita Guseinovaitė (born in 1992) is a 4th year medical student in Faculty of Medicine, Vilnius University. In summer 2013 she took part in summer practice in Klaipeda University Hospital at Oncology Department. Areas of interest include normal and pathological physiology, oncology and oncosurgery.

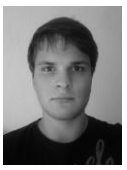

Kazimieras Grigaitis (born in 1991) is a 4th year medical student in Faculty of Medicine, Vilnius University. In summer 2012 he took part in project "Promotion of Student Scientific Activities". In 2013 he participated in summer practice Klaipeda University Hospital at Traumatology Department. Areas of interest include human physiology, biomechanics, orthopaedics and traumatology, surgery.

Antanas Andrius Bielskis is professor, doctor habilitatis of the Informatics, Electrical Engineering Departments of Klaipeda University and of the Department of Informatics of Lithuanian Business University of Applied Sciences He holds the diplomas of radio-engineering in 1959 of Kaunas Institute of Technology, PhD in Electronic Engineering in 1968 of Moscow Institute of Communications, and Doctor of Science in Power Electronics and Communications in 1983 of the Institute of Electrodynamics of Academy of Science of Ukraine.

In 1959-1964, he was the designer, project manager at the Klaipeda Ship Design Institute, in 1964-1990 - senior lecturer, associate professor, head of the departments of Electrical Engineering and Physics - Mathematics, professor of the Klaipeda faculty of the Kaunas Polytechnic Institute (now Kaunas University of Technology), and in 1991 up to now– professor of Klaipeda University.

His research interests include methods of artificial intelligence, knowledge representation techniques, development of smart embedded energy distribution systems.

Real-time Robust Control Using Digital Signal Processor

T. Slavov, L. Mollov, J. Kralev, P. Petkov

***Abstract*—A laboratory system for real-time robust control of multivariable analogue 4th order two input/two output plant is presented. The system consists of Spectrum Digital eZdspTMF28335 development kit with built in Texas Instruments TMS320F28335 Digital Signal Processor (DSP), digital to analogue signal converter, voltage divider, and a test analogue plant. A 16th order discrete-time μ-controller with sampling frequency of 100 *Hz* is implemented by using a DSP. The μ-controller designed ensures robust performance of the closed-loop system in presence of parametric uncertainty in two plant parameters. Frequency domain analysis of the discrete-time closed-loop system is performed. The implementation of high-order robust control law is facilitated by the usage of technology for automatic code generation. An appropriate software in MATLAB®/Simulink® environment is developed which is embedded in DSP by using the Simulink Coder®. Experimental and simulation results are presented which confirm that the control system achieves the prescribed performance.**

Index Terms— **digital signal processor, real-time control, robust control, μ-controller**

I. INTRODUCTION

The Robust Control Theory now is a mature discipline that involves powerful methods for analysis and design of control systems in presence of signal and parameter uncertainties. The most frequently used techniques for robust control design are the H_∞ optimization and the μ-synthesis [1]. The H_∞ optimization is usually preferred in robust design because it produces controller of smaller order which facilitates its implementation. The common disadvantage of all H_∞ optimization methods is that they are suitable for plants with unstructured uncertainties but cannot ensure robust stability and performance in the general case of unstructured and structured (parametric) uncertainties. In contrast, the μ-synthesis which aims at minimization of the structured singular value [2] may ensure robust stability and robust performance in the presence of exogenous disturbances, noises and different type of uncertainties. The high order of the controller obtained is usually pointed out as a disadvantage of μ-synthesis. However, with the appearing of powerful processors in the recent years this peculiarity of the μ-synthesis does not pose a significant difficulty.

In contrast with the theoretical achievements, the practical implementation of robust control laws is still in its beginning. There is a few real life applications of high order robust control laws reported in the literature concerning mainly the control of flying vehicles (see for instance [3] and [4]). The main obstacle of robust control laws implementation is the difficulties related to the development, testing and verification of the necessary real-time software which is highly dependent on the type of digital controller platform used. These difficulties are reduced significantly using the recent technologies for automatic code generation and embedding implemented in MATLAB®/Simulink® program environment [5]. A real-time implementation of linear quadratic control law by using automatic code generation is reported in [6].

In this paper a laboratory system for real-time robust control of multivariable analogue 4th order two input/two output plant is presented. The system consists of Spectrum Digital eZdspTMF28335 development kit with built in Texas Instruments TMS320F28335 DSP, digital to analogue signal converter, voltage divider, and a test analogue plant. A 16th order discrete-time μ-controller with sampling frequency of 100 *Hz* is implemented by using a Digital Signal Processor. The μ-controller designed ensures robust performance of the closed-loop system in presence of parametric uncertainty in two plant parameters. Frequency domain analysis of the discrete-time closed-loop system is performed. An appropriate software in MATLAB®/Simulink® environment is developed which is embedded in DSP by using the Simulink Coder®. Experimental and simulation results are presented which confirm that the control system achieves the prescribed performance.

II. CONTROLLER μ-SYNTHESIS

The block-diagram of the analog two input/two output plant under consideration is shown in Fig. 1.

T. Slavov is with the Technical University Sofia, Bulgaria, He is now with the Department of Systems and Control (e-mail: ts_slavov@ tu-sofia.bg).

L. Mollov is with the Technical University Sofia, Bulgaria, He is now with the Department of Systems and Control (e-mail: l_mollov@abv.bg).

J. Kralev is with the Technical University Sofia, Bulgaria, He is now with the Department of Systems and Control (e-mail:jkralev@yahoo.com).

P. Petkov is with the Technical University Sofia, Bulgaria, He is now with the Department of Systems and Control (e-mail: php@tu-sofia.bg).

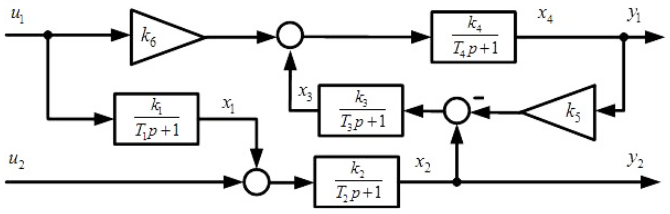

Fig. 1. Block-diagram of the plant

The 4th order plant model is described by the state space equations

$$\begin{vmatrix} \dot{x}(t) = Ax(t) + Bu(t) \\ y(t) = Cx(t) + Du(t) \end{vmatrix}, \quad (1)$$

where $x = \begin{bmatrix} x_1 & x_2 & x_3 & x_4 \end{bmatrix}^T$ is the state vector, $u(t) = \begin{vmatrix} u_1(t) & u_2(t) \end{vmatrix}^T$ is the input vector and $y(t) = \begin{vmatrix} y_1(t) & y_2(t) \end{vmatrix}^T$ is the output vector,

$$A = \begin{vmatrix} -\frac{1}{T_1} & 0 & 0 & 0 \\ \frac{k_2}{T_2} & -\frac{1}{T_2} & 0 & 0 \\ 0 & \frac{k_3}{T_3} & -\frac{1}{T_3} & -\frac{k_5 k_3}{T_3} \\ 0 & 0 & \frac{k_4}{T_4} & -\frac{1}{T_4} \end{vmatrix}, B = \begin{vmatrix} \frac{k_1}{T_1} & 0 \\ 0 & \frac{k_2}{T_2} \\ 0 & 0 \\ \frac{k_4 k_6}{T_4} & 0 \end{vmatrix},$$

$$C = \begin{vmatrix} 0 & 0 & 0 & 1 \\ 0 & 1 & 0 & 0 \end{vmatrix}, D = 0_{2\times 2},$$

$k_1, k_2, ..., k_6$ are coefficients of proportionality, $T_1, T_2, ..., T_4$ are time constants.

The model parameters are estimated by identification procedure using the MATLAB® function *lsqnonlin* based on the nonlinear least square method. The performance criteria minimized is

$$I_e = \int_0^t (y_p(t) - y(t))^T (y_p(t) - y(t)) dt, \quad (2)$$

where $y_p(t) = [y_{p_1}(t) \quad y_{p_2}(t)]^T$ is the analog plant output. The identification input signal is

$$u_{ident}(t) = [1(t) \quad 1(t)]^T$$

where $1(t)$ is a step function. The signal $y_p(t)$ is obtained by real time measuring of the two analogue plant outputs with sample time 100 ms. After minimization of (2) taking $t = 10s$ we obtain

$$I_e = 6.36 \times 10^{-4}.$$

The analog plant output signals and model output signals are shown in Fig. 2 and Fig.3. As can be seen the model outputs coincide very well with the measured plant output signals.

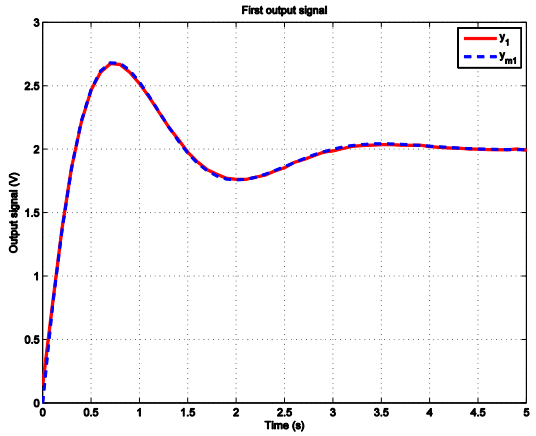

Fig. 2. First output signal

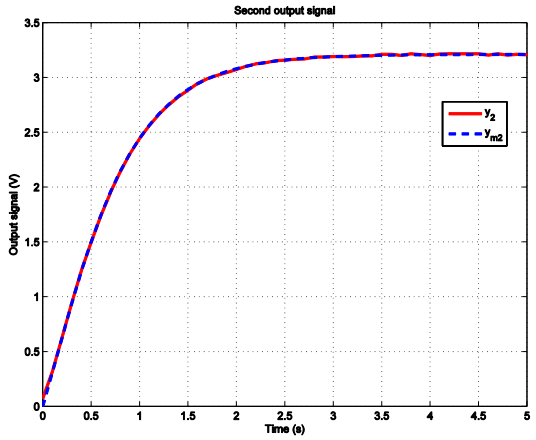

Fig. 3. Second output signal

The nominal model parameters determined are presented in

TABLE I
NOMINAL PANT PARAMETERS

Parameter	Value	Parameter	Value
k_1	1.0463	T_1	0.3308
k_2	1.5689	T_2	0.5291
k_3	0.4213	T_3	1.1142
k_4	3.0000	T_4	0.7063
k_5	3.0558		
k_6	1.8970		

Table 1.

Further on it is assumed that the coefficient k_1 is a subject of 25% change around the nominal value and the parameter T_4 undergoes 40% change around its nominal value. In this

way the plant involves structured (parametric) uncertainty which is set by using the function *ureal* from Robust Control Toolbox® [7]. In order to ensure robust stability and robust performance of the closed-loop system in the presence of such uncertainty and to ensure acceptable suppression of the disturbances and noises, it is appropriate to design a μ-controller.

The block-diagram of the closed-loop system which includes the performance and control weighting functions is shown in Fig. 4. The transfer function matrix of the uncertain plant is denoted by G and the controller transfer function matrix -by K. The system has a reference vector *ref* and an

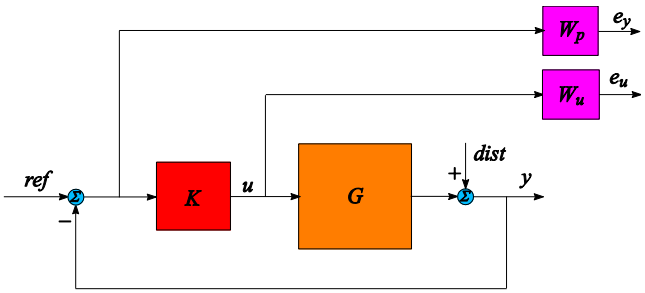

Fig. 4. Closed-loop system with performance requirements

output disturbance vector *dist*.

The closed-loop system is described by the equations

$$\begin{aligned} y &= T_o r + S_o d \\ u &= S_i K (r - d) \end{aligned}, \qquad (3)$$

where the matrix $S_i = (I + KG)^{-1}$ is the input sensitivity transfer function matrix, $S_o = (I + GK)^{-1}$ is the output sensitivity transfer function matrix and $T_o = (I + GK)^{-1} GK$ is the output complementary sensitivity function. (Here and further on the reference vector is denoted for brevity by r and the disturbance vector - by d).

The weighted closed-loop system outputs e_y and e_u satisfy the equation

$$\begin{bmatrix} e_y \\ e_u \end{bmatrix} = \begin{bmatrix} W_p S_o & -W_p S_o \\ W_u S_i K & -W_u S_i K \end{bmatrix} \begin{bmatrix} r \\ d \end{bmatrix}. \qquad (4)$$

The performance criterion requires the transfer function matrix from the exogenous input signals r and d to the output signals e_y and e_u to be small in the sense of $\|\cdot\|_\infty$, for all possible uncertain plant models G. The transfer function matrices W_p and W_u are used to reflect the relative importance of the different frequency ranges for which the performance requirements should be fulfilled.

The μ-synthesis is done for the performance weighting function

$$W_p = \begin{bmatrix} 0.92\dfrac{0.15s+1}{0.24s+10^{-4}} & 0 \\ 0 & 0.92\dfrac{0.18s+1}{0.30s+10^{-4}} \end{bmatrix}$$

and for the control weighting function

$$W_u = \begin{bmatrix} 0.02\dfrac{0.005s+1}{0.001s+1} & 0 \\ 0 & 0.02\dfrac{0.005s+1}{0.001s+1} \end{bmatrix}.$$

The performance weighting functions are chosen as low pass filters to suppress the system error $y - r$, and the control weighting functions are chosen as high pass filters with appropriate bandwidth in order to impose constraints on the high frequency spectrum of the control actions [7].

In order to determine a discrete-time μ controller the extended open-loop system including the plant and weighting functions is discretized with sampling period of 0.01 s corresponding to sampling frequency of 100 Hz. The μ-synthesis is performed by using the Robust Control Toolbox® function *dksyn* [8]. Four iterations are performed that decrease the maximum value of μ to 1.000. The final controller obtained is of 16th order.

The singular value plot of the discrete-time controller is shown in Fig.5. The controller has a high low-frequency gains which allows to attenuate efficiently the low-frequency

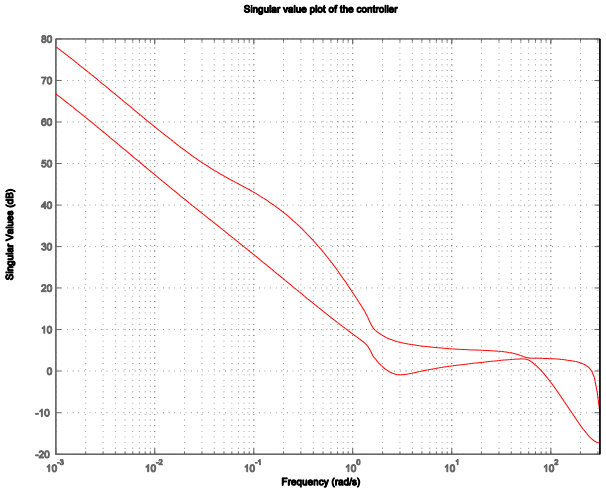

Fig. 5. Controller singular values

disturbances and to ensure accurate reference tracking.

The frequency-response plot of the structured singular value for the case of robust stability, obtained by using the function *robuststab* is shown in Fig. 6. The closed-loop system can tolerate up to 201% of the modeled uncertainty which means that the stability is preserved for uncertainty that may be up to two times larger than the assumed one.

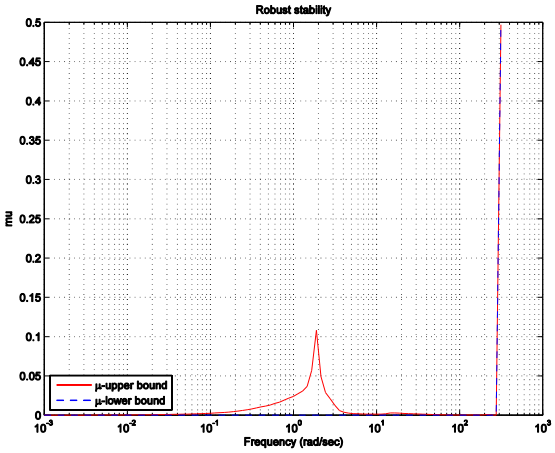

Fig. 6. Robust stability for μ -controller

The frequency response of the structured singular value for the case of robust performance, obtained by using the function *robustperf* is shown in Fig.7. The closed-loop system achieves a robust performance margin of 1.011 which means that the system will satisfy the performance requirements for all possible values of the uncertain parameters. The singular values of the complementary sensitivity function T_o plotted in Fig.8 show that the closed-loop system will track accurately references with frequencies up to 5 rad/s.

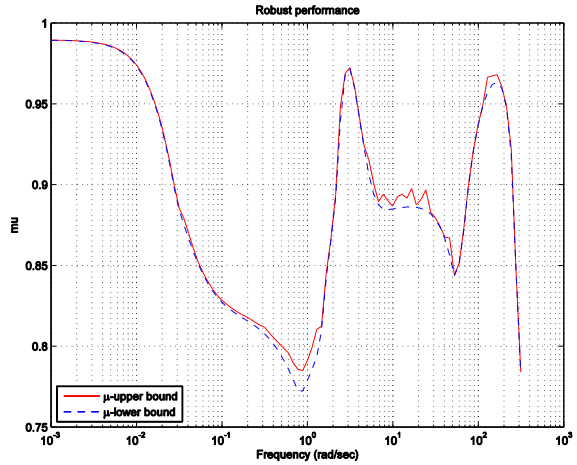

Fig. 7. Robust performance for μ -controller

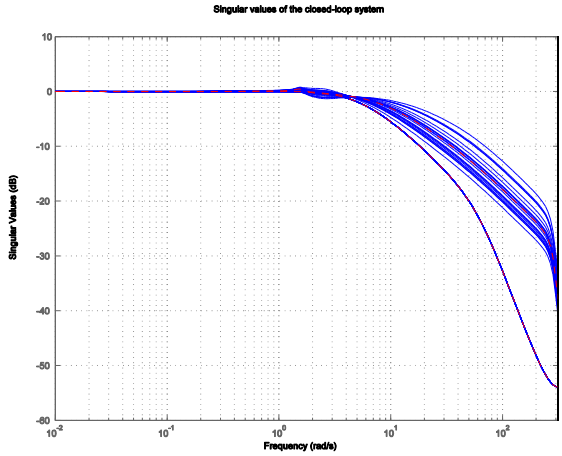

Fig. 8. Singular values of the complementary sensitivity function

In Fig.9 we show the singular value plot of the output sensitivity function S_o compared with the singular value plot of the inverse performance weighting function W_p^{-1}. The plot confirms that the system attenuates more than 10^3 times low frequency output disturbances. The singular value plot of the transfer function matrix $S_i K = KS_o$ which, according to (3) determines the control action u , is shown in Fig.10. It is seen that the high frequency contents of the control actions is attenuated in accordance with the requirements imposed by the inverse control weighting function W_u^{-1}.

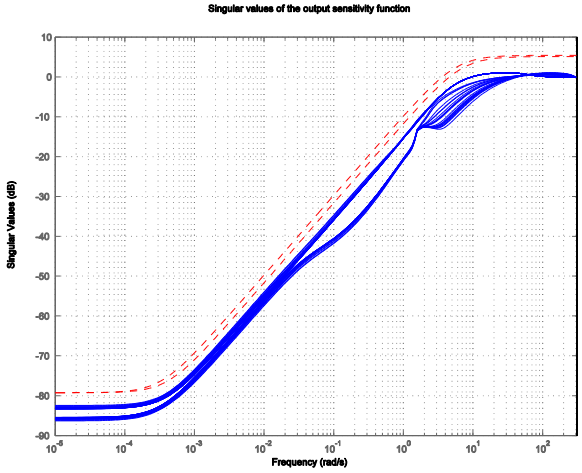

Fig. 9. Singular values of the output sensitivity function

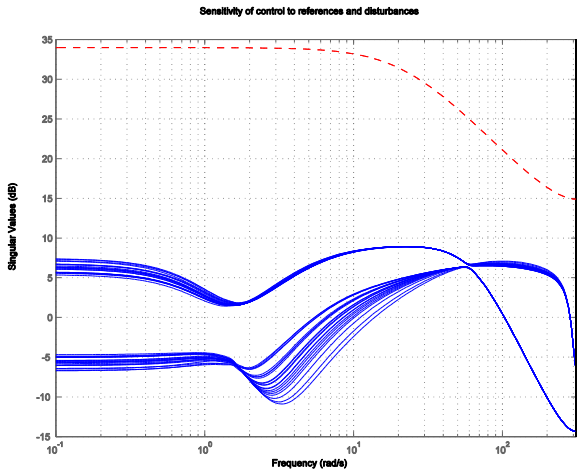

Fig. 10. Singular values of disturbance-to-control transfer function matrix

III. IMPLEMENTATION OF THE μ - CONTROLLER

The experimental setup of the analog plant control system is shown in Fig. 11. The two input/two output plant (1) is modeled on an analog modeling board, consisting of a bus on which functional blocks are operating independently. The bus is powered by a DC power supply. The linear range of input-output signals is ±10 V. The main linear blocks are adder, differentiator, inverter, integrator, aperiodic unit and gain unit.

The analog system makes it easy to model plants with a time constant up to 1 s and gain factor up to 10.

The block-diagram of developed control system with DSP is shown in Fig. 12.

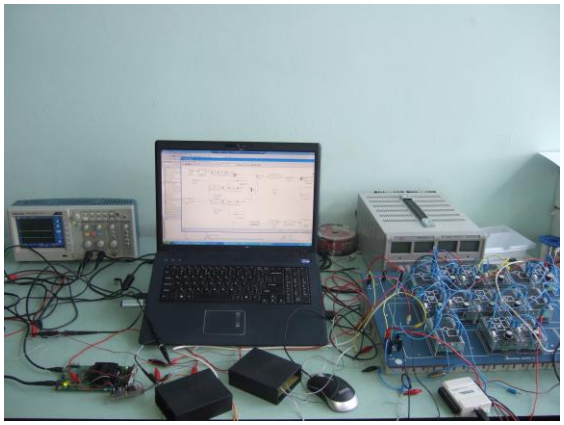

Fig. 11. Experimental setup

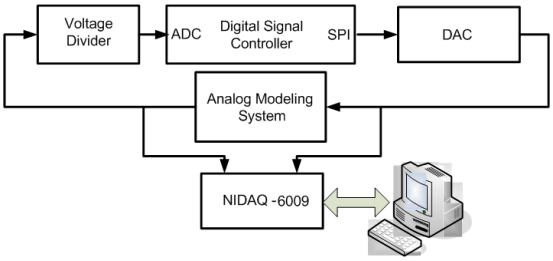

Fig. 12. Block-diagram of the control system with DSP

The block ``Digital Signal Controller'' (DSC) is the Spectrum Digital eZdspTMF28335 development board with an integrated Digital Signal Processor Texas Instruments TMS320F28335 [9]. This controller works at 150 MHz and may perform single precision (32-bit) computations by using The process of generation and implementation of the execution code in the Simulink® model is illustrated in Fig.13. This process relies heavily on the use of Simulink Coder® and Embedded Coder®.

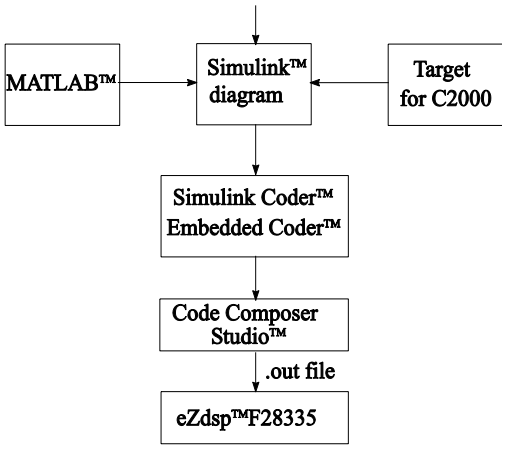

Fig. 13. Generation and embedding of the control code;

FPU (Floating-Point Unit). It has 68K bytes on-chip RAM, 256K bytes off-chip SRAM memory, 512K bytes on-chip Flash memory and on-chip 12 bit Analog to Digital (A/D) converter with 16 input channels.

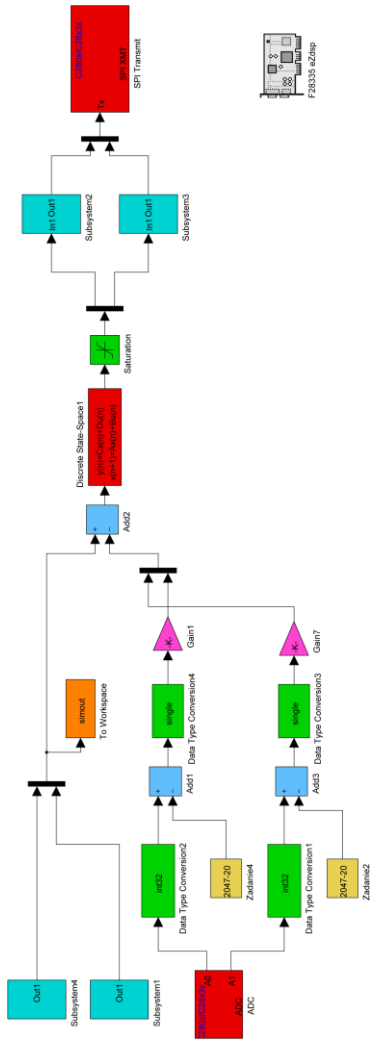

Fig. 14. Block-diagram of the Simulink® model

The block "Voltage Divider" is a specially designed dual channel board, which converts linearly two input analog signals with range -5 to 5 V into two analog output signals with range 0 to 3 V.

The block "DAC" is a digital to analogue converter DAC8734EVM produced by Texas Instruments [10]. The DAC is 16-bit, quad-channel and can be configured to outputs ±10V, ±5V, 0V to 20V or 0V to 10V. It features a standard high-speed serial peripheral interface (SPI) that operates at clock rates of up to 50MHz to communicate with a DSP.

The block ``NIDAQ-6009'' is a specialized module for data acquisition NIDAQ-6009 of National Instruments [11]. A specially developed software provides the user interface, connection and exchange input/output data with a standard PC in real time.

The control algorithm is embedded and runs with

frequency 100 Hz on the DSC. The software development environment includes MATLAB® v.7.11.0.584(R2010b), \Simulink® v.7.6, Simulink Coder® v.7.6 [5(5)], Embedded Coder® v. 5.6 [12], Microsoft Visual C++ v.8.0 and CodeComposer® (CCS) v.3.3. A technology for automatic generation and embedding the code using the Simulink Coder® is implemented. The main advantages of this technology are the relatively easy implementation of complex control algorithms and the short time to translate the control algorithm from the working simulation environment to the real working environment with physical plants, reducing the overall time for application testing and verification of the developed algorithm.

The block-diagram of the Simulink® model used to generate the execution code is shown in Fig. 14. Some blocks are taken from the specialized library for Texas Instruments C2000 of Simulink®. The experimental results are saved on the PC and are visualized in MATLAB®.

IV. Experimental Results

The performance of the developed robust control system with μ-regulator implemented using digital signal controller is confirmed by experimental investigations. Several experiments are done with the nominal plant and for different combinations of the uncertain plant parameters.

A. Experiment with the nominal plant

In case of nominal plant parameters, an experiment is done in which the reference varies every 10 s at three levels: -1V, 0V and 1V. The output and control signals (here and further on all signals are measured in volts) from simulation and experiments are shown in Fig. 15-18 (the experimental results are shown by continuous lines). It is seen from the Fig.15 nd Fig.16 that the experimental signals coincide well with the output signals obtained by simulation.

The Figures displaying control signals show the presence of some deviations from simulation results whose magnitudes may reach values of up to 0.2V. According to the frequency responses shown in Fig. 10, small disturbances and errors may be amplified in the control signals which explain the presence of relatively large noises in these signals.

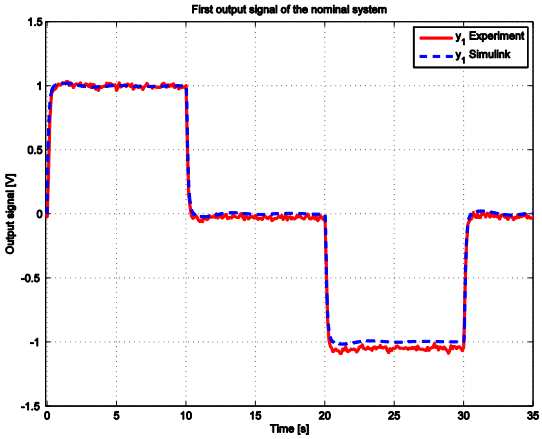

Fig.15. First output signal

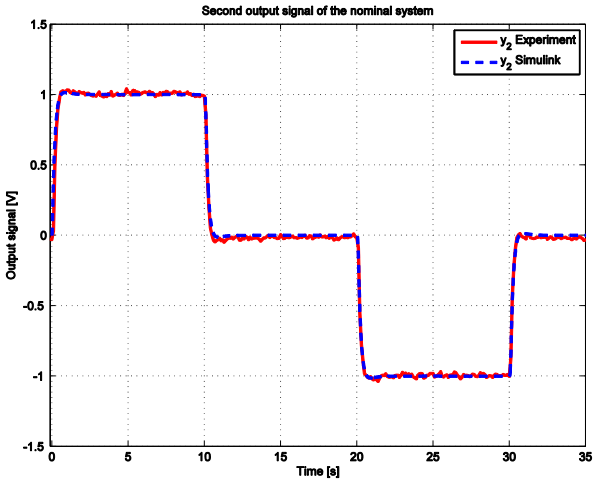

Fig.16. Second output signal

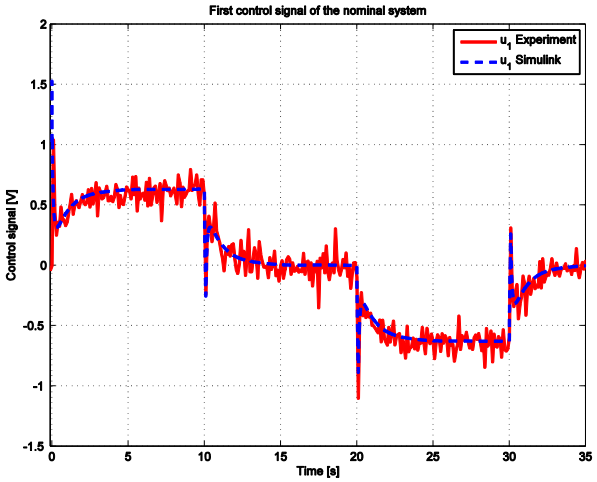

Fig.17. First control signal

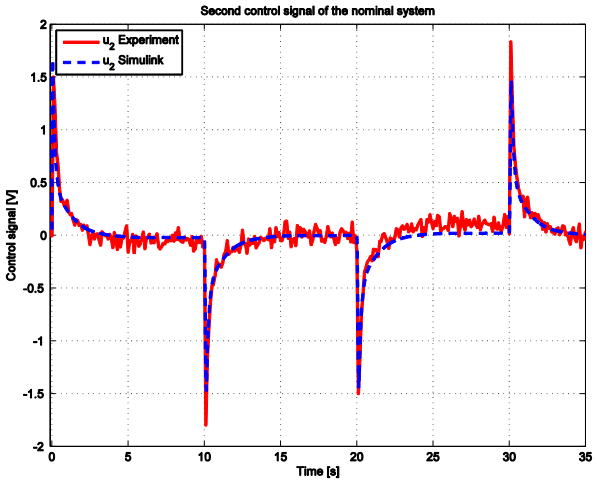

Fig.18. Second control signal

B. Experiment with different plant parameters

Five experiments for different values of the uncertain parameters are performed in order to access the influence of the uncertainties on the closed-loop system behavior. The set of uncertain parameters contain combinations of the minimum and maximum values of the uncertain parameters as shown in

Table II.

TABLE II
PARAMETERS VARIATION

Parameter set	k_1	T_4
1	0.75	0.35
2	0.75	1.05
3	1.25	0.35
4	1.25	1.05
nominal parameters	1.0463	0.7063

The set of nominal parameters is also included in order to estimate the maximum possible deviations of the output and control signals from their nominal values.

In Fig.19 and Fig.20 we show the output signals of the system for all five parameter sets. It is seen that the deviations of the outputs from their nominal values are relatively small which a result of the robust performance achieved is. The two control signals shown in Fig.21 and Fig.22 have more significant deviations from their nominal values which is again explained by the large gains associated with the transfer matrix $S_i K$.

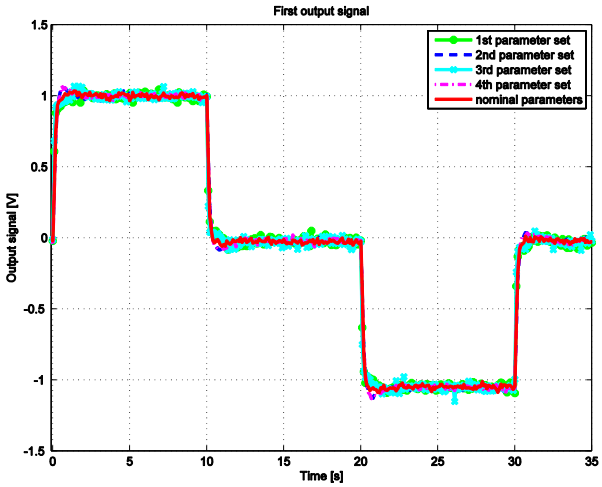

Fig.19. First output signal

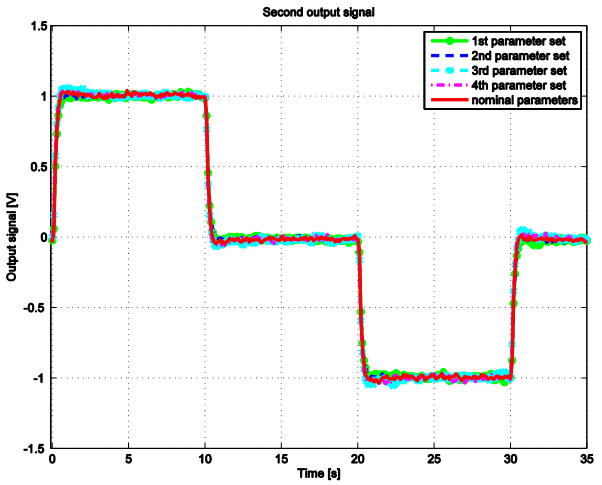

Fig.20. Second output signal

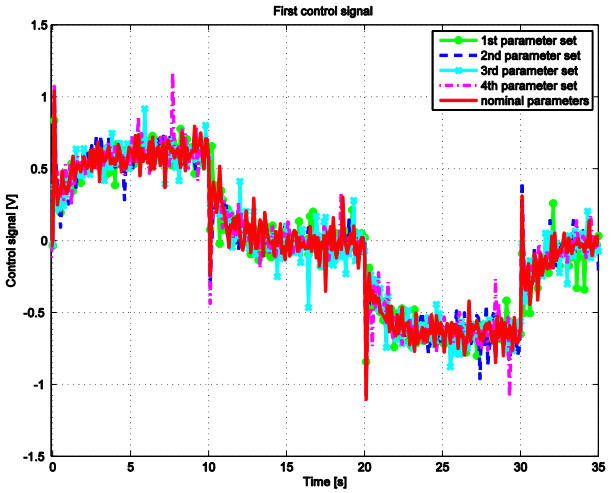

Fig.21. First control signal

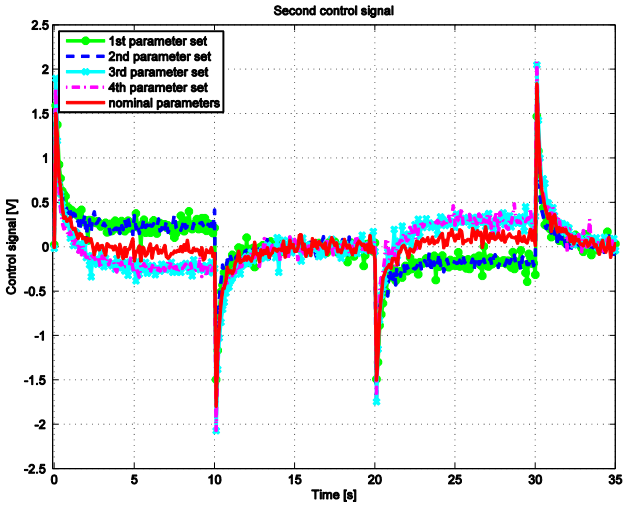

Fig.22. Second control signal

V. CONCLUSION

The paper presents a system for robust real-time control of fourth order plant using Digital System Processor. A specialized software for automatic generation of the control code is developed that facilitates the implementation of high order control algorithms for multivariable plants. The main conclusion is that the existing technologies allow implementing easily a 16th order μ-controller that ensures robust stability and robust performance of the closed-loop system. The experimental results confirm the performance of the closed-loop system whose parameters vary in prescribed boundaries. The control code may be easily modified for control of other plants.

REFERENCES

[1] S. Skogestad, I. Postlethwaite, *Multivariable Feedback Control 2nd ed*, John Wiley and Sons Ltd, Chichester, UK, 2005.

[2] K. Zhou, J.C. Doyle, K. Glover. *Robust and Optimal Control*. Prentice Hall, Upper Saddle River, NJ, 1996.

[3] M. La Civita, G. Papageorgiou, W.C. Messner, T. Kanade, "Design and flight testing of a high-bandwidth loop shaping controller for a robotic

helicopter", *Journal of Guidance, Control, and Dynamics*, vol.29, no 2, pp. 485-495, 2006.
[4] X. Wang, X. Zhao. "A practical survey on the flight control system on small-scale unmanned helicopter", in *Proc.WCICA*, Chongqing, China, 2008, pp 364-369.
[5] The MathWorks Inc. (2013, March 15), *Simulink Coder*, [Online]. Available: http://www.mathworks.com/products/datasheets/pdf/simulink-coder.pdf
[6] T. Slavov, L. Mollov, P. Petkov, "Real-time quadratic control using Digital Signal Processor". *TWMS Journal of Pure and Applied Mathematics*, vol.3, no. 2, pp.145-157, 2012.
[7] D.W. Gu, P.Hr. Petkov, M.M. Konstantinov, *Robust Control Design with MATLAB, 2nd ed*, Springer-Verlag, London, 2013.
[8] G. Balas, R. Chiang, A. Packard, M. Safonov. (2013, March). Robust Control Toolbox User's Guide. The MathWorks, Inc.,Natick, MA. [Online] Available: http://www.mathworks.com/help/pdf_doc/robust/robust_ug.pdf
[9] Spectrum Digital, Inc.(2013, March 15), *eZdspTMF28335 Technical Reference 2007*, [Online] Available : http://c2000.spectrumdigital.com/ezf28335/docs/ezdspf28335c_techref.pdf.
[10] Texas Instruments. (2013, March 15), *DAC8734 Evaluation Module*, [Online] Available: http://www.ti.com/tool/dac8734evm
[11] National Instruments.(2013, March 15), *NI USB-6009 14-Bit, 48 kS/s Low-Cost Multifunction DAQ*. [Online] Available: http://sine.ni.com/nips/cds/view/p/lang/en/nid/201987
[12] The MathWorks, Inc.(2013, March 15), *Embedded Coder*. [Online] Available from: http://www.mathworks.com/products/datasheets/pdf/embedded-coder.pdf.

BIOGRAPHIES

Tsonyo Slavov was born in Sofia, Bulgaria in 1978. He graduated from the Department of Systems and Control of the Technical University of Sofia in 2002. He received Ph.D degree in control engineering from the Technical University of Sofia in 2007. Presently, he is an Associated Professor in the Department of Systems and Control at the Technical University of Sofia

Luben Mollov graduated from the Department of Systems and Control of the Technical University of Sofia in 2008. Presently, he is a assistant professor in the same department.

Jordan Kralev has M.S. degree in Automatics, Information and Control Technologies. Since 03.2013 he is a Ph.D. student in the Department of Systems and Control, Technical University of Sofia. His work is in the field of implementation of complex control structures with programmable platforms.

Petko Petkov received M.S. and Ph.D. degrees in control engineering from the Technical University of Sofia in 1971 and 1979. Since 1995, he has been a Professor of Control Theory in the Department of Systems and Control at the Technical University of Sofia. He is coauthoring *Computational Methods for Linear Control Systems* (Prentice Hall, Hemel Hempstead, U.K., 1991), *Perturbation Theory for Matrix Equations* (North-Holland, Amsterdam, 2003), and *Robust Control Design with MATLAB* (Springer, London, 2005, 2013).

Estimating Optimal Wind and Storage Capacity to Avoid Conventional Power Plants Expansion Using Monte Carlo Method

S. Shojaeian, H. Akrami

***Abstract*— Considering the growing trend of the electric power demand and the global tendency to substitute new renewable energy sources, this paper proposes a Monte Carlo based method to determine an optimal level of this substitution. Because of the limitation of the wind farms in continuous supply of electric power, hydrostatic power storage facilities are used beside them so that the electric power could be stored and fed in a continuous flow into power systems. Due to the gradual exclusion of conventional generators and a reasonable percent annual load growth, Loss Of Load Expectation (LOLE) index was used in order to calculate the amount of the wind power and the capacity of the necessary power storage facility. To this end, Loss Of Energy Expectation (LOEE) index was calculated for the first year as the reference index for the estimation of the amount of wind power and the capacity of the storage facility in consequent years. For the upcoming years, calculations have been made to account for the gradual exclusion of conventional generators in proportion to load increments. The method proposed has been implemented and simulated on IEEE-RTS test system.**

Index Terms— **Hydroelectric Storage, LOLE, Monte Carlo, Reliability, Wind Power**

I. INTRODUCTION

ENVIRONMENTAL concerns, due to the limitations of conventional fossil fuels such as coal, oil and natural gas used in the production of electricity and emissions an pollutions thereof, has elevated the global tendency to use and promote the use of renewable sources of energy. With the advent and development of power generation techniques using renewable sources of energy, and promotion of the use of these techniques in meeting electric power needs of the nations, probing into and assessment of the power generated and fed into the power systems by these sources gains high importance. Wind energy had the fastest growth rate among these renewable sources of energy and has been recognized as the most successful renewable source of energy. A lot of research has been carried out in order to model the wind speed behavior in terms of planning and analysis the reliability of the wind energy conversion system (WECS) or combination power systems including wind power [1,2,3].

S. Shojaeian is with the faculty of electrical engineering, Khomeinishahr Branch, Islamic Azad University, 8418848499 Isfahan, Iran, (corresponding author e-mail: shojaeian@iaukhsh.ac.ir).

H. Akrami was a M. Sc. student in the faculty of electrical engineering, Khomeinishahr Branch, Islamic Azad University, 8418848499 Isfahan, Iran, (e-mail: hadi.akrami@iaukhsh.ac.ir).

In previous studies, Wind speed distributions are often characterized by Weibull distributions in system evaluation using analytical methods [4]. However, these techniques cannot recognize the chronology in wind speed variation at a geographic location. Given the changes in the wind speed in time, Auto Regressive Moving Average (ARMA) time series model is the right model for simulating the wind speed [1]. The relation between the wind speed and power output of the wind turbine generators (WTGs) is shown by a non-linear equation in the name of wind power curve1 [5].

References [4-17] presented different techniques in order to reliability evaluate of the powers systems include wind power. References [4-9] use analytical techniques in the assessment of the reliability of power systems that include wind power generators.

Sequential Monte Carlo simulation (SMCS) methods are used for the assessment of the reliability of power systems with unpopular storage sources have been introduced in [10 – 17]. References [10-15] use ARMA time series model in the reliability evaluation of the power systems include WTGs based on the Monte Carlo method.

Power systems that include wind power face many restrictions in the absorption of wind energy because of the fluctuations of the wind power. If it is possible to use sources for the storage of the wind energy beside WTGs, this restriction could be largely overcome. There are different methods for the storage of the energy. New battery technologies, such as the Vanadium Redox Battery (VRB) [18], are being considered and successfully tested for large scale on-grid applications of wind energy. In reference [19], the general probabilistic method of a WECS has been used that include wind power generators and energy storage batteries.

This paper uses IEEE-RTS test system that has been used in many studies as the test system. ARMA time series model was used to simulate the hourly wind speed and SMCS simulation technique was used in the calculation of, Loss Of Load Expectation (LOLE) and Loss Of Energy Expectation (LOEE) indices. The kind of storage facility used is the hydraulic storage system. All simulations have been used the MATLAB software.

II. MODELLING OF THE SYSTEM COMPONENTS

A. Basic concepts

The main function of an electric system is to be of an acceptable level of reliability and price [10]. The reliability of a system is defined as its ability to perform its functions within a definite span of time. In general the reliability associated

with a power system is a measure of the overall ability of the system to satisfy the customer demand for electrical energy [20].

The most important issue in evaluating the efficacy of a power system including wind power is the ability of the system to supply the power needed to meet the load of the system. Reliability assessment of power systems takes place in the three Hierarchical levels of generation (HL1), transmission (HL2) and distribution (HL3). Considering the fact that failure or fault in generation facilities to the outage of the whole system, the adequacy evaluation of the power systems at the generation level is of particular importance. That is why this study is focused on the reliability of the power systems that include WTGs and storage facilities using the HL1. The transmission and distribution systems are considered as quite reliable in this paper.

Reliability evaluation of the power systems including wind power is carried out using different techniques. Analytical and simulation methods are among the most important techniques used in the evaluation of the reliability of these systems, and as far as simulation techniques are concerned, the Monte Carlo simulation method (MCS), which has been adopted in this study, prevails.

Analytical methods use statistical and mathematical models for the description of the system elements, and risk indices are obtained using mathematical models. The analytical method cannot readily take into account the chronology of the random events and relation between load, wind power, and charge and discharge states of the power storage facilities. On the other hand, the statistical technique is practical and useful for the evaluation of systems that have a great number of random variables.

The Monte Carlo method is a calculative algorithm that uses random sampling for the calculation of the results. The MCS technique provide different methods for the evaluation the reliability indices of the power systems through the simulation of real processes and the random behavior of the system, and takes into account all dimensions and intrinsic probabilities of the system in planning, design and operation of the power systems.

In recent decades, MCS has found widespread uses due to the rapid development of the calculation tools. MCS method involves the sequential and non-sequential techniques. In the sequential technique, the behavior of the system is taken as continuous, whereas in the non-sequential technique, the system's behavior is taken as discrete. Therefore, the sequential method is more precise in terms of the temporal and chronological continuity [21].

B. Generation model

Each power generator within the power systems can be demonstrated by a two-state or multi-state Markov model. In the two-state Markov model the power generation unit is either in a fully functional load or a forced outage rate (FOR) state. As shown in Fig. 1, the generation unit transits between the two states of λ and μ, where λ is the failure rate and μ is the repair rate of the generating unit.

If the failure rate (λ) and repair rate (μ) is available, it is possible to calculate the value of unavailability (U),

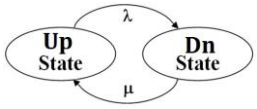

Fig. 1: Two-state model for a generation unit.

availability (A) and FOR of the generator unit with use (1) to (3) [20].

$$U = \frac{\lambda}{\lambda + \mu} \tag{1}$$

$$A = 1 - U = \frac{\mu}{\lambda + \mu} \tag{2}$$

$$FOR = \frac{\sum_i DownTime_i}{\sum_i DownTime_i + \sum_i UpTime_i} \tag{3}$$

C. Load Model

Different load models can be suggested for a system's demand within a definite period of time. The simplest model that can be taken for a load is to use a constant load for the whole period in question. In such conditions, the maximum load of the system is taken as the constant load. Daily peak load variation curve (DPLVC) and load duration curve (LDC) are extensively used as load models in the assessment of the efficacy of the generator units.

The DPLVC is created by arranging the individual daily peak load data, usually collected over a period of one year, in descending order. The LDC is created when the individual hourly peak loads are used, and in this case the area under the curve represents the total energy demand for the system in the given period [1]. In practice, LDC reflects the system load more completely than DPLVC.

Using the hourly load data it is possible to obtain the chronological model of the load. The amount of the load L(t) at time t can be obtained using equation (4).

$$L(t) = L_y + P_w + P_d + P_h(t) \tag{4}$$

Where L_y is the annual peak load, P_w is the percentage of weekly load in terms of the annual peak, P_d is the percentage of daily load in terms of the weekly peak load and $P_h(t)$ is the percentage of hourly load in terms of the daily peak

Using the load conditions on annual, weekly and daily bases, and making use of (4), it is possible to simulate the hourly load for one year. Given the load changes in seasons, months, days and even hours, it will be wrong to consider a fixed amount of load for all hours of a year. That is why this paper load changes in the time spans above have been taken from IEEE-RTS loads with the peak load of 2850 MW for the simulation of the load model. This paper assumes that the load will be increased in 5 percent increments per year...

D. System risk model

The system risk model is obtained by combining the generation model with the load model. Therefore, it is possible to obtain the system risk index of the system using the risk model, that is LOLE and LOEE indexes. LOLE is the number of hours or days in a year when the total power output of the system has failed to meet load demands. LOEE is the loss of energy expectation when the system has failed to meet its demand because the demand outweighs the total power

generation capacity. The load model used in sequential Monte Carlo model has been developed in hourly steps; however, it is possible to use it for even lesser time spans. LOLE and LOEE indices can be obtained using (5) and (6). Estimates of the reliability indices for a number of sample years (N) can be obtained using equations (5) and (6).

$$LOLE = \frac{1}{N}\sum_{i=1}^{N} t_i \qquad [days/year] \tag{5}$$

$$LOEE = \frac{1}{N}\sum_{i=1}^{N} e_i \qquad [MWh/year] \tag{6}$$

Where, t_i is loss of load duration in load curtailment i, e_i is energy not supplied in load curtailment i, N is total number of simulated years and n is number of load curtailments. The LOLE and LOEE present an overall status of the system's ability to estimate the power needed by the system.

E. Wind energy conversion model

Methods used for modeling Wind energy conversion model (WECS) fall into the two categories of simulating wind speed data and extraction of the energy conversion systems model. In the first step, the wind speed random variable should be recognized. This random value consists of the right model for the reflection of the status and chronological correlation for a particular geographical location. In the second step, a non-linear relation between the wind turbine generator power output and the wind speed is taken into account. This relation is obtained by using the WTG operational parameters and modeling techniques of the power curve.

E.1. Wind energy conversion model

The power output of the WTG depends on the wind speed at a certain site. The wind speed changes in time and location. Therefore wind speed at a certain hour depends also on the wind speed in previous hours. Numerous studies have been made for the purpose of planning and analyzing the reliability of the wind energy convertors or compound systems that include wind power [1-3].

Using the ARMA time series it is possible to simulate the wind speed with its seasonal or daily distribution. Therefore, this model can be used in power system reliability studies including WECS. Information on wind speed time series for a wind farm from an ARMA model at the level of (n, n-1) is obtained from (7).

$$y_t = \sum_{i=1}^{N} \varphi_i y_{i-1} + \alpha_t - \sum_{j=1}^{N-1} \varphi_j \alpha_{j-1} \tag{7}$$

Where φ_i (i=1,2,…,p) and θ_i (i=1,2,…,q) are autoregressive (AR) and moving average (MA) respectively and α_t is the white noise process with the zero mean and σ_a^2 variance (that is $\alpha_t \epsilon NID(0, \sigma_a^2)$ where NID is indicative of the independent normal distribution. The minimum squares method is used in order to estimate the amounts of p, q, ϕ_i and θ_i at ARMA (p, q) [22], and the amount of α_t is calculated from an initially guessed value. The 15-year history of wind speed at Swift Current in the Province of Saskatchewan, Canada has been used for obtaining the ARMA time series model. The information recorded goes back to the height of 10 meters, and the wind speed at this site is approximately 20 km/h. The hourly wind speed information at a 15-year sample from 1989 to 2003 has been used in modeling at ARMA time series. Using the information mentioned above, the ARMA time series for this region is calculated from (8).

$$y_t = 0.8782 y_{t-1} - 0.0061 y_{t-2} + 0.0265 y_{t-3} + \alpha_t - 0.2162 \alpha_{t-1} + 0.0091 \alpha_{t-2} \tag{8}$$
$$\alpha_t \in NID(0, 0.55792^2)$$

where y_t is the time series value of time t, α_t is the white noise process with a mean of zero and variance of 0.55792^2. The above time series model provides a logical picture of the wind regime. Using the y_t time series the wind speed for the above site can be calculated using the equation (9).

$$SW_t = \mu_t + \sigma_t . y_t \tag{9}$$

Where μ_t and σ_t are the historical hourly mean wind speed and the standard deviation of wind speed respectively for the wind sites.

E.2. WTG model

The power output of the WTG is different from that of the conventional generators. The conventional power generator units can provide a constant power output for all times. One of the most effective factors on the WTG's power output is the wind speed. There is a nonlinear relation between the power output of the WTG and wind speed that is shown by the power curve in Fig. 2.

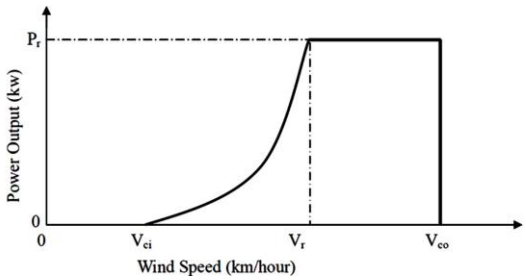

Fig. 2: Power curve of a typical WTG unit.

The relation of this curve with the power output becomes clear by describing the operational parameters of the WTG. The important parameters of this relation are: the cut-in wind speed, rated wind speed, and the cut-out wind speed. A WTG starts generating power at the cut-in wind speed. WTGs have their power output rate (P_r) between the rate speed and cut-out speed. As soon as the wind speed reaches the Cut-out speed, WTG units are shut down for safety reasons.

Equation (10) is used for the calculation of the power output of the wind turbine. This equation is the mathematical expression of the power curve. So using (10) and the simulated wind speed, it is possible to simulate the power output of the WTG.

$$P(SW_t) = \begin{cases} 0 & ,0 < SW_t \le V_{ci} \\ (A + B.SW_t + C.SW_t^2)P_r & ,V_{ci} < SW_t \le V_r \\ P_r & ,V_r < SW_t \le V_{co} \\ 0 & ,V_{co} < SW_t \le 0 \end{cases} \tag{10}$$

where P_r, V_{ci}, V_r and V_{co} are the rated power output, the cut-in wind speed, the rated wind speed and the cut-out wind speed

of the WTG respectively. The constants A, B, C are determined by V_{ci}, and V_r as expressed in (11) [5]. The cut-in, rated and cut-out wind speed values used in this paper are 14.4, 36, and 80km/hour respectively [24].

$$A=\frac{1}{(V_{ci}-V_r)^2}\left\{V_{ci}(V_{ci}+V_r)-4V_{ci}V_r\left[\frac{V_{ci}+V_r}{2V_r}\right]^3\right\},$$
$$B=\frac{1}{(V_{ci}-V_r)^2}\left\{4V_{ci}V_r\left[\frac{V_{ci}+V_r}{2V_r}\right]^3-(3V_{ci}+V_r)\right\}, \quad (11)$$
$$C=\frac{1}{(V_{ci}-V_r)^2}\left\{2-4\left[\frac{V_{ci}+V_r}{2V_r}\right]^3\right\}$$

With used equation (11), the constants A, B and C for the WTG were calculated to be equal to 0.0311, - 0.00215 and 0.0013. This paper assumes that all WTG units are the same and with the same output rate of 1MW. In a particular geographical location, each WTG has been assumed to have been subjected to the same wind regime and all WTGs have been assumed to deliver a constant power output during a certain period of time.

III. Evaluation of the Reliability of Power Systems with Wind Power and Energy Storage

A. Strategy statement

Wind penetration expressed as the ratio of the installed wind capacity relative to the system generation capacity in many power systems around the world is rapidly increasing. The output power of WTGs is widely different from that of conventional generators. The WTGs wind power is random and cannot be used as a constant source in meeting the load of the system except where it is used together with a storage facility. Different kinds of storage techniques have been proposed for the improvement of the performance of power systems. Investigating the effect of energy storage on the reliability large power systems that include a considerable portion of wind power is very important. Storage facilities are very popular and useful where the system faces difficulties in meeting the load.

The main purpose of adding storage facilities in conventional power systems that include wind power is to level out the fluctuations created by WTGs. In practice, usually, the surplus energy of conventional power sources is not stored. The model shown in Fig. 3 stores surplus energy produced by WTGs and delivers it back to the system at low powers (low winds). Energy storage facilities are located adjacent to the wind farms and are connected to the system through a connection line.

When the wind portion is relatively low with little effect on the system's performance, the priority in delivering load services is given to the wind power. In such conditions the whole wind power produced by wind farms is absorbed by the system. The ability of power systems in absorbing wind energy is reduced by the increase in the wind power portion due to the system's need for the stability of power supply. When a great portion of the system load is to be met by the wind power, the probability of system's being unstable goes up. Therefore, due to the limitations created by the system's instability, only part of the power needed by the system can be provided by the wind power. This limitation occurs when a definite percentage of the whole system load is borne by the wind power. When the sum of the wind and conventional powers is not enough to answer the system load, the stored energy is used to meet the load and supplement the system's power supply.

B. Hydro-electric units

Hydroelectric units are able to change their power output rapidly. On the other hand WTG power output is quite variable and random, and their extensive use in the system can lead to the instability of the system. Coordination between WTGs and hydroelectric units, most of the constraints of the application of wind power in the system in a continuous manner will be overcome. Limited hydroelectric units are used to investigate into the advantages of these units in terms of the reliability of power systems incorporating wind power and coordinate wind and hydroelectric powers. This paper assumes the use of two reservoirs or dams for the storage of electric power.

C. Using two water reservoirs or two consecutive dams as micro-hydroelectric power storage facilities

Here, two consecutive dams or two voluminous reservoirs are used for storage purposes. During the period when there is surplus wind energy available, this energy is stored by pumping up water to the upper reservoir to be used when there is a shortage of energy. It is assumed some of water can be added in to reservoir from rain and snow. The potential energy in the water stored in a reservoir is transformed into electrical energy by means of hydro turbines and generators.

When there is a shortage of energy, water flows from the upper reservoir to the lower reservoir and produces energy. This paper assumes 70 percent efficiency for the motor state and 80 percent efficiency for the generator state. The basic data of the project and the constrictions of the hydroelectric units are shown in Table 1.

TABLE I
MEAN VALUE OF WATER IN-FLOW

Number of hydro units		6
Maximum output capacity		62.5
Generator efficiency		0.8 p.u.
Motor efficiency		0.7 p.u.
Maximum water head (m)		180
Reservoir coefficients	a	0.00241
	b	0.111
	c	2
Maximum water volume (Mm^3)		100
Minimum water volume (Mm^3)		5
Initial water volume (Mm^3)		80
Maximum discharge rate (m^3/sec)		53
Minimum discharge rate (m^3/sec)		10.6
Maximum flow area (m^2)		1.1

D. Energy limited hydroelectric unit model

The power outputs from hydroelectric units are depending on the capacity and condition of the reservoir. The potential energy is stored in the water reservoirs and later on it is converted to the electric power by turbines. The water inflow to the upper reservoirs mainly comes from precipitation (which is largely dependent on weather conditions) and pumped from downer reservoir. Three model of weather conditions are shown in Table 1. In this paper the dry state is

default and a year is divided into 13 equal parts each 672 hours with similar weather conditions. The water in-flow data in the three weather conditions are shown in Table 2.

TABLE II
MEAN VALUE OF WATER IN-FLOW

Period	Wet (Mm^3)	Dry(Mm^3)	Normal (Mm^3)
1	20.5	12.0	12.5
2	34.0	14.5	19.5
3	46.0	23.5	30.0
4	57.0	29.0	42.0
5	31.0	14.0	20.0
6	24.0	11.0	16.0
7	18.0	8.0	12.0
8	12.0	5.0	8.0
9	12.0	5.0	8.0
10	12.0	4.0	7.0
11	18.0	8.0	10.0
12	18.0	10.0	16.0
13	28.0	12.0	18.0

The hourly water in-flow (I_i, i=1, …, 8736) into the reservoir can be obtained using (12).

$$I_i = \frac{Z_j}{672} \tag{12}$$

The amount of water spilled from reservoir (S_i) and the amount of water existing in the reservoir (V_i) in the beginning of the i^{th} hour is calculated using (13) to (15).

$$V_{pi} = V_{i-1} - R_{i-1} + I_i \tag{13}$$

$$S_i = \begin{cases} 0 & , V_{pi} \le V_{\max} \\ V_{pi} - V_{\max} & , V_{pi} > V_{\max} \end{cases} \tag{14}$$

$$V_i = \begin{cases} V_{pi} & , V_{pi} \le V_{\max} \\ V_{\max} & , V_{pi} > V_{\max} \end{cases} \tag{15}$$

where, V_{pi} is volume of the reservoir at i^{th} hour before the spillage of extra water, V_{max} is the maximum reservoir volume, R_{i-1} is the water utilized to generate electricity during $(i-1)^{th}$ hour, S_i is the water spilled during i^{th} hour.

The net head H_i of the hydro plant at hour i is then calculated using the following approximate equation (16) when V_i is greater than the minimum reservoir volume (V_{min}):

$$V_i = c + bH_i - aH_i^2 \tag{16}$$

where a, b, and c are constant coefficients of the model. When the power output from WTG and conventional units are enough to answer the system load, the hydroelectric units are not in use. In these conditions the water is stored in the reservoirs. When the power output of the other units (conventional and WTG units) are not enough to meet the load, a right number of the hydroelectric units (K_r) join the circuit to meet the load. The power output of the hydroelectric unit (P_{hi}) is obtained using (17) and (18).

$$P_{hi} = g\beta H_i Q s / 10^6 \tag{17}$$

$$Q_t = G\sqrt{2gH_i} \tag{18}$$

where, g is gravitational constant (in m/sec^2), β is overall efficiency of the hydro plant, Q is turbine discharge rate (in m^3/sec), s is specific weight of water in (10^3 kg/m^3), G is opening area of the guide for each hydro turbine in (m^2). The water used at the I^{th} hour (R_i) is calculated using (19).

$$R_i = 3600 K_r Q \tag{19}$$

The basic data of the project and the constrictions of the hydroelectric units are shown in Table 1.

IV. SIMULATION AND RESULTS

In the reliability evaluation of power systems using the SMCS in the two-state Markov model, the system's generation considers the forces outage rate and it is fully probability.

In the MCS technique, first a value with the normal distribution is selected the within the span of [0, 1]. This value shows the state of the system for the fully functional state or FOR. In this state the value thus produced is compared with FOR value and in case the value is greater than to that of FOR value, the system is in the 'Up' state, and in case the selected value is smaller than or equal to that of FOR value, the system is in the 'Down' state. This process is repeated for all of the power generator units of the system, and after the state of the whole units has been determined, the production output of all units are summed up and total generation (C_c) is delivered to the comparison section for collation. In the comparison section the total production output of the system (C_c) is compared with the system load (L) and in case the total generation does not meet the load of the system, the unmet load is calculated and the counter adds one unit to the number of hours the load has not been met. This procedure is repeated until the reliability indices used are convergent enough. As mentioned before, this trend is quite random, and is of high importance for finding a reliable answer, and for attaining this convergence in the process of simulation. Fig. 4 shows the Monte Carlo convergence process of the LOEE index for the IEEE-RTS.

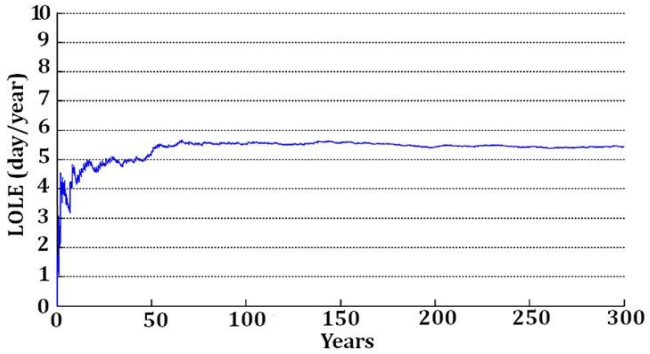

Fig. 4: convergence process of LOEE

Then, given the load growth rate of 5 percent per year, the LOLE index at each stage is calculated and compared with the reference index and wind power generation capacity and the storage needed is calculated. It has been assumed that in the fifth year, one of the conventional 400 MW generator unit and in the eighth year a conventional 350 MW generator unit will be excluded from the circuit and the power requirement will be supplied from the WTG and power storage facility. The hydraulic storage facilities store the excess wind energy at high winds and use it at low winds. Table 3 shows an example of the calculation of the wind power needed and the needed capacity of the hydraulic wind energy storage facility.

Figures 5 and 6 show the wind power needed and the storage facility, and the amount of load increments for each reduction

of conventional power reductions during the eight-year simulation period.

TABLE III
CAPACITY OF WIND POWER AND HYDRODYNAMIC STORAGE FACILITIES REQUIRED IN THE LOLE CONSTANTS TERMS IN EIGHT YEARS

Year	Base load	Conventional generation	Wind power	Hydrodynamic storage capacity	LOLE
1	2850	3405	300	0	5.68
2	2993	3405	420	100	6.06
2	2993	3405	425	107	5.8
2	2993	3405	400	111	5.72
2	2993	3405	383	114	5.69
2	2993	3405	385	114	5.68
3	3143	3405	450	130	12.56
3	3143	3405	730	200	6.12
3	3143	3405	740	205	6.01
3	3143	3405	744	210	5.69
3	3143	3405	745	211	5.67
4	3300	3405	457	150	26.43
4	3300	3405	1107	300	7.47
4	3300	3405	1157	320	6.32
4	3300	3405	1162	327	5.78
4	3300	3405	1083	332	5.68
5	3465	3005	865	597	17.34
5	3465	3005	1400	690	7.42
5	3465	3005	1420	700	6.61
5	3465	3005	1445	735	5.85
5	3465	3005	1449	740	5.67
6	3638	3005	873	607	42.29
6	3638	3005	1523	757	13.74
6	3638	3005	1823	832	8.1
6	3638	3005	1873	852	7.03
6	3638	3005	1922	884	5.68
7	3820	3005	882	617	96.79
7	3820	3005	1532	767	34.5
7	3820	3005	2182	917	12.6
7	3820	3005	2532	1012	6.74
7	3820	3005	2547	1035	5.67
8	4011	2655	1241	987	139.94
8	4011	2655	1891	1137	53.77
8	4011	2655	2541	1287	19.18
8	4011	2655	3191	1437	6.11
8	4011	2655	3160	1446	5.68

V. CONCLUSION

This paper examined the wind power and the hydraulic storage facility needed for the gradual exclusion of the conventional power generation units and annual 5 percent load increments. The simulations and calculations were carried out on the basis of the LOLE index obtained in the first stage and the amount of the wind power generation and storage were calculated and assessed on the basis of the initial LOLE index. All of the operations mentioned above were tested and the values were extracted successfully in IEEE-RTS system.

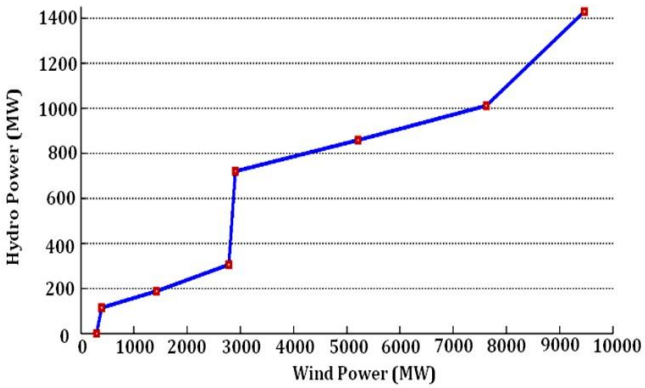

Fig. 5: required the wind power and hydrodynamic storage capacities in the LOLE constants terms

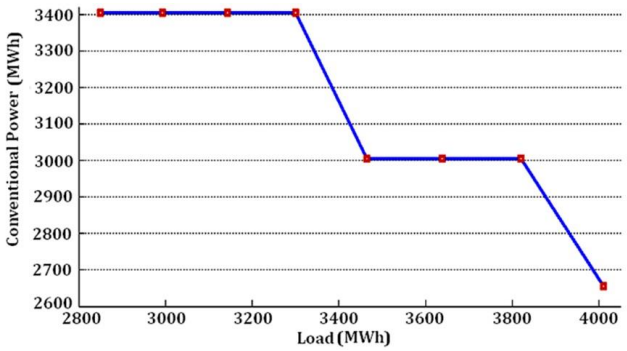

Fig. 6: process of the load growth and reduce of the conventional power in the next eight years

REFERENCES

[1] R. Billinton, H. Chen and R. Ghajar, "Time-series models for reliability evaluation of power systems including wind energy", *Microelectronics Reliability*, Vol. 36, no. 9, pp. 1253-1261, September, 1996.

[2] K. C. Chou and R. B. Corotis, "Simulation of hourly wind speed and array wind power", *Solar Energy*, Vol. 26, no. 3, pp.199-212, 1981.

[3] M. Blanchard and G. Desrochers, "Generation of auto-correlated wind speeds for wind energy conversion system studies", *Solar Energy*, Vol. 33, no. 6, pp.571-579, 1984.

[4] I. Abouzahr and R. Ramakumar, "An approach to assess the performance of utility-interactive wind electric conversion systems", *IEEE Transactions on Energy Conversion*, Vol. 6, no. 4, pp. 627-638, 1991.

[5] P. Giorsetto and K. F. Utsurogi, "Development of a new procedure for reliability modeling of wind turbine generators", *IEEE Transactions on Power Apparatus and Systems*, Vol. 102, no. 1, pp. 134-143, 1983.

[6] X. Wang, H. Dai and R. J. Thomas, "Reliability modeling of large wind farms and electric utility interface systems", *IEEE Transactions on Power Apparatus and Systems*, Vol. 103, no. 3, pp. 569-575, March, 1984.

[7] R. Karki and P. Hu, "Wind power simulation model for reliability evaluation", *Proceedings of the IEEE Canadian Conference on Electrical and Computer Engineering*, Saskatoon, May 1-4, pp. 541-544, 2005.

[8] R. Karki, P. Hu and R. Billinton, "A simplified wind power generation model for reliability evaluation", *IEEE Transactions on Energy Conversion*, Vol. 21, no. 2, pp.533 – 540, June, 2006.

[9] R. Karki, P. Hu and R. Billinton, "Reliability evaluation of a wind power delivery system using an approximate wind model", *41st International Universities Power Engineering Conference*, Newcastle, UK, September 6th-8th, 2006.

[10] W. Wangdee, "Bulk electric system reliability simulation and application", Ph. D. thesis, University of Saskatchewan, 2005.

[11] R. Karki and R, Billinton, "Maintaining supply reliability of small isolated power systems using renewable energy", *IEE Proceedings Generation, Transmission and Distribution*, Vol. 148, no. 6, pp.530 - 534, 2001.

[12] R. Karki and R. Billinton, "Cost-effective wind energy utilization for reliable power supply", *IEEE Transactions on Energy Conversion*, Vol. 19, no. 2, pp. 435-440, June, 2004.

[13] R. Billinton and G. Bai, "Generating capacity adequacy associated with wind energy", *IEEE Transactions on Energy Conversion*, Vol.19, no. 3, pp. 641-646, September, 2004.

[14] R. Billinton, H. Chen, and R. Ghajar, "A sequential simulation technique for adequacy evaluation of generating systems including wind energy", *IEEE Transactions on Energy Conversion*, Vol. 11, no. 4, pp. 728-734, December, 1996.

[15] R. Karki and R. Billinton, "Reliability/cost implications of PV and wind energy utilization in small isolated power systems", *IEEE Transactions on Energy Conversion*, Vol. 16, no. 4, pp. 368-373, December, 2001.

[16] C. Singh and A. Lago-Gonzalez, "Reliability modeling of generation systems including unconventional energy sources", *IEEE Transactions on Power Apparatus and Systems*, Vol. 104, no. 5, pp.1049-1056, May, 1985.

[17] G. Desrochers, M. Blanchard and S. Sud, "A Monte Carlo simulation method for the economic assessment of the contribution of wind energy to power systems", *IEEE Transactions on Energy Conversion*, Vol. 1, no. 4, pp. 50-56, December, 1986.

[18] A. G. Bakirtzis, "A probabilistic method for the evaluation of the reliability of stand-alone wind energy systems", *IEEE Transactions on Energy Conversion*, Vol. 7, no. 1, pp. 99-107, March, 1992.

[19] S. H. Karaki, R. B. Chedid and R. Ramadan, "Probabilistic performance assessment of wind energy conversion systems", *IEEE Transactions on Energy Conversion*, Vol. 14, no. 2, pp. 217-224, 1999.

[20] R. Billinton and R.N. Allan, "*Reliability Evaluation of Power Systems"*, 2nd Edition, Plenum Press, New York, 1996.

[21] R. Billinton and W. Li, "*Reliability Assessment of Electrical Power Systems Using Monte Carlo Methods"*, Plenum Publishing, New York, 1994.

[22] S. M. Pandit, SM. Wu, "*Time Series and System Analysis with Application"*, John Wiley & Sons, Inc, 1983.

[23] Available at: " http://www.climate.weatheroffice.gc.ca "

[24] Y. Gao, "Adequacy assessment of electric power systems incorporating wind and solar energy", M. Sc. Thesis, University of Saskatchewan, 2006.

[25] S. A. Papathanassiou, N. G. Boulaxis, "Power limitations and energy yield evaluation for wind farms operating in island systems", *Renewable Energy*, Vol. 31, no. 4, pp. 457-479, June, 2006.

[26] Po Hu, " Reliability evaluation of electric power systems including wind power and energy storage" Ph. D. thesis, University of Saskatchewan, 2009.

BIOGRAPHIES

S. Shojaiean received the B.Sc and M.S. degree from Isfahan University of Technology, Isfahan, IRAN, in 1997 and 2001 respectively and Ph.D from Islamic Azad University, science and research branch, Tehran, Iran in 2012. He is currently an assistant professor in the department of electrical engineering Khomeini-Shar branch, Islamic Azad University, Isfahan, IRAN. His research interests are nonlinear control application in power system and power system stability and reliability.

H. Akrami received the B. Sc. and M.S. degree from Islamic Azad University Khomeini-Shar branch, Isfahan, Iran in 2007 and 2011 respectively. His research interests are power system reliability and renewable energy sources.

Quasi-Resonant Full-Wave Zero-Current Switching Buck Converter Design, Simulation and Application

G. Yanik and E. Isen

***Abstract*—This paper presents a full wave quasi-resonant zero-current switching buck converter design, simulation and application. The converter control uses with zero-current switching (ZCS) technique to decrease the switching losses. Comparing to conventional buck converter, resonant buck converter includes a resonant tank equipped with resonant inductor and capacitor. The converter is analyzed in mathematical for each subintervals. Depending on the desired input and output electrical quantities, converter is designed with subinterval equations. The converter is simulated in PSIM with design parameters. The simulation results are verified with experimental setup. The converter is controlled by UC3867N integrated resonant mode power supply controller.**

Index Terms—**Buck converter, resonant converter, zero current switching,**

I. Introduction

THE switching frequency or output filter components values must be increased to improve the output performance of conventional hard switching PWM DC-DC converters. Increased switching frequency causes increase in switching losses and electromagnetic noise. Furthermore, more losses cause warming problems, thus bigger heat sink or higher current capacity switching device usage is needed. To solve the problems occurs during switching zero-current switching (ZCS) and zero-voltage switching (ZVS) techniques have been improved [1]-[3]. Using a series connected inductor and a parallel connected capacitor to switching device ZCS and ZVS techniques can be applied [4]. In addition, these soft switching techniques can be applied with resonant circuits [5]. The switch current is decreased to zero with resonant, and then switching signal is off to turn-off the switching device. Thus, switching loss could be significantly decreased with ZCS. In ZVS technique, the voltage on the switch is forced to be zero with resonant before turn-on. When the current decreases to zero, switching signal is applied to turn-on the switch. Hence, the loss occurs during the turn-on greatly decreased [6].

G. YANIK, is with the Electrical Engineering Department, Electrical & Electronics Faculty, Yildiz Technical University, Istanbul, 34220, TURKEY. (e-mail: gyanik@yildiz.edu.tr).

E. ISEN, is with the Electrical & Electronics Engineering Department, Engineering Faculty, Kirklareli University, Kirklareli, TURKEY. (e-mail: evren.isen@kirklareli.edu.tr).

Soft switching techniques are mostly used in DC-DC converters, such as buck converter, boost converter [7],[8]. The placed resonant circuit between output filter and input source is utilized to force the current and voltage to become zero. The resonant circuits are classified in three categories, conventional, quasi-resonant and multi-resonant.

Quasi-resonant converters can be performed as half-wave [9] and full-wave [10]. Considering the quasi-resonant buck converter, conventional buck converter can be worked with resonant by connecting a series inductor to the switch utilized in the input and a parallel capacitor to the output diode. While a unidirectional switching device is used in half-wave quasi-resonant converter, bidirectional switching device is used in full-wave quasi-resonant converter. Operating principle is the same for both converters. However, reverse inductor current can flow through the anti-parallel diode of switch, thus resonant interval increases. Therefore, this condition lets resonant energy be transferred back to input source in low load operating, and the dependence of output voltage to the load decreases. As a result, use of quasi-resonant converter instead of conventional DC-DC converter provides low switching losses, high efficiency, ability of working in higher frequencies, low EMI and low value of output filter elements.

In this study, 60 W quasi-resonant full-wave (QRFW) zero-current switching (ZCS) buck converter is analyzed, simulated and implemented. Operating intervals of the converter are examined, circuit equations for each interval are derived and circuit parameters are calculated. The converter is simulated with calculated parameters and the simulation results are verified with experimental results.

II. Series Resonant Circuits

In this section, operating principle of series resonant circuits is explained to understand quasi-resonant full-wave converter operating. As shown in Fig. 1, series resonant circuit includes series connected an inductor and a capacitor. When the input voltage is applied to resonant circuit, a resonant occurs between these resonant elements. Circuit equations during the resonant are given in (1)-(3) and waveforms are shown Fig. 2.

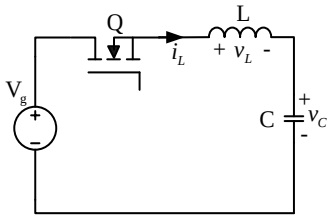

Fig. 1. Series resonant circuit

$$i_L = I_{L0}\cos\omega t + \frac{V_g - V_{C0}}{Z}\sin\omega t \quad (1)$$

$$V_L = (V_g - V_{C0})\cos\omega t - ZI\sin\omega t \quad (2)$$

$$V_C = -(V_g - V_{C0})\cos\omega t + ZI_{L0}\sin\omega t + V_g \quad (3)$$

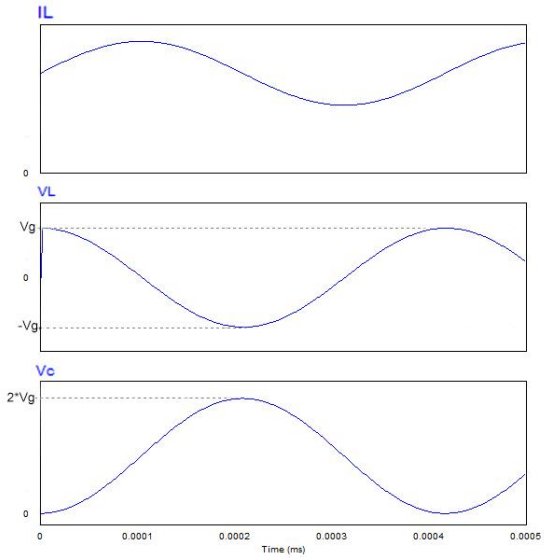

Fig. 2. Series resonant circuit waveforms

III. THEORETICAL ANALYSIS

QRFW buck converter is a special version of the traditional buck converter that uses resonant intervals to ensure soft switching of the semiconductor device. In this section, operation principle of the QRFW buck converter that is shown in Fig. 3 along with subintervals of the converter will be analyzed.

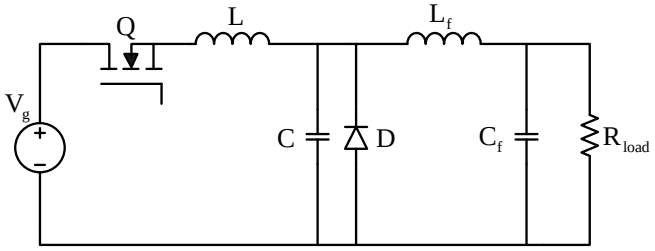

Fig. 3. Full Wave Quasi Resonant Buck Converter Topology

Before subinterval 1, converter is assumed to be working in steady state. Inductor current and output voltage are set to nominal values. The output diode D conducts the filter inductor current I_{Lr}. Filter inductor is assumed to be so large that output current I_{Lf} is constant during one switching cycle. Subinterval 1 starts with the signal applied to the switch Q.

A. Subinterval 1

The switch Q turns on and input voltage V_g is applied to the resonant inductor L. Therefore, resonant inductor current rises linearly, with the slope of V_g/L and diode current decreases from I_{Lf} to zero, with the same slope. Switch current increases linearly with a slightly slow slope, therefore ZCS turn on of the switch is provided. Fig. 4 shows the subcircuit in this interval.

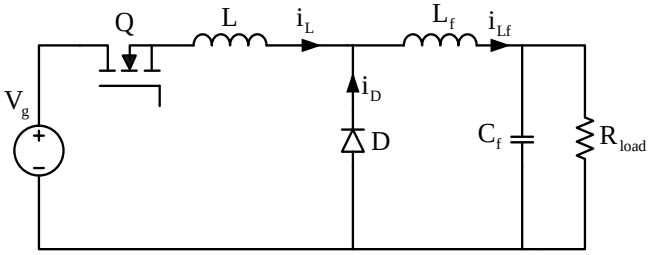

Fig. 4. Subcircuit in subinterval 1

$$I_L = \frac{V_g}{L}t \quad (4)$$

$$V_C = 0 \quad (5)$$

When resonant inductor current reaches to I_{Lf} and the diode turns off, this interval ends.

B. Subinterval 2

Fig. 5 shows the subcircuit in this interval. In the input side of the converter, a series resonant tank occurs where L and C are the resonant elements.

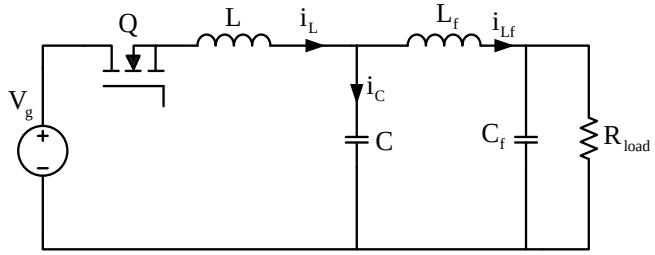

Fig. 5. Subcircuit in subinterval 2

Resonant inductor has initial current I_{Lf} and inductor current continues to increase in sinusoidal. Resonant capacitor voltage also starts to increase, simultaneously. Related state equations can be calculated from (1) and (3).

$$I_L = I_{L0} + \frac{V_g}{Z}\sin\omega t \quad (6)$$

$$V_C = V_g - V_g\cos\omega t \quad (7)$$

When inductor current decreases to zero, this interval ends.

C. Subinterval 3

Fig. 6 shows subcircuit in this interval. As it is seen in the figure, the subcircuit is the same with the previous subinterval but resonant inductor and resonant capacitor currents are reversed.

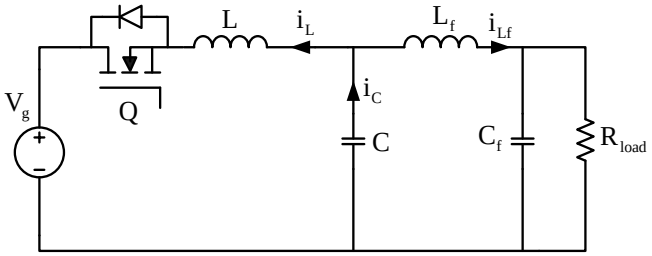

Fig. 6. Subcircuit in subinterval 3

In the beginning of this interval, a negative ringing between resonant elements starts. Resonant current flows through the body diode of the switch. This is the ZCS interval where control signal applied to the switch must be cut off to ensure turn the switch off with ZCS. State equations of the resonant elements are the same with the previous one and given below.

$$I_L = I_{Lf} + \frac{V_g}{Z}\sin \omega t \tag{8}$$

$$V_C = V_g - V_g \cos \omega t \tag{9}$$

This interval ends when resonant current reaches to zero.

D. Subinterval 4

The subcircuit of this interval is shown in Fig. 7. At the start of this interval, resonant capacitor is not discharged completely therefore, output current I_{Lf} flows through resonant capacitor, discharging it linearly with the slope of I_{Lf}/C.

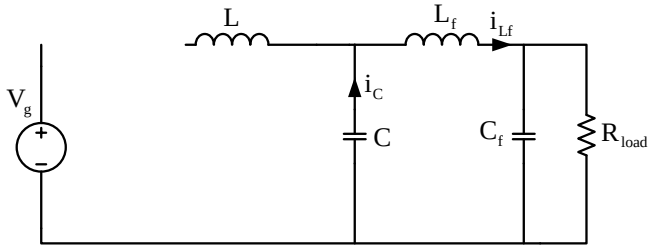

Fig. 7. Subcircuit in subinterval 4

State equations of the resonant elements are given below.

$$I_L = 0 \tag{10}$$

$$V_C = \frac{I_{Lf}}{C} \tag{11}$$

This interval ends when capacitor voltage decreases to zero and output diode turns on.

E. Subinterval 5

When capacitor voltage decreases to zero, output inductor current turns on the diode. Corresponding subcircuit is shown in Fig. 8. This subinterval is the off state of the traditional converter. Output current is conducted by the diode and this interval ends when the switch is back on. Unlike the traditional buck converter, this subinterval is the control interval. In the traditional buck converter, duration of the on state of the switch controls output voltage. In QRFW buck converter, off stage duration is adjusted to control the output voltage. Therefore, the on time of the switch is constant and defined by the resonant elements.

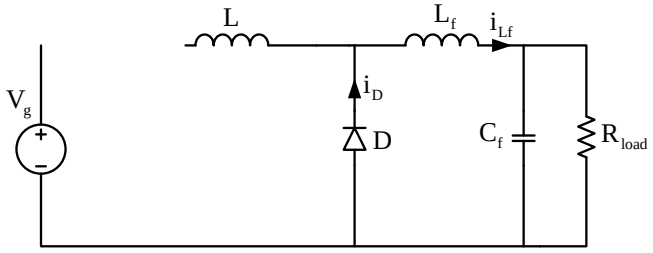

Fig. 8. Subcircuit in subinterval 5

Theoretical waveforms of the resonant tank are shown in Fig. 9.

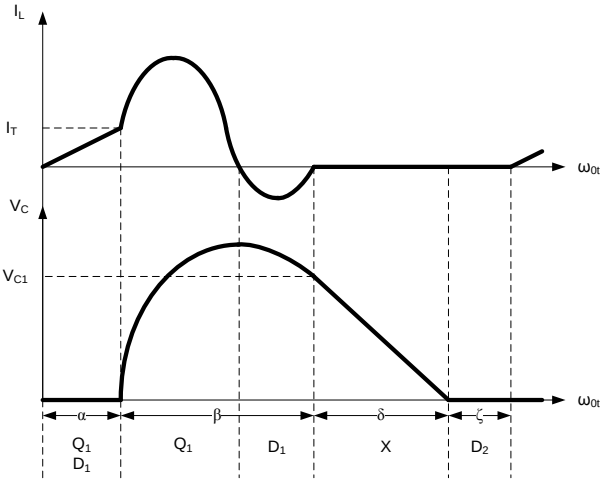

Fig. 9. Theoretical waveforms of the resonant tank

IV. Design Consideration

To design any SMPS circuit, output power, input and output voltages and switching frequency must be considered. These parameters of the designed converter are shown in TABLE I.

TABLE I
DESIGN CONSIDERATION

Symbol	Quantity	Value
P_0	Output power	60 W
V_g	Input voltage	48 V
V_0	Output voltage	12 V
f_s	Switching frequency	200 kHz

In a QR converter, values of the resonant elements are crucial for the operation. In this section, selections of the resonant elements are explained.

In the second interval of the converter, a series resonant circuit tank, loaded with a current source, occurs as shown in Fig. 10.

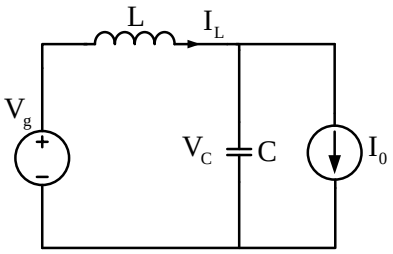

Fig. 10. Series resonant tank loaded with constant current source

In this resonant circuit, resonant inductor current is calculated as below.

$$I_L = I_O + \frac{V_g}{\sqrt{\frac{L}{C}}}\sin \omega t \tag{12}$$

In a QRFW buck converter, current source value must be lower than resonant current peak level to ensure negative ringing, where switch signal will be cut off. Output current is selected as 5 Amps due to the output power and voltage. Therefore, resonant tank current must be greater than 5.

$$I_{Lres(peak)} > 5 \tag{13}$$

$$I_O = \frac{V_g}{\sqrt{\frac{L}{C}}}\sin \omega t \Rightarrow 5 = \frac{12}{\sqrt{\frac{L}{C}}};\quad \sqrt{\frac{L}{C}} > 2.4 \tag{14}$$

Conversation ratio of the QRFW buck converter is as given below.

$$V_o = FV_g = \frac{f_s}{f_o}V_g \tag{15}$$

For the minimum load, the switching frequency is selected 200 kHz. Therefore,

$$\frac{12}{48} = 200000 \cdot 2\pi\sqrt{LC} \Rightarrow \sqrt{LC} = 198 \cdot 10^{-9} \tag{16}$$

Depending on the (14) and (16), calculated resonant elements are given TABLE II.

TABLE II
RESONANT ELEMENTS

Quantity	Value
Resonant inductor	0.85 µH
Resonant capacitor	47 nF

V. SIMULATION STUDY

Simulation study of the designed converter has been performed in PSIM simulation software. Fig. 11 shows the simulation circuit.

For the closed loop operation, a voltage controlled oscillator is needed to control circuit but this type of a control block is not present in software library. To obtain close loop operation

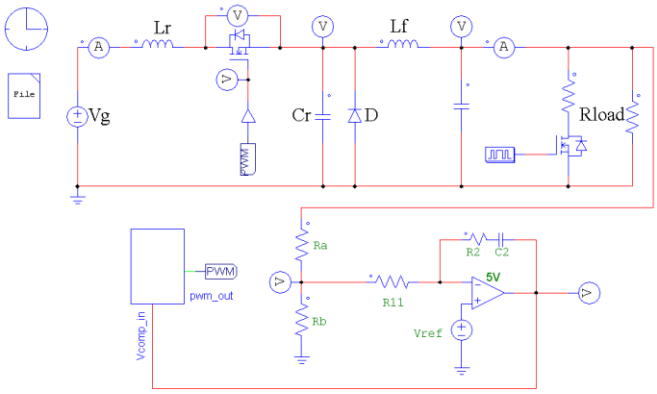

Fig. 11. Simulation circuit

result in simulation, this type of controlled must be designed.

In the designed controller, principle of a capacitor's linear charging with a constant current is used. The capacitor is charged with a constant current source. Then, when the capacitor voltage exceeded a pre-defined limit, another current source starts to discharge capacitor and so capacitor voltage decreases linearly. Second current source is a voltage controlled current source so that a compensating voltage in the output of the closed loop error amplifier will be controlling discharge current of the capacitor.

If the voltage on the capacitor is compared with a constant DC voltage, a desired PWM will be obtained. Frequency of this PWM can be controlled with discharge current. In a ZCSHW buck converter, a frequency controlled fixed on time PWM signal is needed to control output voltage. Although variable frequency is obtained by the described method, on time of the controlled is still varies along frequency. Fig. 12 shows capacitor voltage with reference voltage and PWM signal. As shown in figure, only positive slope of the triangular capacitor voltage must be compared with reference voltage.

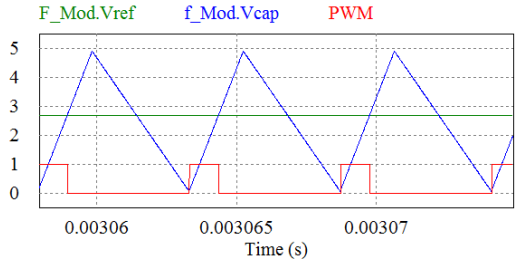

Fig. 12. Controlled capacitor voltage with reference voltage and PWM signal

To compare reference voltage with positive slope only, positive slope on the capacitor voltage must be detected. Derivative of the capacitor voltage will give the slope value. If the derivative of the capacitor voltage is positive, this means capacitor is charging. To use only sign not the value of this derivative, upper and lower limit block is used. Positive derivative gives high signal, and negative derivative gives low signal. The reference and capacitor voltage are compared, and so a signal is generated when reference is higher than capacitor voltage. The output signal is generated with given to AND integrated circuit of obtained signal and a signal of derivative slope. As a result, a fixed on time and variable

frequency PWM signal is obtained where frequency of the signal is controlled with input voltage.

Resonant tank waveforms obtained from simulation study is shown in Fig. 13. Obtained waveforms are completely matching the theoretical analysis.

MOSFET drain source voltage versus drain current which is equal to resonant inductor current is shown in Fig. 14. In the turn-on process of the MOSFET, collision between this current and voltage is very small due to series inductor; hence turn-on switching losses are very small. In the turn-off process of the MOSFET, there are no collisions between voltage and current, so switching loss at turn off process is zero.

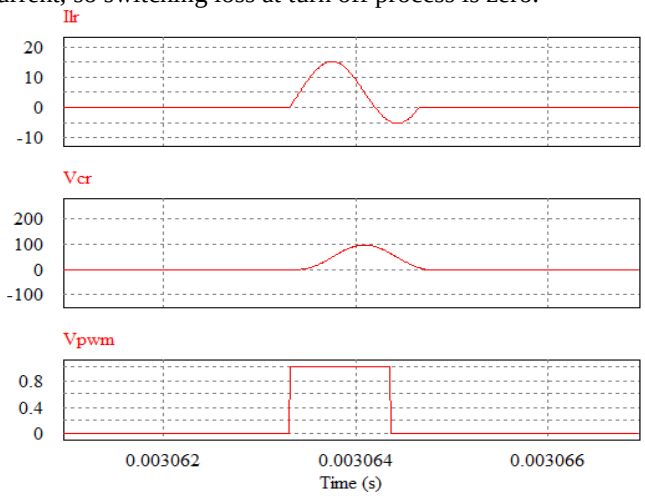

Fig. 13. Resonant tank waveforms and corresponding control signal

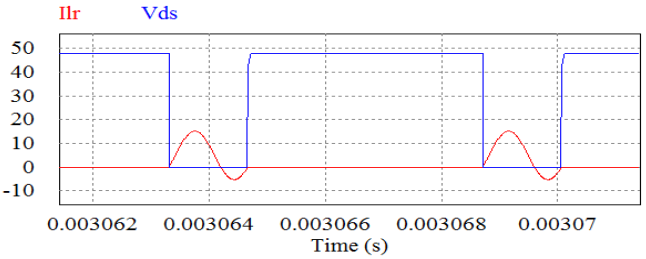

Fig. 14. MOSFET voltage versus MOSFET current

Fig. 15 shows compensated output voltage corresponding to change in output current. As can be seen in the figure, whenever output current changes from half load to full load or from full load to half load, output voltage is settles back the desired value after a small drop or a small overshoot.

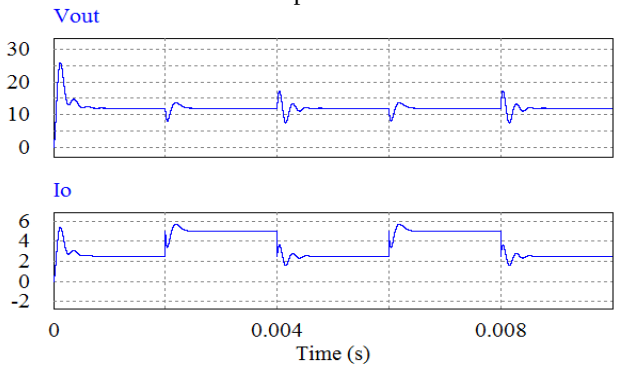

Fig. 15. Output voltage corresponding to step change in output current

VI. Experimental Results

In this section experimental results are given and discussed. Fig. 16 shows oscilloscope plot of the inductor current and V_{DS} voltage on MOSFET. A very high frequency ringing on MOSFET voltage can be seen in the plot. This ringing occurs when MOSFET turns off due to the resonant between MOSFET's parasitic capacitor and resonant inductor. Resonant inductor current increases further than expected in positive direction after negative ringing in resonant tank.

To prevent this parasitic ringing, a RC snubber is added to the circuit. Fig. 17 shows the inductor current and V_{DS} voltage on MOSFET after the RC snubber. As it is seen in the figure, the parasitic ringing is eliminated with the RC snubber. Resonant inductor current, capacitor voltage and MOSFET gate signal is shown in Fig. 18.

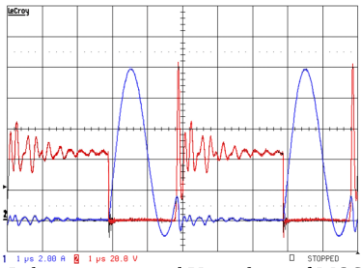

Fig. 16. Inductor current and V_{DS} voltage of MOSFET

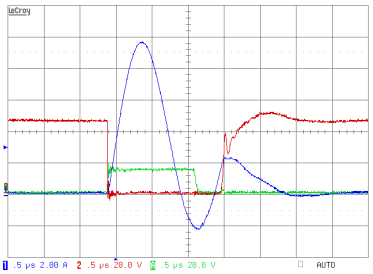

Fig. 17. Inductor current, V_{DS} voltage after the RC snubber and MOSFET gate signal

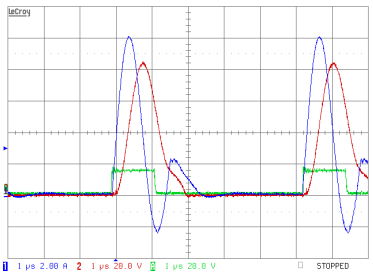

Fig. 18. Resonant capacitor voltage, resonant inductor current and MOSFET gate signal

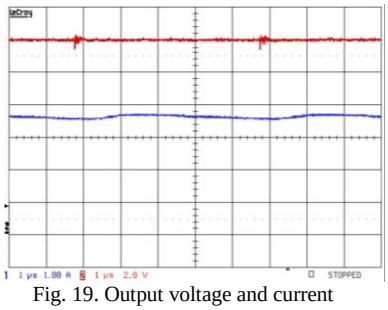

Fig. 19. Output voltage and current

Output voltage and current for open loop operation can be seen in Fig. 19. Closed loop operation of the converter for a positive step in the output current is shown in Fig. 20. After output current rises from half load to full load, output voltage drops for a short time and settles back to desired level. Output voltage response to a negative step in output current is shown in Fig. 21. Output voltage overshoots for a short period of time then settles back to desired level after change in the output current.

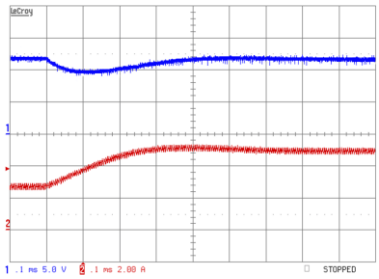

Fig. 20. Output voltage corresponding to positive step in output current

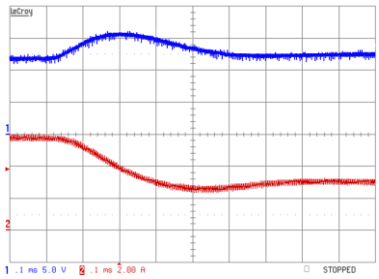

Fig. 21. Output voltage corresponding to negative step in output current

Change in the resonant inductor current for a positive step in output current is shown in Fig. 22 and for a negative step in output current is shown in Fig. 23.

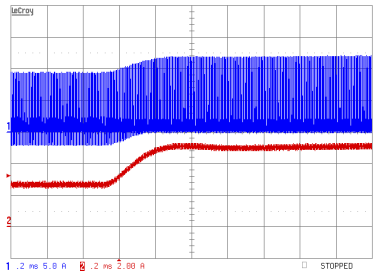

Fig. 22. Resonant inductor current change corresponding to positive step in output current

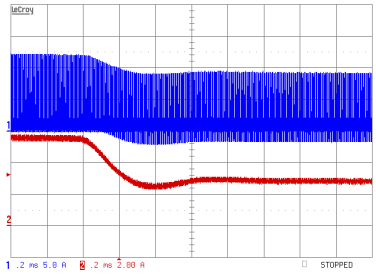

Fig. 23. Resonant inductor current change corresponding to negative step in output current

VII. CONCLUSION

In this study, a 60 W quasi-resonant full-wave zero-current switching buck converter design, simulation and experimental results are given. Although all unwanted parasitic effects on waveforms, desired result is obtained with the experimental setup. Output voltage can be controlled with switching frequency and a well filtered DC voltage with desired value can be obtained in output. Converter can regulate output voltage when the load current changes. Measured efficiency of the experimental setup is around %85. Resonant elements are crucial for a quasi-resonant converter. For a switching frequency around 200 kHz, resonant tank elements are very small, and so it is very hard to measure these elements with a LCR meter. Measurement error and a small change in this element's values, due to the external factors such as temperature, may cause major problems in operation of the converter. PCB design of such a converter has a major effect in operation. High frequency effects on every element must be considered during PCB design process. An air inductor is used for the resonant inductor. Although expected result has been obtained, the effects of an air inductor, such as EMI, should be investigated.

REFERENCES

[1] Y.C. Chuang, Y.L. Ke, H.S. Chuang and Y.S. Wang, "A Novel Single-Switch Resonant Power Converter for Renewable Energy Generation Applications", Industrial & Commercial Power Systems Technical Conf., May, 2013, pp. 1-9.

[2] C.J. Tseng and C.L. Chen, "Novel ZVT-PWM converters with active snubbers", IEEE Trans. on Power Electronics, Vol. 13, Iss. 5, pp. 861-869, 1998.

[3] D.S. Gautam and A.K.S. Bhat, "A Comparison of Soft-Switched DC-to-DC Converters for Electrolyzer Application", Vol. 28, No. 1, pp. 54-63, 2013.

[4] I.H. Baciu and S. Lungu, "Resonance in Power Converters Circuits", IEEE 18th Int. Symp. For Design and Tech. in Electronic Packing, Oct. 2012, pp. 183-187.

[5] S. Urgun, "Zero-voltage transition-zero-current transition pulsewidth modulation DC-DC buck converter with zero-voltage switching-zero-current switching auxiliary circuit", IET Power Electronics, Vol. 5, Iss. 5, pp. 627-634, 2012.

[6] E. Jayashree and G. Uma, "Analysis, design and implementation of a quasi-resonant DC-DC converter", IET Power Electronics, Vol. 4, Iss. 7, pp. 785-792, 2011.

[7] T. Mishima and M. Nakaoka, "A Practical ZCS-PWM Boost DC-DC Converter With Clamping Diode-Assisted Active Edge-Resonant Cell and Its Extended Topologies", IEEE Trans. on Industrial Electronics, Vol. 60, No. 6, pp. 2225-2236., 2013.

[8] L. Jiang, C.C. Mi, S. Li, C. Yin and J. Li, "An Improved Soft-Switching Buck Converter With Coupled Inductor", Vol. 28, No. 11, pp. 4885-4891, 2013.

[9] N.N. Goryashin and A.S. Solomatova, "Analysis of MOSFET Operating in Half-Wave Zero-current Switching Quasi-resonant Converter", XIII Int. Conf. and Seminar on Micro/Nanotechnologies and Electron Devices, July 2012, pp. 333-337.

[10] R.W. Erickson and D. Maksimovic, "Fundamentals of Power Electronics", Springer Press, 1997.

G. YANIK was born in Istanbul, Turkey, in 1985. He received his B.S. and M.S. degrees in Electrical Engineering at Yildiz Technical University, Istanbul, in 2008 and 2011, respectively.
He is a Research Assistant in the Department of Electrical Engineering, Yildiz Technical University since 2008. His research interests include DC-DC converters, soft-switching techniques, power factor correction and inductor design.

E. ISEN was born in Bandırma, Turkey, in 1981. He received his B.S., M.S. and Ph.D. degrees in electrical engineering at Yildiz Technical University, Istanbul, in 2003, 2005 and 2012, respectively.
He was a Research Assistant in the Department of Electrical Engineering, Yildiz Technical University between 2005 and 2012. He is an Assistant Professor in the Department of Electrical and Electronics Engineering, Kirklareli University. His current research interests include grid connected inverters, renewable energy conversion systems and power electronics.

Power System Stabilizer Based on Global Fuzzy Sliding Mode Control

E. Nechadi and M.N. Harmas

***Abstract*—Power systems stability is enhanced through a novel stabiliser developed around a fuzzy sliding mode approach. First, sliding mode control is applied to selected operating point based models of a power system separately then fuzzy logic is used to form a global model encompassing the separate subsystems, thus leading to a fuzzy sliding mode power system control. Stability is insured through Lyapunov synthesis. Severe operating conditions are used in a simulation study to test the validity of the proposed method, indicating better performance and satisfactory transient dynamic behaviour.**

Index Terms—**Power system stabiliser; sliding mode control; sliding surface; fuzzy sliding mode; Lyapunov stability.**

I. INTRODUCTION

THE need for more reliable power margins and less amount of electro-mechanical oscillations that limit power flow in complex power systems, has imposed the addition of stabilizers coined power system stabilizer PSS as early as the mid 40s, nowadays tagged conventional, classical stabilisers or CPSS[1-3]. Highly non linear, time varying, power systems have been and remain a major challenge to control and power engineers alike.

Effectively, power systems are complex nonlinear systems that often exhibit low frequency oscillations due to insufficient damping caused by adverse operating conditions which can lead the underlying machine to lose synchronism. Power system stabilizers are used to suppress these oscillations and improve the overall stability. Conventional stabilizers, consisting of cascade connected lead–lag compensators derived from a linear model representing the power system at a certain operating point, have long been used to damp oscillations regardless of the varying loading conditions or disturbances. However, this linear model based control strategies often fail to provide satisfactory results over a wide range of operating conditions.

Many alternatives have been put forth since pioneering CPSS not only in stabilizer design but in power model elaboration as well. Further research work led to more appropriate adaptive approaches as in [4-6]. Robust control techniques have been also suggested in effort to circumvent parameters uncertainties effect as well as exogenous disturbances leading to sliding mode based PSS [7-10] and Hinf PSS [11].

E. Nechadi is with the Electrical Engineering Department, Ferhat Abbas University of Sétif, Algeria, (e-mail: nechadiamira@yahoo.fr).

M. N. Harmas is with the Electrical Engineering Department, Ferhat Abbas University of Sétif, Algeria, (e-mail: mharmas@yahoo.fr).

Remarkable research effort has been done in the last decade putting forward intelligent fuzzy logic based PSS as well as optimality in adapting to changing operating conditions as in [12-17].Amid the many interesting schemes suggested, the combination of sliding mode technique and the fuzzy approach capitalising on the free model aspect of the latter and the robustness of the first seem to be promising. Based on work developed by Yu [18] we have elaborated a power system stabilizer using fuzzy logic to amalgamate several sliding mode controlled based linear power system models, obtained for selected operating points.

This paper introduces briefly in the next section the sliding mode control approach used, followed by the third section in which Takagi-Sugeno fuzzy technique is tackled. In section IV the design of the global fuzzy sliding mode stabilizer is undertaken and stability issue addressed. The power system model is presented in the ensuing section followed by simulation and a presentation of results for different operating conditions.

II. SLIDING MODE CONTROL

Sliding mode control is a part of the theory of Variable Structure Control (VSC) which is a control technique relying on a practical high-speed switching between different configurations basically inspired by relay control theory. This variable structure control provides an efficient method for nonlinear plants control.

Reluctant at first, control engineers have shown increased interest in variable structure control as advances in electronic circuitry and computer technology took place making feasible many practical implementations such as in robotics[19-20],or in power system control as in[11,21].

Essentially, VSC utilizes a high-speed switching control law to drive the nonlinear plant's state trajectory onto a selected designer chosen sliding surface in the state space and to maintain plant's state trajectories on this surface for all subsequent time. The plant dynamics restricted to this surface represent the controlled system's behaviour.

Consider a SISO dynamical system described by:

$$\dot{x}(t) = Ax(t) + Bu(t), \tag{1}$$

where $x(t)$ is the state vector, $A \in R^{nxn}$, $B \in R^{nxq}$ and $u(t)$ is the sliding mode control input.

Sliding mode control design comprises two phases: first a switching surface imposing desired dynamics in the sliding mode is elaborated, followed by the design of the

discontinuous control law that drives the system state trajectories towards the switching surface. The switching surface is generally defined as:

$$s(x) = Cx(t) \tag{2}$$

C is the sliding vector, which can be determined using different available techniques, we will use pole placement in the sliding phase according to Ackerman's approach [22].
Control law enabling satisfaction of the attraction phase condition (3) and the equivalent control to maintain state trajectories on the sliding surface is typically given by (4) assuming (CB) is non-singular.

$$s(x)\dot{s}(x) \prec 0 \tag{3}$$

$$u = -(CB)^{-1}\left[CAx + k sign(s)\|x\|\right] \; ; k \succ 0 \tag{4}$$

$\|.\|$ indicates the euclidean norm, used here to reduce chattering when approaching the equilibrium point.
Bbackground details for sliding mode theory and sliding surface design can be found in [22-24].

III. Design of fuzzy control

In our control design procedure, a Takagi-Sugeno fuzzy model is used to represent a global model of the underlying non linear plant. The fuzzy model described by fuzzy IF-THEN rules represents local linear input-output relations of the considered nonlinear system. The main feature of a Takagi-Sugeno fuzzy model is to express the local dynamics of each fuzzy implication (rule) by a linear system model.
The global fuzzy model of the system is achieved by fuzzy ''blending'' the operating point based linear system models [18, 19].
The i^{th} rule of the T-S fuzzy models is of the following form:
Rule i:
IF $z_1(t)$ is F_{i1} AND… $z_p(t)$ is F_{ip}, THEN

$$\dot{x}(t) = A_i x(t) + B_i u(t),\; y(t) = D_i x(t) + E_i u(t),\; i = 1,2,3,...,m \tag{5}$$

where, F_{ip} is the fuzzy set and m is the number of model rules, $x(t)$, $u(t)$, $y(t)$ are respectively the state, the input and the output vectors, $A_i \in R^{nxn}$, $B_i \in R^{nxq}$, $D_i \in R^{pxn}$, $E_i \in R^{nxp}$ and $z_1(t),...z_p(t)$ are known premise variables that may be functions of the state variables, external disturbances and time. We will use $z(t)$ to denote the vector containing all the individual elements $z_1(t),...z_p(t)$. Each linear consequent equation represent a called a subsystem.
Let $\mu_i(z(t))$ denote the normalized fuzzy membership function of the inferred fuzzy set F_i where

$$F_i = \bigcap_{j=1}^{p} F_{ij} \quad \text{and} \quad \sum_{i=1}^{m} \mu_i = 1. \tag{6}$$

The global fuzzy state space model is given by:

$$\dot{x}(t) = Ax(t) + Bu(t),$$
$$y = Dx(t) + Eu(t) \tag{7}$$

Where

$$A = \sum_{i=1}^{m} \mu_i A_i \;, \qquad B = \sum_{i=1}^{m} \mu_i B_i \,,$$
$$D = \sum_{i=1}^{m} \mu_i D_i \;, \qquad E = \sum_{i=1}^{m} \mu_i E_i \tag{8}$$

Let us make the assumption that *(A, B)* of the global system is completely controllable based on the assumed controllability if each subsystem.

IV. Design of fuzzy sliding mode control

In their paper X. Yu & al. [18] used a constant sliding surface to developed their remarkable results that we revisit here with our contribution being the use of different sliding surfaces corresponding to different operating points that our application requires, a power system, in order to uphold the desired poles placement. The main drawback in such a system resides in the necessity for a new sliding manifold for each new configuration in order to enable the same pole placement and thus identical dynamic performances.

Theorem 1: Each subsystem of the fuzzy model (5) if we choose the following control u^i law,

$$u^i = -(C_i B_i)^{-1}\left[C_i A_i x + k_i sign(s_i)\|x\|\right] \tag{9}$$

then the system is asymptotically stable.

Proof:
Let the Lyapunov function candidate be given as,

$$V(x) = \frac{1}{2} s_i^T(x) s_i(x) \tag{10}$$

Therefore:

$$\dot{V} = s_i^T(x)\dot{s}_i(x)$$
$$= s_i^T(x)C_i(A_i x + B_i u^i)$$
$$= -k_i s_i^T(x) sign(s_i)\|x\|$$

and thus: $\dot{V} < 0$

Theorem 2: For the fuzzy system (7), if we choose the following control law for ith subsystem u^i:

$$u^i = -(C_i B_i)^{-1}\left[C_i A_i x + k_i sign(s_i)\|x\|\right] \tag{11}$$

and if

$$C_j B_i = C_i B_i \,, sign(s_i) = sign(s_j) \;\; i \neq j \tag{12}$$

Then the system is asymptotically stable.

Proof:
Choosing the Lyapunov function candidate to be

$$V(x) = \frac{1}{2} s^T(x) s(x), \tag{13}$$

and the control law term (14) given here will be designated approach (1)

$$u = \sum_{i=1}^{m} \mu_i u^i \text{ , (1) approach} \quad (14)$$

Therefore,

$$\begin{aligned}\dot{V} &= s^T(x)\dot{s}(x)\\ &= s^T(x)C(Ax+Bu)\\ &= s^T(x)(C\sum_{i=1}^{m}\mu_i A_i x + C\sum_{i=1}^{m}\mu_i B_i u)\\ &= s^T(x)(C\sum_{i=1}^{m}\mu_i A_i x + CB\sum_{i=1}^{m}\mu_i u^i)\\ &= s^T(x)\sum_{i=1}^{m}\mu_i(CA_i x + CB_i u^i)\\ &= -s^T(x)\sum_{i=1}^{m}\mu_i k_i sign(s_i)\|x\|\\ &= -\sum_{i=1}^{m}\mu_i k_i s_i sign(s_i)\|x\|\end{aligned}$$

$\dot{V} < 0$.

Theorem 3: For the global fuzzy system (7), if we choose the following control u^k for another rule k ($i \neq k$)

$$u^k = -(C_k B_k)^{-1}\left[C_k A_k x + k_k sign(s_k)\|x\|\right] \quad (15)$$

and if

$$k_k > k_k^0 = \frac{\left\|CA_i - CB_i(C_k B_k)^{-1}C_k A_k\right\|}{\lambda_{min}(CB_i(C_k B_k)^{-1} + (CB_i(C_k B_k)^{-1})^T)},$$
$$\lambda_{min}(CB_i(C_k B_k)^{-1} + (CB_i(C_k B_k)^{-1})^T)sign(s_k) > 0 \quad (16)$$

Then the system is asymptotically stable.

Proof:
Choosing the Lyapunov function candidate:

$$V(x) = \frac{1}{2}s^T(x)s(x)$$

Therefore

$$\begin{aligned}\dot{V} &= s^T(x)\dot{s}(x)\\ &= s^T(x)C(Ax+Bu)\\ &= s^T(x)(C\sum_{i=1}^{m}\mu_i A_i x + C\sum_{i=1}^{m}\mu_i B_i u^k)\\ &= s^T(x)C(\sum_{i=1}^{m}\mu_i A_i x + \sum_{i=1}^{m}\mu_i B_i\\ &\qquad (-(C_k B_k)^{-1}\left[C_k A_k x + k_k sign(s_k)\|x\|\right]))\\ &= s^T(x)\sum_{i=1}^{m}\mu_i((CA_i - CB_i(C_k B_k)^{-1}C_k A_k)x\\ &\qquad - CB_i(C_k B_k)^{-1}k_k sign(s_k)\|x\|)\\ &\le \sum_{i=1}^{m}\mu_i(\left\|CA_i - CB_i(C_k B_k)^{-1}C_k A_k\right\|\|s\|\|x\|\\ &\qquad - \lambda_{\min}(CB_i(C_k B_k)^{-1} + (CB_i(C_k B_k)^{-1})^T)k_k\|s\|\|x\|)\end{aligned}$$

$\dot{V} < 0$.

Theorem 4: For the global fuzzy system (7), if we choose the global control u law which will be termed approach (2)

$$u = -(CB)^{-1}\left[CAx + ksign(s)\|x\|\right] \text{ (2) approach} \quad (17)$$

Where

$$A = \sum_{i=1}^{m}\mu_i A_i, \quad B = \sum_{i=1}^{m}\mu_i B_i,$$
$$C = \sum_{i=1}^{m}\mu_i C_i, \; s(x) = Cx(t) \quad (18)$$

then the system is asymptotically stable.
Hence, we can write

$$C = \theta^T\xi(x) \quad (19)$$

Where $\theta = [\theta_1, \theta_2, \ldots \theta_m]$ is the vector of parameters, $\xi = [\xi_1, \xi_2, \ldots \xi_m]^T$ is the vector of fuzzy basis functions with θ being bounded: $\|\theta\| \le M_\theta$.
If we let:

$$\dot{\theta} = -\gamma s(x)\xi(x) \quad (20)$$

Where

$$\gamma = \frac{M_\theta}{\|s\|\,\xi(x)\|x\|} \quad (21)$$

Where M_θ and γ are positive constants.

Proof:
Considering the Lyapunov function candidate:

$$V(x) = \frac{1}{2}s^T(x)s(x) + \frac{1}{2\gamma}\theta^T\theta$$

Therefore

$$\begin{aligned}\dot{V} &= s^T(x)\dot{s}(x) + \frac{1}{\gamma}\theta\dot{\theta}\\ &= s^T(x)\left(C(Ax+Bu) + \dot{\theta}\xi(x)x\right) + \frac{1}{\gamma}\theta\dot{\theta}\\ &= s^T(x)\sum_{i=1}^{m}\mu_i C_i\left(\sum_{i=1}^{m}\mu_i A_i x + \sum_{i=1}^{m}\mu_i B_i\left(-(CB)^{-1}\left[CAx + ksign(s)\|x\|\right]\right)\right)\\ &\qquad + s^T(x)\dot{\theta}\xi(x)x + \frac{1}{\gamma}\theta\dot{\theta}\\ &\le -ks(x)sign(s)\|x\| - \gamma\xi^2(x)\|s\|^2\|x\| - \|\theta\|\|s\|\xi(x)\end{aligned}$$

After some straight forward calculations, we obtain the following

$$\dot{V} < -k\, s(x) sign(s) \|x\| - \left(M_\theta + \|\theta\|\right)\|s\|\xi(x)$$

and thus: $\dot{V} < 0$.

V. POWER SYSTEM MODEL

The power system model considered in this paper is a fourth order linearized model representing a synchronous machine connected to an infinite bus via a double circuit transmission line. The power system schematic diagram including turbine, transformer, automatic voltage regulator and PSS is shown in fig.1 [25].

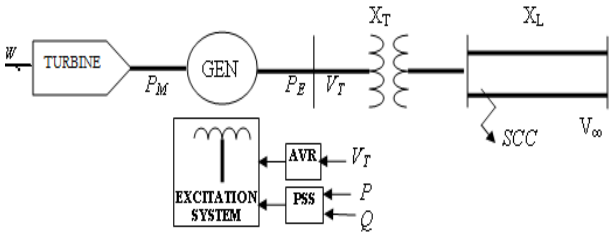

Fig.1 Synchronous machine infinite bus.

A fourth order classic state space representation [9, 25] is given in (22). See appendix for nomenclature.

$$\dot{x} = \begin{bmatrix} -\frac{D}{M} & -\frac{K_1}{M} & -\frac{K_2}{M} & 0 \\ \omega_0 & 0 & 0 & 0 \\ 0 & -\frac{K_4}{T'_{d0}} & -\frac{1}{T'_{d0}K_3} & \frac{1}{T'_{d0}} \\ 0 & -\frac{K_4K_5}{T_A} & -\frac{K_AK_6}{T_A} & -\frac{1}{T_A} \end{bmatrix} x + \begin{bmatrix} 0 \\ 0 \\ 0 \\ \frac{K_A}{T_A} \end{bmatrix} u \qquad (22)$$

Where the state variable are expressed as: $x(t) = \left[\Delta\omega(t)\, \Delta\delta(t)\, \Delta e'_q(t)\, \Delta e_{fd}(t)\right]^T$.

Note that the six constants $K_1 - K_6$ are functions of real power P and reactive power Q [2, 25].

The parameters of the single machine infinite bus system are as follows:

$$x_e = 0.4\,p.u,\ x_q = 1.55\,p.u,\ x_d = 1.6\,p.u,\ x'_d = 0.32\,p.u,\ D = 0,$$
$$T'_{d0} = 6s,\ H = 5s, T_A = 0.05,\ K_A = 50, V = 1\,p.u$$
$$P_0 = 0.75\,p.u,\ Q_0 = 0.015\,p.u.$$

VI. SIMULATION

The soundness of the approach was tested and performance as well as robustness tests were conducted and compared to a classic CPSS [12] confirming, through computer simulations, good transient behaviour with the proposed approaches despite severe operating conditions illustrated by the following case studies.

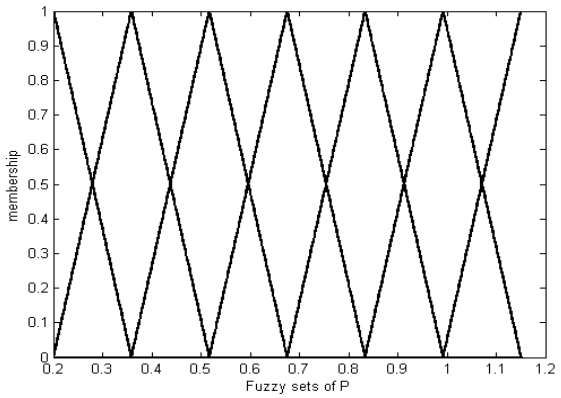

Fig.2 Fuzzy sets for input *P*.

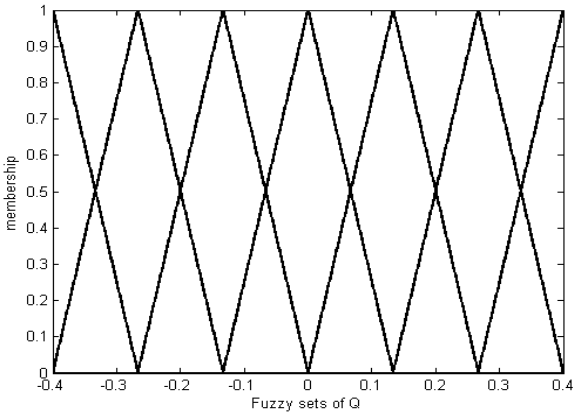

Fig.3 Fuzzy sets for input *Q*.

Case 1: First the simulation results for light load condition are shown in fig.2 with PSS calculated on both approaches. Performances of the second approach are clearly superior while a greater control effort is solicited.

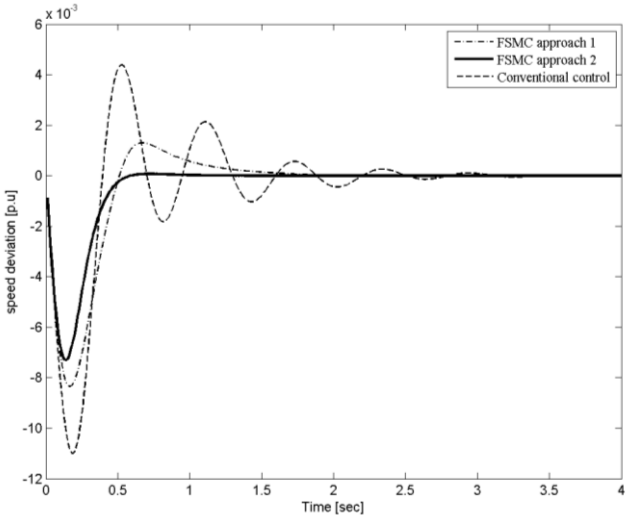

Fig.4 Speed deviation.

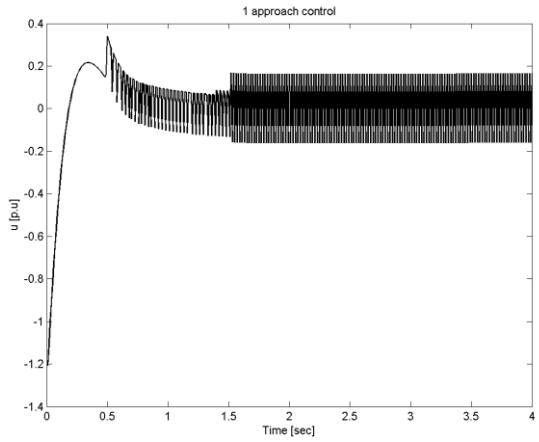

Fig.5 First approach control effort.

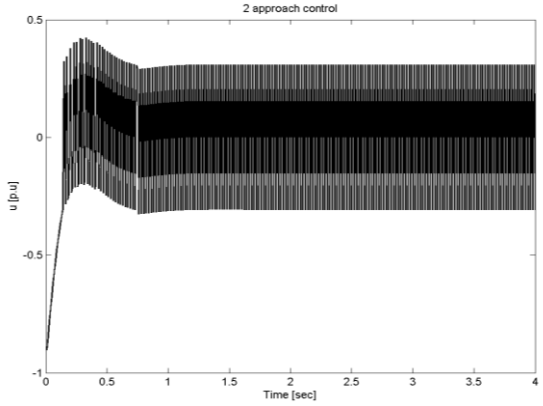

Fig.6 Second approach control effort.

Case 2: Operating conditions change abruptly from light to heavy load condition, i.e. *P* is changed from 0.75 p.u. to *1 p.u.* The simulation results in fig.4 show a better transient performance for the second approach.

Case 3: We now consider the case of the sudden occurrence of heavy reactive power causing a change in Q from the light value of *0.015p.u.* to *0.3p.u.* Again the simulation results shown in fig.5 seem to indicate a good transient behaviour whith superior performance due to the second approach.

Case 4: Two major perturbations are assumed, i.e., heavy load *1p.u.* and a variation in the inertia constant of the synchronous machine from *10s* to *12s.* Appreciable performances are obtained for both approaches with a slight edge for the second control law as can be seen in fig.6.

Case 5: Operating point $P_0 = 0.9$ *p.u.* , $Q_0 = 0.3$*p.u. and* $x_e = 0.2$ *p.u.* Again in this case our global fuzzy approaches indicates rapid elimination of oscillations with better performance in the second approach as shown in simulation results are fig.7.

Case 6: Heavy reactive load and weak connection: $P_0 = 0.9$ *p.u.*, $Q_0 = 0.4$ *p.u. and* $x_e = 0.45$ *p.u.*

As can be seen from the simulation results shown in Fig.8 both global fuzzy approaches indicates a rapid suppression of oscillations and a better response than the response obtained using conventional stabilizer.

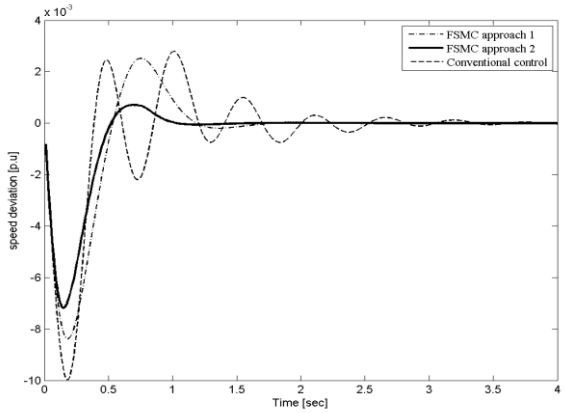

Fig.7 Speed deviation in heavy load condition case.

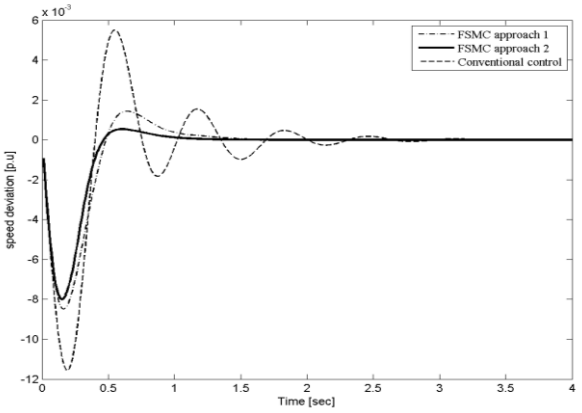

Fig.8 Speed deviation in heavy reactive power case.

Case 7: Import of reactive power and strong connection: $P_0 = 0.9$*p.u.*, $Q_0 = -0.4$*p.u.* and $x_e = 0.1$*p.u.*

The simulation results are show in fig.9 clearly indicating a loss of synchronism with CPSS and an effective damping of oscillations with both suggested approaches.

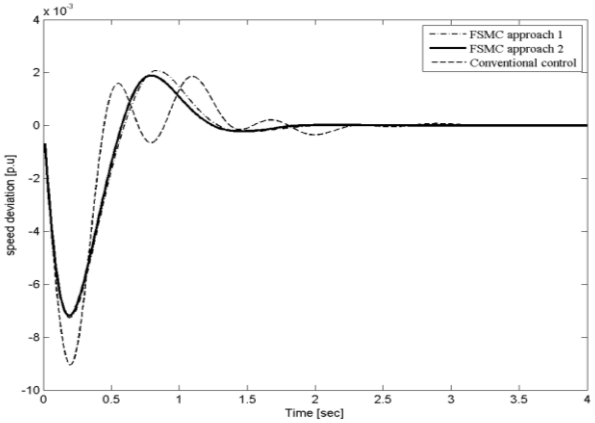

Fig.9 Speed deviation for two major perturbations case.

VII. CONCLUSION

We introduced in this paper, based on the work of Yu & al., a global fuzzy sliding power system stabilizer that enhances damping and thus improves transient dynamics of a single synchronous machine power system. Different load conditions as well as severe perturbations were used to evaluate the proposed global sliding fuzzy power system stabilizer effectiveness in rapidly reducing oscillations that could lead to loss of synchronism if not treated. Simulation results exhibit superior performance over classical PSS and satisfactory transient behaviour for both approaches considered while showing a better performance for the second approach. Multi-machines power system remains to be thoroughly investigated under the proposed technique.

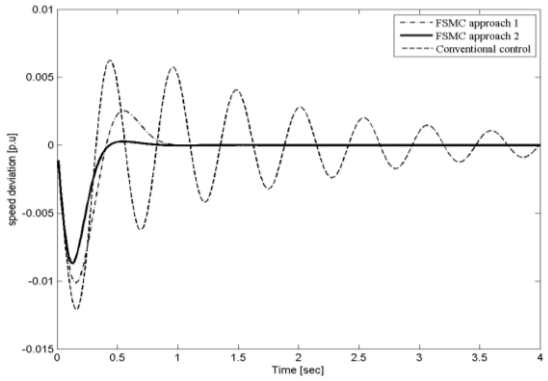

Fig.10 Speed deviation responses for P0 = *0.9p.u. Q0 = 0.3p.u.* and *xe = 0.2p.u.*

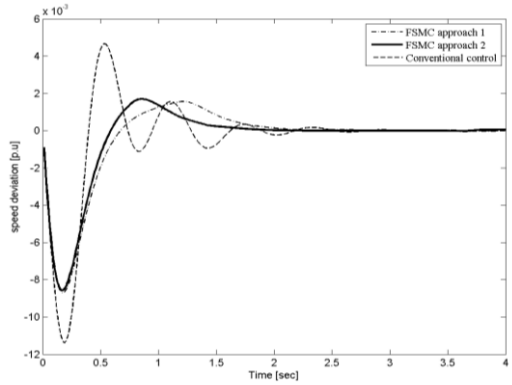

Fig.11 Speed deviation in heavy reactive load and weak connection case.

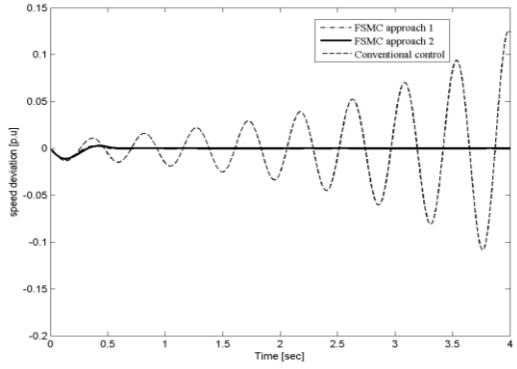

Fig.12 Speed deviation in import of reactive power and strong connection case.

REFERENCES

[1] E.V. Larsen, D.A. Swann, Applying power system stabilizers, Part I, II, III, IEEE Trans. on Power App. and Syst., PAS-100(1981), 3017-3041.
[2] F.P. deMello, C.A. Concordia, Concept of synchronous machine stability as affected by excitation control, IEEE Trans.PAS-103 (1969) 316–329.
[3] P.M. Anderson, A.A. Fouad, Power system control and stability, lowa State University Press, Ames, 1977.
[4] A. Ghosh, G. Ledwich, O.P. Malik, G.S. Hope, Power system stabilizer based on adaptive control techniques,
[5] IEEE Trans. PAS 103 (1984), 1983–1989.
[6] S.J. Chang, Y.S. Chow, O.P. Malik, G.S. Hope, An adaptive synchronous machine stabilizer, IEEE Trans. PWRS 1, (1986), 101–109.
[7] A. Pierre, A perspective on adaptive control of power systems, IEEE Trans. PWRS 2 (1987), 387–396.
[8] A. Y. Sivaramakrishnan, M. V. Hariharan, M. C. Srisailam, Design of a variable-structure load controller using pole assignment technique, Int. J. Contr.,40(1984), 487-498.
[9] Kothari M.L., Nanda J., K. Bhattacharya, Design of variable structure power system stabilizers with desired eigenvalues in the sliding mode, IEE Proc. Gen., Trans. and Distr., 140(1993), 263-268.
[10] Bhattacharya K., Kothari M.L and Nanda J., Design of Discrete-Mode Variable Structure Power System Stabilisers, Electrical power & Energy System, Vol.17, n 6,pp.399-106,1995.
[11] Y.M. Park, W. Kim, Discrete time adaptive sliding mode power system stabilizer with only input/output measurements, Electrical power & Energy systems, 18(1996),509-517.
[12] S.S. Lee and J.K. Park, Design of power system stabilizer using observer / sliding mode, observer/sliding mode model following and H∞ / sliding mode controllers for small signal stability study, Electrical Power & Energy Systems, Vol.20, 8(1998),pp.543-553.
[13] A.L. Elshafei, K. El-Metwally, Power system stabilization via adaptive fuzzy logic, IEEE Proc. of International Symposium on Intelligent Control,(1997),89-95, Istanbul, Turkey.
[14] N.H. Zadeh, A. Kalam, A direct adaptive fuzzy power system stabilizer, IEEE Trans. on Energy Conversion, 14(1999).
[15] H.M. SoIiman, A.L. Eshafei, A.A. Shaltout, M.F. Mors, Robust power system stabiliser, IEE Proc-Elec. Power Appl., 147(2000),285-291.
[16] N.H. Zadeh, A. Kalam, An indirect adaptive fuzzy-logic power system stabiliser, Electrical power & Energy systems, 24(2002), 837-842.
[17] A.L. Elshafei, K. El-Metwally, A.A. Shaltout, A variable structure adaptive fuzzy logic stabilizer for single and multi-machine power systems, Control Engineering Practice,13,(2005),413-423.
[18] H. M. Soliman, A.L. Elshafei, F. Bendary, W. Mansour, LMI static output-feedback design of fuzzy power system stabilizers, Expert Systems with Applications,36(2009),6817-6825.
[19] X. Yu, Z. Man and, B. Wu," Design of fuzzy sliding mode control systems", Fuzzy sets and systems. 9165(1998), 295-306.
[20] J. J. Slotine, S. S. Sastry, Tracking control of non-linear systems using sliding surfaces, with application to robot manipulators, Int. J. Contr., 38(1983), 465-492.
[21] I. R. Petersen, A procedure for simultaneously stabilizing a collection of single input linear systems using non-linear state feedback control, Automatica, 23(1987), 33-40.
[22] K. D. Young, Controller design for a manipulator using the theory of variable structure systems, IEEE Trans. Man Cyber., 8(197, 101-109.
[23] Y.M. Park, W. Kim, Discrete time adaptive sliding mode power system stabilizer with only input/output measurements, Elect. Power & Energy Systems, 18, (1996), 509-517.
[24] J. Ackerman, V. Utkin, Sliding mode control design based on Ackerman's formula, IEEE Trans. on Aut. Control, 43, (1998), 234-237.
[25] V. I. Utkin, Variable structure systems with sliding modes, IEEE Trans. Aut. Cont., AC22 (1977), 212-222.
[26] K. D. Young, V. I. Utkin, U. Ozguner, A control Engineer's guide to sliding mode control, IEEE Trans on Control Syst. Technology, 7 (1999), 328-342.
[27] P. Kundur, Power System Control and Stability, Ed. McGrawHill Inc., 1994.

BIOGRAPHIES

Emira NECHADI received her bachelor degree in control systems, master degree in control systems, and Ph.D. degree in control systems, all from the University of Sétif, Algeria in 2002, 2004, and 2013, respectively. Her research interests include sliding mode control, adaptive fuzzy control, fuzzy systems, synergetic control and power systems.

Mohamed Naguib HARMAS received the Ph.D. degree in control systems from Ferhat Abbas University of Sétif 1, and M. Sc. degree in electrical engineering and electronics from California State University of Sacramento, Sacramento, USA. He is currently a professor at Sétif University, Algeria. His research interests include robust nonlinear control, power system and power electronics control, and fuzzy synergetic design.

Challenges of Marine Power in the Balkan Region

D. Dzhonova-Atanasova, R. Popov, A. Georgiev

***Abstract*—The world power generation is in a process of transition from fossil fuels to renewable and sustainable power sources. The part of the electricity from alternative energy technologies is growing rapidly. New engineering approaches and devices are continuously created by the researchers in the field of power engineering, aimed at obtaining energy with less harm for the environment and the life on the planet. The present work is an initial evaluation of the possibilities for marine energy conversion in the Balkan region. The focus is on energy from the sea including energy from waves, currents, salinity, temperature difference etc. The main purpose of the work is on the basis of assessment of the power potential determined by the geographical characteristics of the seas in the region and the scientific, technological and economical level to make some conclusions about the prospects in this area.**

Index Terms— **assessment, energy conversion, energy resources, marine power, power potential, wave energy.**

I. INTRODUCTION

THE FOSSIL fuel dependent production of energy leads to continuously deepening ecological problems. The scientists and engineers in the field directed their efforts towards energy efficient technologies, decreasing the pollution caused by fuel combustion, as well as inexhaustible and sustainable energy resources like sun, wind and ocean. The share of the energy from renewable sources is rapidly growing, Fig. 1. Despite of the crises of the late years, the renewable electricity cost decreases, due to the growing awareness of the authorities that the transition to sustainable power production is the only way for future development of the mankind. The European Council in 2007 adopted ambitious energy and climate change objectives for 2020 [1] – to reduce greenhouse gas emissions by 20%, to increase the share of renewable energy to 20%, and to make a 20% improvement in energy efficiency.

Compared to 2011, the structure of electricity production in 2012 in EU-27, Fig. 2, taken from [3], is as follows:

D. Dzhonova-Atanasova is with the Institute of Chemical Engineering at the Bulgarian Academy of Sciences, "Acad. G. Bonchev" Str., Bl 103, Sofia 1113, Bulgaria (e-mail: dzhonova@bas.bg, dzhonova@mail.bg).

R. Popov is with the Department of Optoelectronics and Laser Engineering, Technical University of Sofia, Branch Plovdiv, Bulgaria (e-mail: rum_pop@yahoo.com).

A. Georgiev is with the Department of Mechanics, Technical University of Sofia, Branch Plovdiv, Bulgaria (e-mail: AGeorgiev@gmx.de).

- the production of conventional thermal electricity decreased by 4.6 % and accounted for 52.3 % of total production;
- the production of electricity by nuclear power plants decreased by 2.7 % and accounted for 27.1 % of the total;
- the electricity production by hydropower increased by 9 %, while the production by wind increased by 11.5 % and represented respectively 11.7 % and 6.4 % of the total.

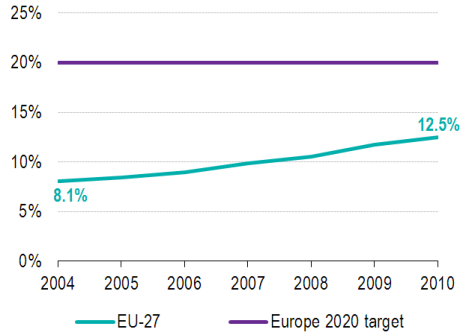

Fig. 1 EU 27 Share of electricity production by renewable sources in gross production, source [2]

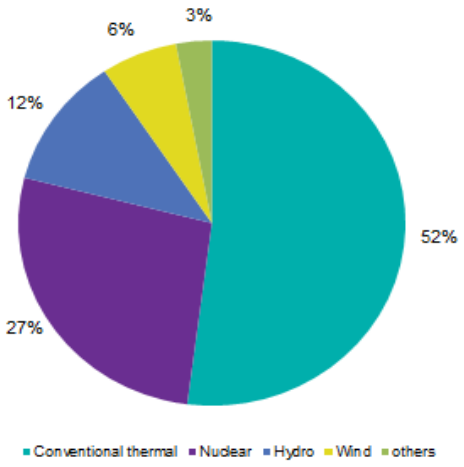

Fig. 2. EU 27 electricity production by source, 2012 (in %), source [3].

II. MARINE RENEWABLE RESOURCES

The ocean contains great amount of energy, but its conversion to useful form like electricity requires advanced technology that is still under development. The main types of ocean energy technologies are wave energy, tidal energy, temperature gradient energy and salinity gradient energy. The ocean energy comes from the sun, which heats the atmosphere

and the ocean water, and thus generates wind and ocean currents. Prospects for the various marine energy sources including their power potential and energy density were assessed after the 1973 energy crisis, Table I from [4].

TABLE I
MARINE RENEWABLE RESOURCES, [4]

Resource	Power potential (TW)	Energy Density (equivalent to meters of hydraulic head)
Ocean Currents	0.05	0.05
Ocean Waves	2.7	1.5
Tides	0.03	10
Thermal Gradient	2.0	210
Salinity Gradient	2.6	240

The comparison of the characteristics of the ocean resources to other renewable resources in Table II, from [5], shows that the marine power density is the highest but at the highest energy cost, the technologies are under development and much research and new approaches are needed.

A. Tidal energy

The tides are created from the Earth-Sun–Moon gravitational interaction. The most practical use for tidal energy is for conversion to electricity. The tide conversion technologies are two main types: using tidal range and tidal currents. The tidal range is used by creating a dam, similar to hydroelectric dams, or barrage containing several gates and turbines, across an estuary. Since the first tidal barrage in La-Rance estuary in France built in 1962 and still in operation, lot of engineering solutions and devices for tidal range and current power have been proposed [6, 7].

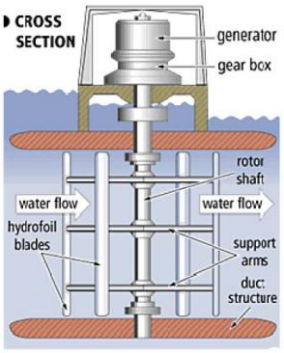

Fig. 3. Vertical Axis Hydro Turbine, Blue Energy Canada Inc., (on the basis of the wind turbine of Darrieus, 1931), source [9].

The current power is more promising than the tide range in the seas around the Balkan Peninsula, where the tides are very limited. Some examples of commercial current energy converters are given in Figs. 3 to 5. Currents are also generated by temperature, pressure, water salinity difference and wind. The ideal locations for tidal current power generation are basins with a relatively narrow entrance, such as areas between islands, narrow straits, and headlands and Aegean islands offer this morphology [5].

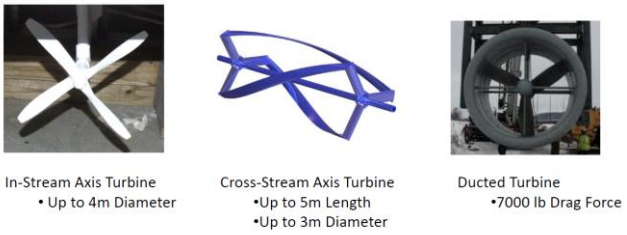

Fig. 4. Horizontal Axis Hydro Turbine tested at the University of New Hampshire, source [10].

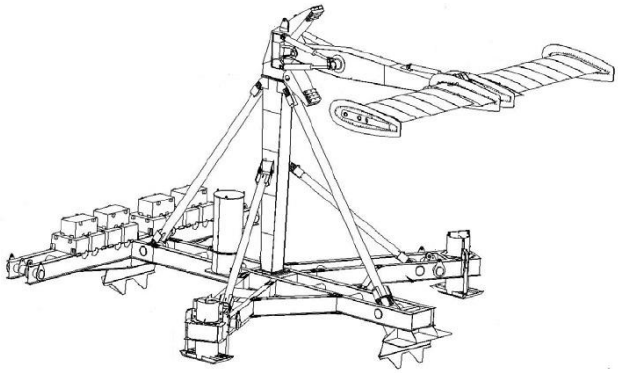

Fig. 5. Oscillating hydrofoil, Stingray Assembly © Engineering Business Ltd 2005, source [11].

The expression for estimation of the power of the current, i.e. the kinetic energy passing per unit time of the column of fluid upstream of turbine, [8], is

$$P_o = \tfrac{1}{2}(\rho A_1 u_o)u_o^2 = \tfrac{1}{2}\rho A_1 u_o^3, \quad (1)$$

where ρ=1025 kg/m^3 -density of the sea water, A_1- cross-sectional area of the turbine disc, m^2, u_o- tide current speed, m/s.

TABLE II
RENEWABLE ENERGY RESOURCES, [5].

	Solar	Wind	Wave	Tidal/ Current
Development Status	Early Commercial	Mature Commercial	Early Commercial	Early Commercial
Source	Sun	Uneven solar heating	Sun-wind	Gravity of moon & sun
Annual Average Power Density	0.175 -0,2 kW/m^2 (fixed tilt at latitude Winnipeg - Calgary - Edmonton	0.6 - 1kW/m^2 (Rocky Mountains, offshore BC)	30 - 45 kW/m (Pacific Coast) 10 - 25 kW/m (Atlantic Coast	4-9 kW/m^2 (Minas Basin) 0.5 - 2 kW/m^2 (other sites)
Intermittency	Day-night; clouds, haze, and humidity	Atmospheric fronts and storms (local winds only)	Sea (local winds) and swell (from distant storms)	Diurnal cycles
Energy Cost	9 c/kWh (Photovoltaic)	4 c/kWh (Wind turbine 6-9 m/s wind spd.)	~ 10 c/kWh	~10 c/kWh

When assuming 40% efficiency of tidal current power to electricity the following relation is obtained:

$$q \approx 0.1\rho u_o^3 . \quad (2)$$

The SeaGen 1.2 MW device, [12], of horizontal axis type was the world's first grid connected commercial scale tidal current device and has continued to lead the way in tidal stream technology. Since installation in 2008 at Strangford Lough, Northern Ireland, SeaGen has generated over 8 GWh of electricity.

B. Ocean thermal energy conversion (OTEC)

Ocean thermal energy conversion (OTEC) allows production of electricity using cold water from the deep seawater (1000 m and 5◦C) and surface water (between 25 and 28◦C) as hot spring. With this temperature gradient, typical for the tropical and equatorial seas, the production of electricity is made possible using a Rankine cycle [8]. Carnot efficiency of the process is

$$\eta_{\text{Carnot}} = (T_E - T_c)/T_E = 20/298 = 6.7\ \%, \quad (3)$$

where T_E and T_c are hot water and cold water temperature respectively, K.

OTEC gross power efficiency is only half the Carnot limit - about 3%.

The systems can be classified into closed, open and hybrid cycle type. The open cycle conversion is accompanied by water desalination. The recent developments are reviewed in [8, 13], including improved variants with higher efficiency, Kalina cycle and Uehara cycle, using two component working fluid [14].

The Balkan region is out of the range of the potential sites between 20°N and 20°S for development of OTEC systems, but there are solutions using hot spring water or hot waste water [15], which are possibly feasible.

C. Salinity gradient conversion

In the review of salinity gradient conversion technologies [16] it has been noted that of all marine renewable energy sources the salinity gradient power is of the highest energy density, as shown in Table I. The osmotic pressure difference between fresh water and seawater is equivalent to 240 m of hydraulic head. Almost all of the proposed conversion schemes rely on the fundamental natural process of evaporation to separate the fresh water from the salt. The overview in [16] of the state of technologies till 2000 includes Pressure-Retarded Osmosis, Reversed Electrodialysis, Vapor Compression and Hydrocratic generator. The authors stated that any strategy to desalinate seawater could be reversed to produce power. The world's first osmotic energy plant has been operating from 2010 in Tofte, Norway, on the Oslo fiord inlet [17].

Aegean Sea, being the place of mixing of water masses of low salinity from the Black Sea and hypersaline water masses from Mediterranean Sea, which leads to formation of currents and water stratification with high salinity at the sea bottom, seems promising for development of marine power plants, but its potential has not yet been fully investigated and assessed.

D. Wave energy

Wave energy conversion is harvesting the power of the sea waves. When the wind energy is converted to wave energy, it is specially concentrated due to reduction of the area of energy distribution to the envisaged area perpendicular to direction of wave propagation. The power carried in the wave at the horizontal axis, per unit width of wave front at any instant [8], can be estimated by

$$P' = \frac{\rho g a^2}{2}\frac{c}{2} = \frac{\rho g a^2 \lambda}{4T} \quad (4)$$

where ρ is the sea water density, kg/m^3, a- wave amplitude, m, c- wave phase velocity, m/s, g- acceleration of gravity, m/s^2, λ- wave length, m, and T- period of motion, s.

The wave power levels near the coasts of the Balkan Peninsula are estimated to reach 7 kW/m of wave crest, [18], and near the Black Sea cost - 3 to 7 kW/m, [19], which is not as much as the potential of the North East Atlantic coast reaching to 70 kW/m, but marks the region as a prospective wave energy site.

The systems can be classified into fixed and floating or on-shore, near-shore and off-shore. Some examples of prototypes and plants put into operation are given in Figs. 6 to 10. The wave energy converting systems are reviewed in [20]. Most of the proposed processes of wave conversion are shown schematically in Fig. 11.

Examples of fixed on-shore converters are:

1. Oscillating water column (OWC), Fig. 6. Incoming waves force air up column to turn the turbine. Outgoing waves suck air down column to turn the turbine. LIMPET (Land Installed Marine Powered Energy Transformer) is a 500 kW rated OWC power plant, developed by the Queen's University of Belfast and Wavegen Ltd in the United Kingdom. A 75 kW prototype was constructed on the island of Islay, Scotland in 1991 [22, 23].

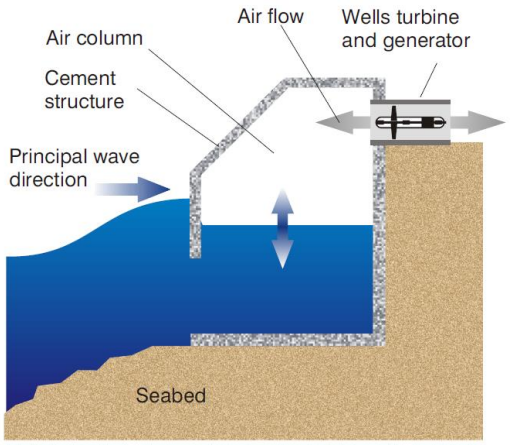

Fig. 6. Oscillating water column (OWC), source [24].

2. Tapered Channel System (TAPCHAN), where the concept is similar to that of traditional hydroelectric devices. Waves feed through tapered channel into reservoir and are then fed through a turbine. Kinetic energy of the moving wave is changed to potential energy as water is collected in the reservoir, Fig. 7. The TAPCHAN is designed by Norwave company, and a 350 kW prototype commenced operation in 1985 on a small Norwegian island.

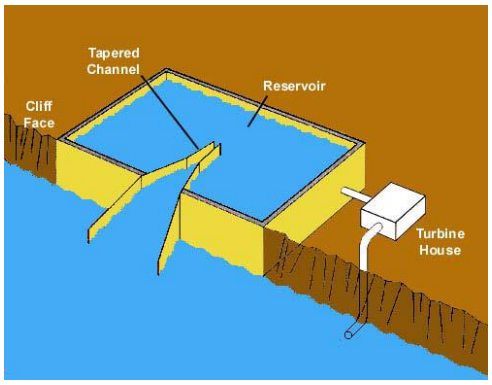

Fig. 7. TAPCHAN, Copyright Boyle, 1996, source [19].

The existing very large variety of off-shore floating devices is reviewed in the [24] and [20]. Some key examples of off-shore systems put into operation are:

1. The PELAMIS device, Fig. 8, consists of semi-submerged cylindrical sections linked by hinged joints, [25]. The wave induced motion of these joints is resisted by hydraulic rams which pump high pressure oil through hydraulic motors via smoothing accumulators. The prototype, a 120 m long and 3.5 m diameter device rated at 375 kW, was first tested at the European Marine Energy Centre in 2004 and became the first commercial scale off-shore wave power machine to successfully generate electricity into the national grid. The first prototype connected to the grid is currently deployed in Nissum Bredning fiord, Denmark in relatively mild wave conditions.

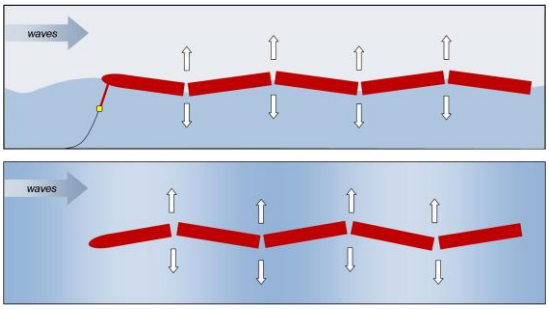

Fig. 8. PELAMIS wave energy converter, source[26]

2. The Archimedes Wave Swing (AWS), [27], is an off-shore, fully submerged (43 m deep underwater), point absorber (that is to say, of negligible size compared to the wavelength). Its two main parts are the silo (a bottom-fixed air-filled cylindrical chamber) and the floater (a movable upper cylinder). Due to changes in wave pressure, the floater heaves, Fig. 9. AWS Ocean Energy, the Scottish company established to commercialize the AWS, tested the technology at full-scale in open water (Portugal 2004).

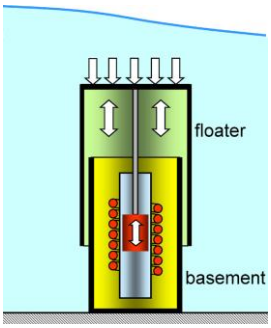

Fig. 9. Archimedes Wave Swing, source [28].

3. Wave Dragon, [29, 30], is a floating, slack-moored energy converter of the overtopping type. The overtopping device, Fig. 10, elevates ocean waves to a reservoir above sea level, where water is let out through a number of turbines and in this way transformed into electricity, i.e. a three-step energy conversion: overtopping (absorption); storage (reservoir); power-take-off (low-head hydro turbines).

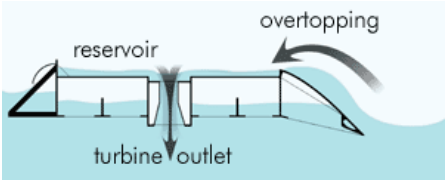

Fig.10. Wave Dragon principle, source [29].

The Wave Dragon prototype of rated power 20 KW tested in Nissum Bredning fiord in Denmark is constructed to match a very humble wave climate at approximately 0.4 kW/m, but the technology has no up-ward restriction from wave heights or wave lengths on its size.

III. MARINE ENERGY CONVERSION IN THE BALKAN REGION

The Balkan region is behind the development of the other European countries in respect to renewable energy resources. The reasons are lack of understanding and resistance of the authorities and the public towards the higher capital costs of the renewable energy, especially in the countries with economic and political difficulties. The authors believe that in this situation the strategy for successful marine power development of the region is cooperation of the researchers from the countries with close natural conditions and potential for higher efficiency and optimization of funding.

The aim of the present work is to show the basis for this cooperation, the engineering and scientific achievements in the area of marine power technologies in the Balkan countries, described as follows.

A. Wave power potential of Turkey

The wave power potential of Turkey was assessed in [31] with the aim to find out the cost effectiveness of a wave power

converter system for the mild climate conditions of Turkish waters. The regions in the west of the Black Sea in the north of Istanbul Straits and off the southwestern coasts of Aegean Sea between Marmaris and Finike were suggested by the authors as the best sites to harness the wave energy and a system of the type of Wave Dragon was assessed in this conditions. It was concluded that the Baltic Sea and devices designed for that sea can be a sample for the studies in Turkey.

B. Sea current power of Greece

The work plan for marine power development in Greece given in the assessment of the energy potential of the Greek seas [32] can serve as a basis for the development of the Balkan region. The authors focused on measures for enhancement of the current measurement system and data base concerning speed/ direction of current/ wind, sea temperature etc. On the basis of a review of projects running in other countries the authors selected a vertical axis system (KOBOLD) [33] as a low-cost, easily deployable system ideal for the Greek seas. In addition SeaGen turbine would be an interesting alternative for covering large scale energy needs.

C. Wave power potential of Bulgaria

In the project report [34] the low-power wave conditions in the Black Sea and the large costs of the sea converters determine the aim of the studies – to develop devices which can be applied in sites of the world with better energy conditions for high capacity energy production or for small rescue vessels. On the basis of preliminary studies [35] in the Laboratory of Mechatronics at the Bulgarian Academy of Sciences on development of a wave converter utilizing the horizontal movement of the sea waves, an experimental device was constructed in 2010 and successfully tested in the sea [36]. The device floats on the sea surface and absorbs the wave energy by means of two vertical plates. A linear electric generator is connected to the plates moving back-and-forth. The device adapts to the changes of the wave length by changing the distance between the plates using only the power of the waves.

D. Wave energy conversion in sheltered seas

Very useful are the conclusions from the studies concerning sheltered seas, like the Baltic Sea and the Mediterranean Sea.

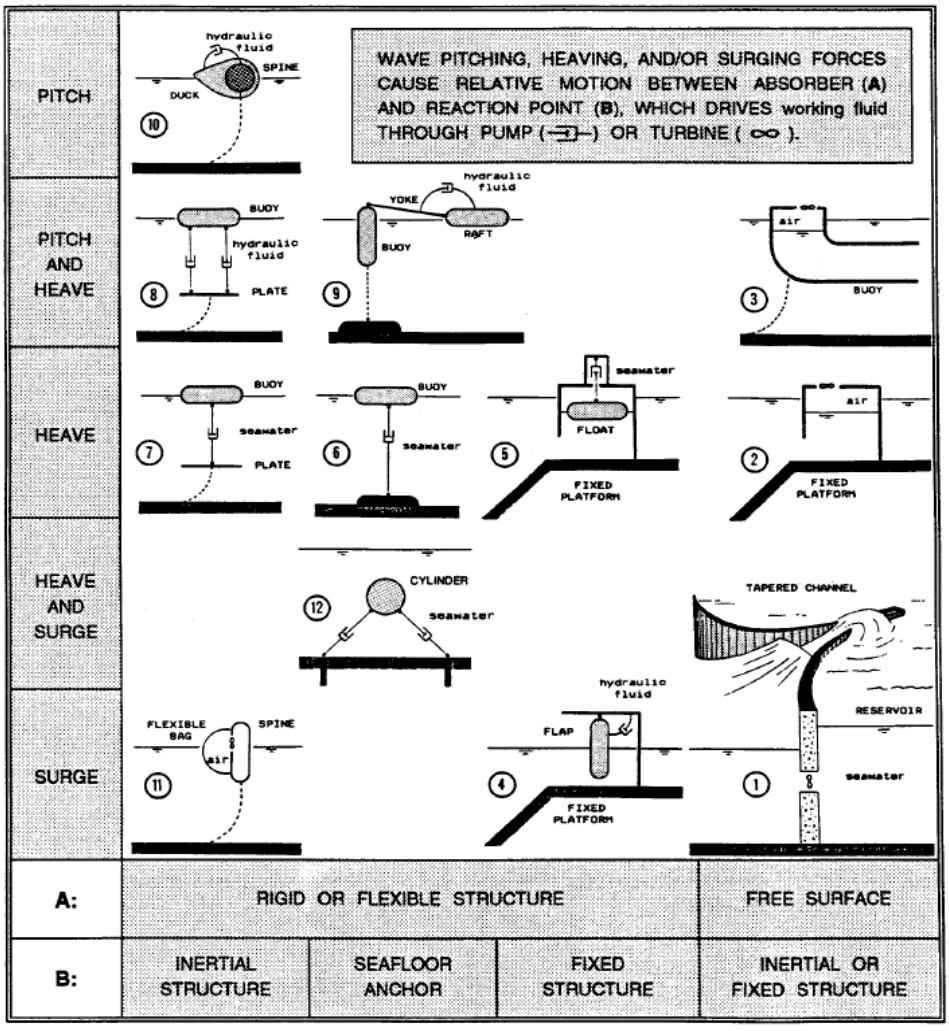

Fig. 11. Processes of wave conversion, source [21]

In the assessment of the potential of the Baltic Sea in [37] the dominating idea to use one large unit, which can convert a lot of power is opposed by systems where a number of small specifically designed generators are connected in arrays. The authors proposed for the sheltered seas with milder but steady wave climate, wave power plants consisting of a number of small wave energy converters, forming large arrays. They look at advantageous arrangements of point absorbers, [38], and their operation in the conditions of the Baltic Sea.

The concept of the wave power plants consisting of large arrays of small direct driven wave energy converters, having specifically designed linear generators driven by a point absorbing buoy, Fig. 12, was studied for the moderate climate of the Mediterranean Sea in [39] and for the Black sea near the Romanian coasts in [40].

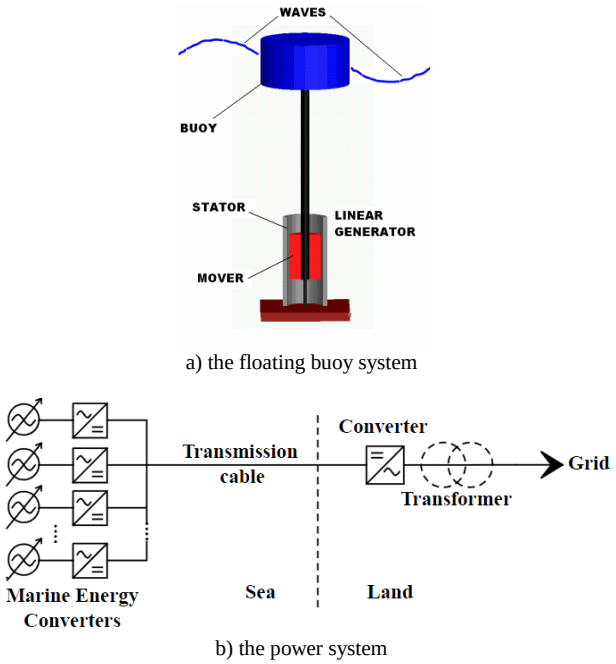

a) the floating buoy system

b) the power system

Fig. 12. The direct drive power take off system, source [40].

The feasibility of the Seabased device [41], designed by Uppsala University for deployment in the Swedish seas, was studied in [39] for wave energy exploitation under Mediterranean Sea conditions by a numerical model of the coupled buoy-generator system, developed to simulate the behavior of the wave energy converter in regular waves of different wave heights and periods. The wave energy potential of the Black Sea near the Romanian coasts, a possible power take off system, Fig. 12, and respectively the linear generators to be used in such wave energy power converters was discussed in [40].

IV. THE UNIQUE POSSIBILITIES OF THE BLACK SEA

The Black Sea is unique with the presence of hydrogen sulfide dissolved in the water under the level of about 200 m depth, reaching constant concentration of 9.5 mg/l under 1500 m depth [42]. It is the world's largest anoxic basin, where almost 90% of the seawater is anaerobic [43]. The hydrogen sulfide in natural sea waters forms through bacterial sulfur cycle. The interest in production of hydrogen, the fuel of the future, is growing. Hydrogen sulfide can be converted to hydrogen and sulfides with much less energy than that required for splitting water [43]. Therefore many technologies are under development for hydrogen production from H_2S found either in industrial waste gases and waters or in natural sea water.

The potential for hydrogen and sulfur production from H_2S in the Black Sea is studied by many authors, especially from the countries surrounding the sea (Turkey, Romania, Bulgaria, Ukraine), and those using renewable energy sources, especially solar and wind are expected to be the most perspective [43]. The available methods for hydrogen production from H_2S at different stages of development include thermal, thermochemical, electrochemical, photochemical and plasmochemical methods [42]. In [42] a catalytic thermal decomposition process operated on solar energy for process heat generation is considered for hydrogen and sulfur production from H_2S in the Black Sea, Fig. 13. The authors selected the most promising site for such a plant, Amasra, Turkey, for the following favorable conditions:

- the 2000 m bathymetric contours pass nearest to the shore;
- sufficient insulation and solar radiation;
- mild wind and sea currents conditions;
- seaport and highway connection.

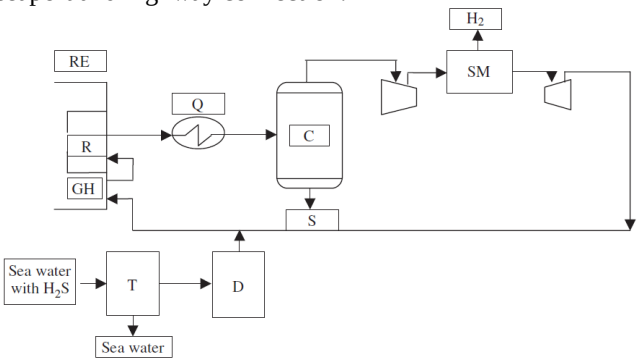

Fig. 13. Solar H_2S thermolysis process (C: condenser, D: dehumidifier, GH: H_2S heater, Q: quencher, R: reactor, RE: solar receiver, SM: membrane separator, T: sea water storage tank), source [42].

The authors of [43] proposed and studied a process of electrolysis of H_2S using renewable energy, Fig 14. Another technology under investigation, [44], is using electrochemical method of removal of sulfides from the deep Black Sea water by oxidation to sulfites or sulfates. The authors developed a fuel cell with a catalyst incorporated into activated carbon matrix.

The economical assessments [42, 43] show that no commercial technology has been developed yet. The high costs of the produced hydrogen and sulfur make the available solutions not economically feasible, but they have considerable ecological significance for counteracting the dangerous increase of the hydrogen sulfate content in the Black Sea.

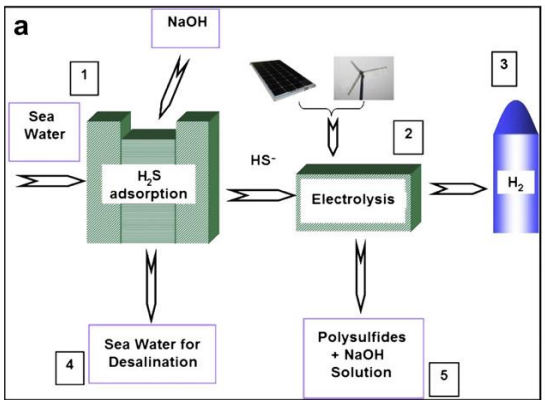

Fig. 14. Electrolysis of H_2S, source [43].

V. CONCLUSIONS

The present review of the current state of marine technologies for power production in the Balkan region aims at implications of further research and prospects. Although the energy potential of the seas surrounding the Balkan Peninsula is estimated as low power, sea energy conversion has its place, since large portions of the world marine energy potential are possessed by sheltered seas with mild conditions like the Mediterranean Sea, the seas surrounding the Balkan Peninsula and the Baltic Sea. The most promising for the region are expected to be wave and current energy conversion and decomposition of hydrogen sulfide from the Black Sea. For higher efficiency they can be combined with solar or wind converters. Because of the high cost for the development, installation, maintenance and testing of large-scale marine energy devices, the projects should be performed in cooperation of a number of countries and should be supported by national and European funds. It is necessary to promote international cooperation in the efforts to study and enhance the sea technologies in order to lower the cost of green energy production and to gain the support of the society and the governments. An important part of the studies is careful assessment of the social as well as environmental impact of the sea power technologies.

REFERENCES

[1] *ENERGY 2020 - A strategy for competitive, sustainable and secure energy*, Directorate Generale for Energy, EC, (2010, Nov.) [Online]. Available: http://ec.europa.eu/energy/publications/doc/2011_energy2020_en.pdf.

[2] M. Šturc, (2012, Nov. 8) Renewable energy .Analysis of the latest data on energy from renewable sources, *Environment and energy, EUROSTAT Statistics in focus*, [Online], Issue No *44*, Available: http://epp.eurostat.ec.europa.eu/cache/ITY_OFFPUB/KS-SF-12-044/EN/KS-SF-12-044-EN.PDF

[3] *Electricity production and supply statistics* (2012) EC EUROSTAT, [Online], Available: http://epp.eurostat.ec.europa.eu/statistics_explained/index.php/Electricity_production_and_supply_statistics

[4] J. D. Isaacs, W. R. Schmitt, "Ocean Energy: Forms and prospects", *Nature*, Vol. 207, Number 4428, pp. 265-273, 18 Jan. 1980.

[5] S. Alatsathianos, P. Fafali, "Wave and current energy: A viable scheme to exploit the energy potential of Greek seas", [Online], Available: http://www.researchgate.net/publication

[6] *Tidal Resources*, [Online], Available: http://www.see.murdoch.edu.au/resources/info/Res/tidal/index.html

[7] L B Bernshtein (1996) *Tidal Power Plants*. Seoul: Korea Ocean Research and Development Institute (KORDI). [Online], Available: http://repository.tudelft.nl/assets/uuid:46a59861-0817-4bf7-a252-b3a9562fdcd6/L.B._Bernshtein_-_Tidal_power_plants.pdf

[8] J. Twidell, T. Weir, *Renewable Energy Resources*, (2nd ed.), Taylor & Francis, 2006

[9] S. S. Khalid, Z. Liang, N. Shah, "Harnessing Tidal Energy Using Vertical Axis Tidal Turbine" *Research Journal of Applied Sciences, Engineering and Technology* 5(1) 2012, pp. 239-252, [Online], Available: http://maxwellsci.com/print/rjaset/v5-239-252.pdf

[10] J. Byrne, K. Baldwin, B. Celikkol, R. Swift, M. Wosnik, (2010, Feb. 11) Development of a tidal energy test platform, Univ. of New Hampshire, CORE, [Online], Available: http://www.mrec.umassd.edu/media/supportingfiles/mrec/agendasandpresentations/2ndconference/jeff_byrne_development_of_a_tidal_energy_test_platform.pdf

[11] Technology: Oscillating Hydrofoil, Marine Current Resource and Technology Methodology' Website: http://www.esru.strath.ac.uk/EandE/Web_sites/05-06/marine_renewables/technology/oschydro.htm]

[12] Sea Generation Ltd, [Online], Available: http://www.seageneration.co.uk/index.php.

[13] L.A. Vega, (1999) "Ocean Thermal Energy Conversion (OTEC)", [Online], Available: http://www.otecnews.org/portal/otec-articles/ocean-thermal-energy-conversion-otec-by-l-a-vega-ph-d/#economic

[14] H. Kobayashi, S. Jitsuhara, H. Uehara, (2001) "The Present Status and Features of OTEC and Recent Aspects of Thermal Energy Conversion Technologies", National Maritime Research Institute, Japan, [Online], Available: http://www.nmri.go.jp/main/cooperation/ujnr/24ujnr_paper_jpn/Kobayashi.pdf

[15] Nam Jin Kim , Kim Choon Ng , Wongee Chun, Using the condenser effluent from a nuclear power plant for Ocean Thermal Energy Conversion (OTEC), *International Communications in Heat and Mass Transfer*, 36, pp. 1008–1013, 2009.

[16] A. T. Jones, W. Finley, "Recent Developments in Salinity Gradient Power", *OCEANS 2003 Proceedings*, Vol. 4, 22-26 Sept. 2003, pp. 2284 – 2287.

[17] Tofte prototype plant, [Online], Available: http://www.statkraft.com/energy-sources/osmotic-power/prototype/

[18] V. Vannucchi, L. Cappietti and A.F.O. Falcão, "Estimation of the offshore wave energy potential of the Mediterranean Sea and propagation toward a nearshore area", *4th International Conference on Ocean Energy*, 17 October, Dublin, 2012, [Online], Available: http://www.icoe2012dublin.com/ICOE_2012/downloads/papers/day2/POSTER%20SESSION%202/Valentina%20Vannucchi,%20Universita%20Di%20Firenze.pdf

[19] V. Galabov, (2013) "On the Wave Energy Potential of the Western Black Sea Shelf", [Online], Available: http://arxiv.org/ftp/arxiv/papers/1304/1304.7806.pdf

[20] Feasibility of Developing Wave Power as a Renewable Energy Resource for Hawaii, (2002), Department of Business, Economic Development, and Tourism, [Online], Available: http://energy.hawaii.gov/wp-content/uploads/2011/10/Feasibility-of-Developing-Wave-Power-as-a-Renewable-Energy-Resource-for-Hawaii.pdf

[21] G. Hagerman, "Wave Energy Resource and Economic Assessment for the State of Hawaii," Prepared by SEASUN Power Systems for the Department of Business, Economic Development, and Tourism, Final Report, 1992

[22] Isley LIMPED Wave Power Plant, The Queen's University of Belfast Contract JOR3-CT98-0312 Publishable Rep., 1 November 1998 to 30 April 2002, [Online], Available: http://mhk.pnnl.gov/wiki/images/2/25/Islay_LIMPET_Report.pdf

[23] Technology: Oscillating water column (OWC) [Online], Available: http://www.wavegen.com

[24] Wave Energy in Europe Current Status and Perspectives, (2002) Centre for Renewable Energy Sources (CRES), [Online], Available: http://www.cres.gr/kape/pdf/download/Wave%20Energy%20Brochure.pdf

[25] R. Yemm, (1999) "The history and status of the Pelamis Wave Energy Converter", "Wave power – Moving towards commercial viability", *IMECHE Seminar*, London, UK

[26] Pelamis Technology, Pelamis Wave Power, [Online], Available: http://www.pelamiswave.com/pelamis-technology
[27] L. Hamilton (2006, Oct. 25), "AWS MK II. Deployment, monitoring and evaluation of a prototype advanced wave energy device", AWS Ocean Energy Ltd, [Online], Available: http://ec.europa.eu/research/energy/pdf/gp/gp_events/ocean_energy/1200_aws-mkii_en.pdf
[28] A. F. de O. Falcao, "Wave energy utilization: A review of the technologies, *Renewable and Sustainable Energy Reviews* 14, 2010, pp.899–918=
[29] J. P. Kofoed, P. Frigaard, E. Friis-Madsen, H. C. Sørensen, "Prototype testing of the wave energy converter Wave Dragon", *Renewable Energy*, Vol. 31, Issue 2, Feb. 2006, pp 181–189.
[30] Wave Dragon, [Online], Available: http://www.wavedragon.net
[31] M. Saglam, "Wave Energy and Technical Potential of Turkey", *Journal of Naval Science and Engineering*, Vol. 6, No.2, 2010, pp. 34-50
[32] S. Alatsathianos, P. Fafali, (2008) "Wave and current energy: A viable scheme to exploit the energy potential of Greek seas", [Online], Available: http://www.docin.com/p-385061618.html
[33] P. Kracht, J. Giebhardt, M. Lutz, M.Vecchio, A. Moroso, J. Bard, "Implementation of a Vertical Axis Marine Current Turbine for Off-grid Village Electrification in Indonesia", *4th International Conference on Ocean Energy*, 17 October, Dublin, [Online], Available:http://www.icoe2012dublin.com/ICOE_2012/downloads/papers/day1/1.2%20Tidal%20Stream%20Technologies/Peter%20Kracht%20-%20Fraunhofer%20IWES.pdf
[34] Innovation technologies for wind and wave energy in the coastal zone, INWECO (2009-2011), funded by the Bulgarian Science Fund , [Online], Available: http://waveconverter.alle.bg
[35] G. Stainov, "Device for converting the energy of the sea waves", Bulgarian Patent BG 66042 B1 (Priority Doc. 10.06.2008)(in Bulg.).
[36] B. Vassilev, G. Stainov, "Adaptive control of linear electro generator for experimental sea waves energy extracting device", *20th Int. Conference "ROBOTICS & MECHATRONICS '10"*, 6-9 Oct. 2010, Varna, Bulgaria, [Online], Available: http://waveconverter.alle.bg
[37] H. Bernhoff, E. Sjöstedt, M. Leijon, "Wave energy resources in sheltered sea areas: A case study of the Baltic Sea" *Fifth European Wave Energy Conference*, 17-20 September 2003, Cork, Ireland, [Online], Available: http://www.el.angstrom.uu.se/meny/artiklar/Wave%20energy%20resources%20in%20sheltered%20sea%20areas.pdf
[38] J. Falnes, *Ocean Waves and Oscillating Systems: Linear Interactions Including Wave-Energy Extraction*, Cambridge Univ. Pr. 2013.
[39] S. Bozzi, A. M. Mique, A. Antonini, G. Passoni, R. Archetti, "Modeling of a Point Absorber for Energy Conversion in Italian Seas", *Energies*, 6, 2013, pp. 3033-3051, [Online], Available: www.mdpi.com/journal/energies
[40] L. Szabo, C. Oprea, "Linear Generators for Wave Power Plants to Be Set up Near the Romanian Coasts of the Black Sea", [Online], Available: http://www.researchgate.net/publication/228680531
[41] M. A. Mueller, et al., "Low Speed Linear Electrical Generators for Renewable Energy Applications," *Proceedings of the Conference on Linear Drives in Industrial Applications, LDIA '2003*, Birmingham (UK), pp. 121-124.
[42] S. Z. Baykara, E. H. Figen, A. Kale, T. N. Veziroglu, Hydrogen from hydrogen sulphide in Black Sea, *International Journal of Hydrogen Energy* 32, 2007, pp. 1246 – 1250
[43] K. Petrov, S. Z. Baykara, D. Ebrasu, M. Gulin, A. Veziroglu, "An assessment of electrolytic hydrogen production from H_2S in Black Sea waters" *International Journal of Hydrogen Energy*,36, 2011, pp. 8936-8942
[44] E. N. Razkazova-Velkova, M. S. Martinov, L. A. Ljutzkanov, N. Dr. Dermendzhieva, V. N. Beschkov, (2013),Catalytic Oxidation of Sulfide Ions in Black Sea Water, *Journal of International Scientific Publications: Materials, Methods &Technologies*, Vol. 7, Part 1, pp. 456-463, [Online], Available: http://www.scientific-publications.net/download/materials-methods-and-technologies-2013-1.pdf.

Daniela Dzhonova-Atanasova was born in Vidin, Bulgaria in 1963. She graduated from the Technical University of Sofia, Bulgaria. There she received her MSc degree in Mechanical Engineering in 1988 and her PhD degree in 1992.

Her research interests are in the area of Heat and Mass Transfer Processes, Fluid Dynamics, Energy Efficiency in Chemical Engineering and Renewable Energy Resources. Since 1994 she has been working at the Institute of Chemical Engineering at the Bulgarian Academy of Sciences, Sofia, Bulgaria, as a researcher and Assistant Professor. Since 2011 she has been an Associate Professor at the Institute of Chemical Engineering. She was a lecturer in Fluid Mechanics at the Technical University of Sofia, and in Ocean Energy Conversion (in English) at the European Polytecnical University, Pernik.

Dr. Dzhonova is a member of the Union of Chemists in Bulgaria.

Rumen Popov was born in Plovdiv, Bulgaria, in 1964. He received the M.S. degree (Automatic Control Systems) in Technical University of Tula, Russia, in 1990 and the Ph.D. in Technical University of Ruse, Bulgaria in 2009.

From 1990 to 1991, he was a Research Engineer with the Aviotechnics SA, Plovdiv at Radio Electronic Systems department. Since 1991, he has been an Assistant Professor with the Control Systems Department, Technical University of Sofia, branch Plovdiv. He is the author of more than 45 articles. His research interests include Measurement and Automation, Renewable Energy Systems, Sun - Tracking systems.

He became an associated professor at the Technical University of Sofia, Bulgaria in 2011. His main courses are in Measurement Systems, SCADA Systems, and Aviation Electricity and Electronics. Assoc. Prof. Popov is a member of the Bulgarian Geothermal Association since 2011.

Aleksandar Georgiev was born in Dobrich, Bulgaria in 1958. He received the MSc degree in Mechanical Enginieering from the Technical University (TU) of Sofia, Bulgaria in 1981 and received the PhD degree in 1988 at the same university.

His research interests are in Renewable Energy Sources, Solar Heating and Cooling Systems, Sun - Tracking systems and Shallow Geothermal Energy.

He became a full professor at the European Polytecnic University in Pernik (EPU), Bulgaria. Prof. Georgiev is a member of the Bulgarian Geothermal Association since 2011. He is presently active at the Department of Mechanics at the TU Sofia, branch Plovdiv in Bulgaria.

His lectures (in Bulgarian and English) are in the field of the Thermal Energy Systems, they are hold in both universities (EPU Pernik and TU Sofia).

Hybrid Fuzzy sliding mode performance control applied to a DFIG system for the production and integrated wind energy into a power grid based three-level converters

B. Belabbas

***Abstract*— In this paper we have developed a hybrid nonlinear robust control law, called fuzzy sliding mode (FSMC), which combines the advantages of both: the sliding mode (SMC) and fuzzy logic (FLC). This controller has the feature to eliminate the ripples caused by SMC; it will be applied to a doubly fed asynchronous generator to produce power from the wind. We have used the FSMC to control the active and reactive power exchanged between the stator and the grid. The two powers are decoupled by the mean of using an indirect vector control with power loop. The performance of this cascade and control are analyzed by simulation of Matlab / Simulink software.**

Index Terms—**Wind System, GADA, Fuzzy logic, SMC, FSMC, Vector control.**

I. INTRODUCTION

WIND energy is one of the fastest growing renewable energy in the world. The generation of wind energy is clean, non-polluting, it produces no harmful was to the environment. Conventional techniques were used to adjust the wind, but assuming the wind operation in balanced conditions. Advances in technology of wind led to the design of a more powerful drive to improve their behavior and make it more robust and reliable. One of the current areas of research is the generation of electrical energy by means of double-fed asynchronous machine, using driving means such as wind power incorporated into a wind energy system, the function can DFIG on wide range of wind speed and get the maximum possible power for each wind speed. Its stator circuit is connected directly to the mains. A second circuit disposed on the rotor is connected to the network but also via power converter structure NPC three levels [1-4].

But the DFIG is subject to many constraints, such as the effects of parametric uncertainty "due to the heating, saturation ..... "And the disturbance variable speed. These constraints could thus divert the system optimal operation [5].

B. Belabbas is with the Department of Electrical Engineering of the University of Ibn Khaldoun Tiaret, Algeria (e-mail: belabbas_1986@yahoo.fr)

This is why control should be concerned about the robustness and performance. To do this, we referred to the use of Fuzzy Sliding mode control [7-9].

Our work falls within this context and aims to control powers. It is organized as follows: Section 2 is dedicated to the modeling of the wind turbine. Then, the model and the vector control of DFIG are studied in Section 4 devoted to the development of a FSMC of DFIG, Section 5 discusses the operating principle of the rotor side converter. The system being studied is shown in Fig. 1.

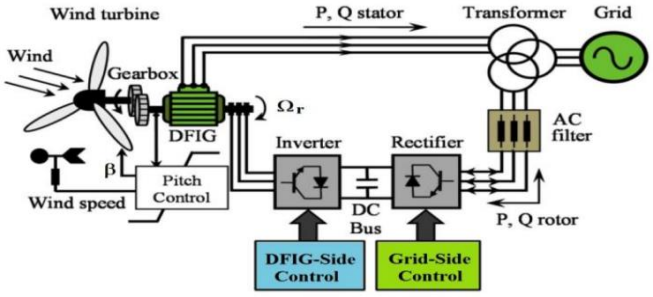

Fig.1. Diagram of a Conversion of Wind Energy.

II. MODELING OF WIND TURBINE

II.1. MODEL TURBINE

Mechanical power available on the shaft of a wind turbine is expressed by [1,5]:

$$P_{aero} = \frac{1}{2}.C_p(\lambda,\beta).\rho.\pi.R^2.V^3 \quad (1)$$

$$\lambda = \frac{R.\Omega_{mec}}{G.V} \quad (2)$$

The aerodynamic torque is directly determined by [1]:

$$C_{aero} = \frac{P_{aero}}{\Omega_{Turbine}} = C_P.\frac{\rho.S.V_1^3}{2.\Omega_{Turbine}} \quad (3)$$

The multiplier is mathematically modeled by the following equations:

$$C_g = \frac{C_{aero}}{G} \tag{4}$$

$$\Omega_{turbine} = \frac{\Omega_{mec}}{G} \tag{5}$$

The power factor $C_p(\lambda,\beta)$ represents the aerodynamic efficiency of the wind turbine. The wind turbine is a complex model, however simple mathematical models are often used aerodynamic system. The expression of power coefficient that we will use in our study is given by [1]:

$$Cp(\lambda,\beta) = 0.5176.\left(116.\frac{1}{\lambda i} - 0.4.\beta - 5\right).\exp\left(\frac{-21}{\lambda i}\right) + 0.0068.\lambda i \tag{6}$$

$$\frac{1}{\lambda_i} = \frac{1}{\lambda + 0.08.\beta} - \frac{0.035}{1+\beta^3} \tag{7}$$

The fundamental equation of dynamics to determine the evolution of the mechanical speed from the total mechanical torque (C_{mec}) applied to the rotor:

$$\begin{aligned} &J.\frac{d\Omega_{mec}}{dt} = C_{mec} \\ &C_{mec} = C_g - C_{em} - C_{vis} \\ &C_{vis} = f.\Omega_{mec} \\ &J = \frac{J_{turbine}}{G^2} + J_g \\ &f = \frac{f_{turbine}}{G^2} + f_g \end{aligned} \tag{8}$$

In this section, we present a different strategy to control the electromagnetic torque to adjust the mechanical speed to maximize the electric power generated. This principle is known as the terminology (MPPT).

We are interested in controlling the electromagnetic torque servo mechanical speed using a conventional PI controller. For this study, we assume that the electrical machine and its drive are ideal and therefore, regardless of the power generated, the electromagnetic torque is developed at all times equal to its reference value. The maximum power extraction techniques include determining the speed of the turbine, which provides maximum power generated [7].

$$\frac{d\Omega_{mec}}{dt} = \frac{1}{J}.(C_g - C_{em} - f.\Omega_{mec}) \tag{9}$$

$$\begin{aligned} &C_{emref} = PI.(\Omega_{ref} - \Omega_{mec}) \\ &\Omega_{ref} = G.\Omega_{turbine\ ref} \\ &\Omega_{turbine\ ref} = \frac{\lambda.C_{p\max}.V}{R} \end{aligned} \tag{10}$$

II.2. MODEL OF DFIG

Applying the Park transformation to electrical equations DFIG [1] in the referential linked to the rotating field allows us to achieve the following electrical system of equations:

The stator and rotor equation in the referential synchronous are given by:

$$\begin{cases} V_{sd} = R_s i_{sd} + \frac{d\Phi_{sd}}{dt} - \omega_s \Phi_{sq} \\ V_{sq} = R_s i_{sq} + \frac{d\Phi_{sq}}{dt} + \omega_s \Phi_{sd} \\ V_{rd} = R_r i_{rd} + \frac{d\Phi_{rd}}{dt} - \omega_r \Phi_{rq} \\ V_{rq} = R_r i_{rq} + \frac{d\Phi_{rq}}{dt} + \omega_r \Phi_{rd} \end{cases} \tag{11}$$

$$\begin{cases} \Phi_{sd} = L_s i_{sd} + M_{sr} i_{rd} \\ \Phi_{sq} = L_s i_{sq} + M_{sr} i_{rq} \\ \Phi_{rd} = L_r i_{rd} + M_{sr} i_{sd} \\ \Phi_{rq} = L_r i_{rq} + M_{sr} i_{sq} \end{cases} \tag{12}$$

$$C_{em} = P\frac{M_{sr}}{L_s}\left(\Phi_{sq} i_{rd} - \Phi_{sd} i_{rq}\right) \tag{13}$$

II.3. POWER CONTROL

To easily control the production of electricity from wind, we will achieve an independent control of active and reactive power by the stator flux orientation. The idea is to align along the axis of the rotating frame [2-4] stator flux. We therefore: $\Phi_{sq} = 0$ and consequently $\Phi_{sd} = \Phi_s$.

This choice is not random but is justified by the fact that the machine is often coupled with a powerful network voltage and constant frequency, which leads to a finding stator flux of the machine. Neglecting the resistance of the stator windings, often accepted hypothesis for high power machines: The systems of equations (11) and (12) can be simplified as follows:

$$\begin{cases} V_{sd} = 0 \\ V_{sq} = V_s = \omega_s \Phi_s \\ V_{rd} = R_r i_{rd} + \frac{d\Phi_{rd}}{dt} - \omega_r \Phi_{rq} \\ V_{rq} = R_r i_{rq} + \frac{d\Phi_{rq}}{dt} + \omega_r \Phi_{rd} \end{cases} \tag{14}$$

$$\begin{cases} \Phi_s = L_s i_{sd} + M_{sr} i_{rd} \\ 0 = L_s i_{sq} + M_{sr} i_{rq} \\ \Phi_{rd} = L_r i_{rd} + M_{sr} i_{sd} \\ \Phi_{rq} = L_r i_{rq} + M_{sr} i_{sq} \end{cases} \tag{15}$$

$$Cem = -P\frac{Msr}{Ls}\Phi s\, irq \tag{16}$$

The stator active and reactive power in the orthogonal coordinate system can be written:

$$\begin{cases} P = v_{sd} i_{sd} + v_{sq} i_{sq} \\ Q = v_{sq} i_{sd} - v_{sd} i_{sq} \end{cases} \tag{17}$$

Under the assumption of a stator flux oriented, this system of equations can be simplified as:

$$\begin{cases} P = v_s i_{sq} \\ Q = v_s i_{sd} \end{cases} \tag{18}$$

From the expressions of the stator flux, we can write:

$$\begin{cases} i_{sd} = \dfrac{V_s}{\omega_s L_s} - \dfrac{Msr}{L_s}.i_{rd} \\ i_{sq} = -\dfrac{Msr}{L_s}.i_{rq} \end{cases} \tag{19}$$

$$\begin{cases} P = -\dfrac{V_s M_{sr}}{L_s} i_{rq} \\ Q = -\dfrac{V_s M_{sr}}{L_s} i_{rd} + \dfrac{V_s^2}{L_s \omega_s} \end{cases} \tag{20}$$

$$\begin{cases} \Phi_{rd} = \left(L_r - \dfrac{M_{sr}^2}{L_s} \right) i_{rd} + \dfrac{M_{sr} V_s}{\omega_s L_s} \\ \Phi_{rq} = \left(L_r - \dfrac{M_{sr}^2}{L_s} \right) i_{rq} \end{cases} \tag{21}$$

By introducing these expressions in the equations of the rotor voltages are found:

$$\begin{cases} V_{rd} = R_r i_{rd} + \left(L_r - \dfrac{M_{sr}^2}{L_s} \right) \dfrac{di_{rd}}{dt} - g\omega_s \left(L_r - \dfrac{M_{sr}^2}{L_s} \right) i_{rq} \\ V_{rq} = R_r i_{rq} + \left(L_r - \dfrac{M_{sr}^2}{L_s} \right) \dfrac{di_{rq}}{dt} + g\omega_s \left(L_r - \dfrac{M_{sr}^2}{L_s} \right) i_{rd} + g\dfrac{M_{sr} V_s}{L_s} \end{cases} \tag{22}$$

III. INDIRECT CONTROLS WITH POWER LOOP

It is based on the equations governing the operation of the machine defined in the preceding paragraph, while keeping the same assumptions.

By combining the different flow equations, the rotor voltages, currents and powers, we can write the equations of the rotor voltage depending on the power. Thus power from the stator as a function of the rotor currents and voltages of the rotor in terms of the rotor current function [1]:

From the control unit we can develop a structure ensures good stability of the network, so we have a control unit consists of two subsystems. The first calculates the reference currents from the references (active and reactive powers), the second calculates the reference voltage from the rotor currents calculated by the first. In this spirit, we have used SMC to the inner loop (current loop) and classic PI outer loop to controlling powers. It then sets the control system given by the figure (2).

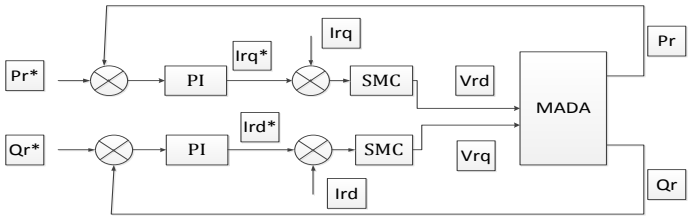

Fig.2. Block diagram of indirect control with loop power controlled by SMC.

IV. DEVOLOPING OF THE HYBRID CONTROL

IV.1. INDIRECT CONTROL OF THE DFIG WITH LOOP POWER

The basic idea of the SMC is primarily attracting states of the system in a suitably selected, and then designs a control law that will always keep the system in this region [1] region. In summary SMC is divided into three parts: [1-6].

IV.1.1. CHOICE OF SWITCHING SURFACE

For a non-linear system shown in the following form:

$$\begin{aligned} &\dot{X} = f(X,t) + g(X,t) \quad u(X,t); \\ &X \in R^n, u \in R. \end{aligned} \tag{23}$$

There f(X, t), g(X, t) are two continuous and uncertain nonlinear functions, assumed bounded. It takes the form of general equation proposed by J.J. Slotine to determine the sliding surface given by Slotine and all [7-9]:

$$S(X) = \left(\frac{d}{dt} + \lambda \right)^{n-1} .e \quad et \quad e = X^d - X \tag{24}$$

With, e: error on the controlled variable, λ: positive coefficient, n: order system, X^d: desired size, X: state variable of the controlled variable.

IV.1.2. CONVERGENCE CONDITION

The convergence condition is defined by the Lyapunov equation (Lopez et al, 2006), it makes the area attractive and invariant $S(X).\dot{S}(X) \le 0$.

IV.1.3. CONTROL CALCULATION

The control algorithm is defined by the relation $u = u^{eq} + u^{n}$ *et* $u^{n} = u^{\max}.sign(S(X))$

With: u: control variable, u^{eq}: size equivalent command, u^{n}: term control switch, sign(S(X)): sign function.

IV.2. CONTROL OF ROTOR CURRENT NEXT AXIS "D"

To control the rotor current is taken n = 1, the expression of the current control surface along the axis "d" of the marker to form Park $S(I_{rd}) = (I_{rd}^{*} - I_{rd})$

Deriving the surface with the replacement of the current expression I_{rd}, obtained:

$$\dot{S}(I_{rd}) = (\dot{I}_{rd}^{*} - \frac{1}{\sigma.L_r}(V_{rd} - R_r.I_{rd}) \quad (25)$$

The control voltage V_{rd} is defined by: $V_{rd} = V_{rd}^{eq} + V_{rd}^{n}$ During the sliding mode and steady state was: $\dot{S}(I_{rd} = 0); S(I_{rd} = 0); V_{rd}^{n} = 0;$ or of pulling: $V_{rd}^{eq} = \sigma.L_r.\dot{I}_{rd}^{*} + R_r.I_{rd}$ During the convergence mode, the condition $S(X).\dot{S}(X) \le 0$ should be checked with: $V_{rd}^{n} = K.V_{rd}.sign(S(I_{rd}))$ *et* $K.V_{rd}$ positive gain.

IV.3. CONTROL OF ROTOR CURRENT NEXT AXIS "Q"

To control the rotor current is taken n = 1, the expression of the current control surface along the axis "q" of the marker to form Park $S(I_{rq}) = (I_{rq}^{*} - I_{rq})$

Deriving the surface with the replacement of the current expression I_{rq}, on gets:

$$\dot{S}(I_{rq}) = (\dot{I}_{rq}^{*} - \frac{1}{\sigma.L_r}(V_{rq} - R_r.I_{rq}) \quad (26)$$

The control voltage V_{rq} is defined by: $V_{rq} = V_{rq}^{eq} + V_{rq}^{n}$ During the sliding mode and steady state was: $\dot{S}(I_{rq} = 0); S(I_{rq} = 0); V_{rq}^{n} = 0;$ or of pulling: $V_{rq}^{eq} = \sigma.L_r.\dot{I}_{rq}^{*} + R_r.I_{rq}$ During the convergence mode, the condition $S(X).\dot{S}(X) \le 0$ should be checked with: $V_{rq}^{n} = K.V_{rq}.sign(S(I_{rq}))$ *et* $K.V_{rq}$ positive gain.

V. FUZZY SLIDING MODE CONTROL OF INTERNAL LOOP DFIG

The disadvantage of the SMC is that the term switching control where we have lot of ripples. To reduce it, we replace it by a fuzzy structure (Wong et al, 2001). FSMC, which is designed to control the rotor current, is shown in Fig.3 [9-16].

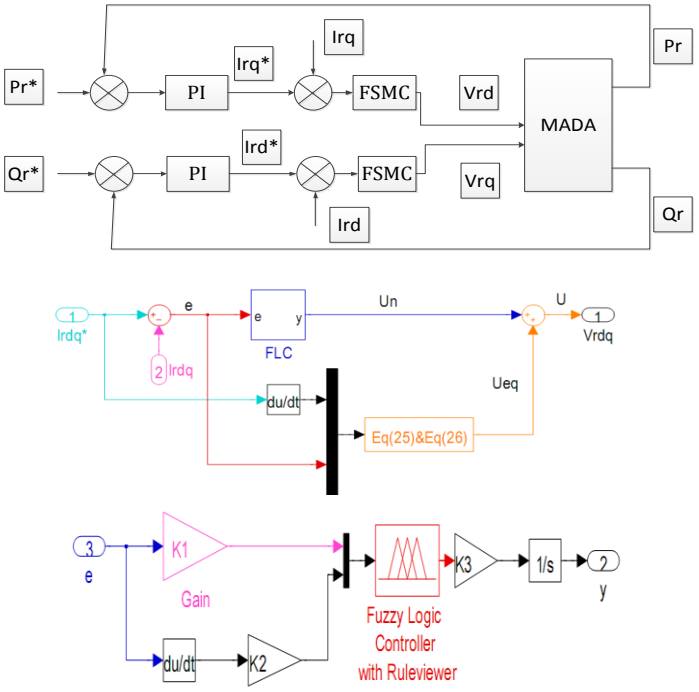

Fig.3. Block diagram of indirect control with loop controlled power FSMC.

The fuzzy logic control is expanding. Indeed, this method provides a very effective law often set without doing extensive modeling. As opposed to a standard regulator or a regulator of state-reaction against the controller fuzzy logic does not address a well-defined mathematical relationship, but uses inferences with multiple rules, based on linguistic variables. By inference with several rules, it is possible to take account of experience gained by the operators of a technical process.

Three linguistic variables input-output are shown in Fig.4. The fuzzy rules can be written as shown in Table 1. For this purpose, it is used a system of Mamdani-type fuzzy logic. The member ship function resulting from the aggregation of using the operator max. The Defuzzification of the output control is accomplished using the method of center of gravity [5-7-9].

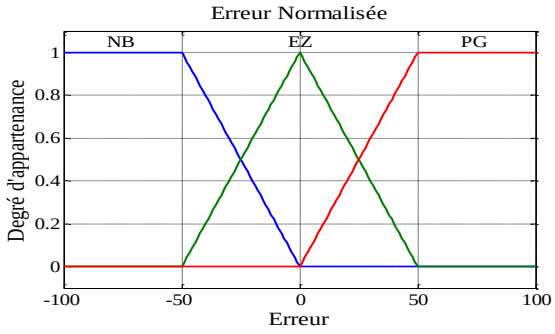

Fig.4. Membership functions of the different linguistic variables.

TABLE1. Rules for RFL.

E_X / ΔE_X	NP	EZ	PG
NP	NP	NP	EZ
EZ	NP	EZ	PG
PG	EZ	PG	PG

VI. MODELING AND CONTROL OF THE THREE LEVELS STRUCTURE NPC VSI

VI.1. THE THREE-LEVEL NPC VSI STRUCTURE

The three phases three-level NPC VSI is constituted by three arms and two DC voltage sources. Every arm has four bi-directional switches in series and two diodes (Fig. 5) [2].

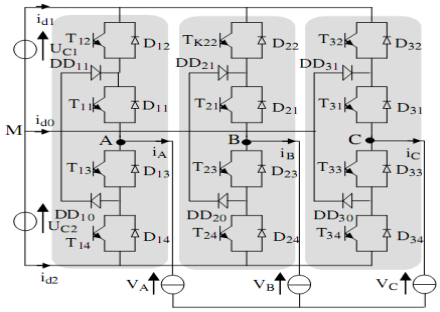

Fig.5. The three-level NPC inverter.

VI.2. KNOWLEDGE MODEL

The switch connection function F_{ks} indicates the opened or closed state of the switch T_{ks}.

We define to a half arm connection function F_{km}^{b} with:

K: Arm number.

$$m=\begin{cases}1 \ for\ the\ lower\ half\ arm\\ 0 \ for\ the\ \text{upper}\ half\ arm\end{cases}$$

For an arm k of the three-phase three-level NPC VSI, several complementary laws controls are possible. The control law which lets an optimal control of this inverter is [3]:

$$\begin{cases}B_{k1}=\overline{B}_{k4}.\\ B_{k2}=\overline{B}_{k3}.\end{cases} \quad (27)$$

Where B_{ks} represents the gate control of the switch T_{ks}. We define the half arm connection function F_{i1}^{b} and F_{i0}^{b} associated respectively to the upper and lower half arms.

Where i is arm number $i\in\{1,2,3\}$

$$\begin{cases}F_{11}=1-F_{14}\\ F_{12}=1-F_{13}\end{cases}\quad\begin{cases}F_{21}=1-F_{24}\\ F_{22}=1-F_{23}\end{cases}\quad\begin{cases}F_{31}=1-F_{34}\\ F_{32}=1-F_{33}\end{cases} \quad (28)$$

The output voltages of the inverter relatively to the middle point M are defined as follows:

$$\begin{bmatrix}V_{AM}\\ V_{BM}\\ V_{CM}\end{bmatrix}=\begin{bmatrix}F_{11}^{b}\\ F_{21}^{b}\\ F_{31}^{b}\end{bmatrix}.U_{c1}-\begin{bmatrix}F_{10}^{b}\\ F_{20}^{b}\\ F_{30}^{b}\end{bmatrix}.U_{c2} \quad (29)$$

The system (29) shows that the three-level NPC VSI can be considered as two two-level voltage source inverters in series. The input currents of the inverter are given as follow:

$$\begin{cases}i_{d1}=F_{11}^{b}.i_1+F_{21}^{b}.i_2+F_{31}^{b}.i_3\\ i_{d2}=F_{10}^{b}.i_1+F_{20}^{b}.i_2+F_{30}^{b}.i_3\end{cases} \quad (30)$$

The current i_{d0} is defined by the following relation:

$$i_{d0}=F_{11}.F_{13}.i_1+F_{21}.F_{23}.i_2+F_{31}.F_{33}.i_3 \quad (31)$$

VI.3. PWM STRATEGY OF THE THREE-LEVEL NPC VSI

The inverter is controlled by the space vector modulation strategy which uses two bipolar carriers. This strategy is characterized by two parameters:

Modulation index m defined as ratio between the carrier frequency f_p and the reference voltage frequency:

$$m=\frac{f_p}{f} \quad (32)$$

Modulation rate r is the ratio between the magnitudes V_m of the reference voltage and three times of the carriers magnitude U_{pm}:

$$r=\frac{V_r}{V_p}\le 1 \quad (33)$$

VII. CASCADE (RECTIFIER, FILTER AND INVERTER) WITH DFIG

In this part of the chapter, the dynamic behavior of the wind turbine based on doubly fed machine (DFIG) connected to the network is studied. The stator of the DFIG is directly connected to the network, against the rotor is connected to it via a cascade (rectifier, filter and inverter). This changer allows indirect frequency from a fixed network frequency and amplitude has a system output voltage frequency and variable amplitude.

The general structure of this cascade is shown in Fig.6. The rectifier and inverter are controlled by the two sinusoidal carrier strategy triangular saw tooth.

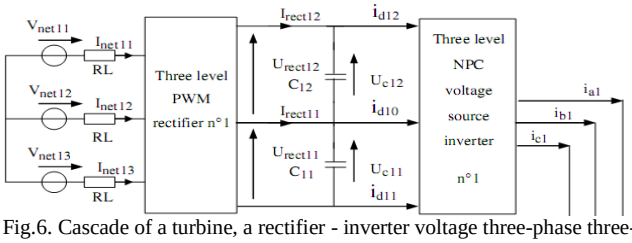

Fig.6. Cascade of a turbine, a rectifier - inverter voltage three-phase three-level feeding the DFIG.

VII.1. MODELLING OF THE INTERMEDIATE FILTER

The model of the intermediate filter is defined by the following system:

$$\begin{cases} U_{C1}=\frac{1}{C_1}\int\left(I_{rect1}-I_{d1}\right)dt \\ U_{C2}=\frac{1}{C_2}\int\left(I_{rect2}-I_{d2}\right)dt \end{cases} \quad \begin{cases} C_1.\frac{dU_{C1}}{dt}=I_{rect1}-I_{d1} \\ C_2.\frac{dU_{C2}}{dt}=I_{rect2}-I_{d2} \end{cases} \tag{34}$$

VIII. THE HALF CLAMPING BRIDGE

To improve the input voltages of the three-level NPC inverter, we propose to use a half clamping bridge, constituted by a transistor and a resistor [3]. The transistors are controlled to maintain equal the different input DC voltages of the inverter (Fig. 7).

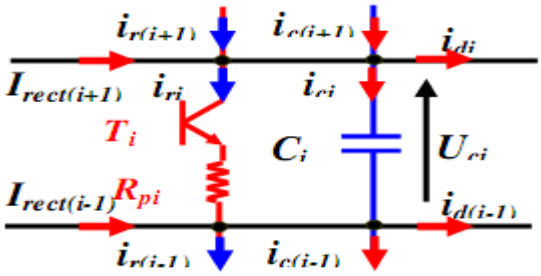

Fig.7. Structure Bridge clamping with intermediate filter.

VIII.1. MODELLING OF THE INTERMEDIATE FILTER

Figure 8 shows the structure of the intermediate filter of the studied cascade.

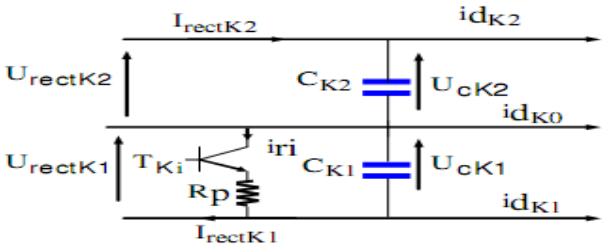

Fig.8. Structure of the intermediate filter of the of the half clamping bridge cascade.

The model of the half clamping bridge-filter set is defined by the following equation:

$$\begin{cases} U_{C1}=\frac{1}{C_1}\int\left(I_{rect1}-I_{r1}-I_{d1}\right)dt \\ U_{C2}=\frac{1}{C_2}\int\left(-I_{rect2}-I_{r2}+I_{d2}\right)dt \end{cases} \tag{35}$$

$$I_{ri}=T_i.\frac{U_{Ci}}{R_{Pi}} \qquad \text{Avec} \quad i=\{1,2\} \tag{36}$$

The control algorithm of the resistive clamping circuits can be summarized as follows:

$$\begin{cases} \left(U_{Ci}-U_{ref}\right)=\varepsilon_i \\ if\ \ \varepsilon_i \succ 0\ Then\ T_i=1\Rightarrow I_{ri}=T_i.\frac{U_{Ci}}{R_{Pi}} \\ if\ \ NO\ T_i=0\Rightarrow I_{ri}=0 \end{cases} \tag{37}$$

VIII.2. VOLTAGE LOOP MODEL

The modeling of this loop is based on principle of instantaneous power conservation with no loss hypothesis. This boucle imposes efficacy network reference current. The input power is calculated as:

$$P_e=\sum_{K=1}^{3}\left(V_{netK}.i_{netK}-R_{net}.i_{netK}^2-\frac{L_{net}}{2}\frac{di_{netK}^2}{dt}\right) \tag{38}$$

The output power is calculated as:

$$P_e=U_{C1}.\left(i_{C1}+i_{load1}\right)+U_{C2}.\left(i_{C2}+i_{load2}\right)=U_{rect1}.I_{rect1}-U_{rect2}.I_{rect2} \tag{39}$$

It is assumed that the following: $U_{C1}=U_{C2}=U_C$ *and* $C_1=C_2=C.$
Define variables. i_C, i_{laod} *and* U_C

$$\begin{cases} i_C=\frac{i_{C1}+i_{C2}}{2} \\ i_{Ch}=\frac{i_{d1inv}-i_{d2inv}}{2} \\ U_C=U_{Cmoy}=\frac{U_{C1}+U_{C2}}{2} \\ i_{rec}=i_C+i_{laod} \end{cases} \tag{40}$$

Using the principle of conservation of power and neglecting the Joule losses in the resistance Rnetw, we can write:

$$\sum_{K=1}^{3}\left(V_{netwK}.i_{netwK}\right)=\sum_{K=1}^{3}\frac{L_{netwK}}{2}\frac{di_{netwK}^2}{dt}+2.U_C.\left(i_C+i_{Laod}\right) \tag{41}$$

$$3.V_{eff}.I_{eff}=2.U_C.\left(i_C+i_{laod}\right) \tag{42}$$

Where E_{eff} is the *rms* value of grid voltages and Ie is the *rms* value of grid currents. Uc is the constant value of the DC capacitor voltage and *Irect* is the DC current. A IP regulator is used to regulate the DC voltage. The general principle feedback of three-level rectifier is shown on Fig.9.

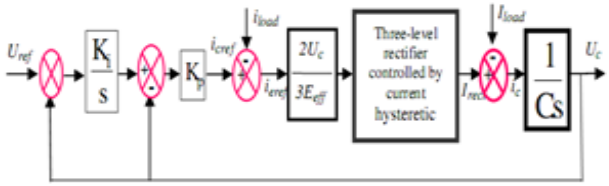

Fig.9. Enslavement algorithm of output voltage of three-level rectifier.

IX. SIMULATION RESULTS

In this section, we present the work on the modeling of a chain of wind conversion based on an asynchronous machine is comprised of dual power controlled by the technique of PWM rectifier and a DC bus, all connected to the network via a PWM inverter and a filter. Modeling the overall wind conversion chain and the associated control device are developed in the form of an equivalent continuous model which takes into account the relevant components of the currents and voltages at the machine, and the DC bus network.

We applied a control algorithm on the voltages (U_{c1}, U_{c2}) with the aim of stabilizing the past to balance the midpoint M.

The strategy of indirect control based controllers SMC and FSMC rotor currents of DFIG were implemented in MATLAB environment to perform tests of control.

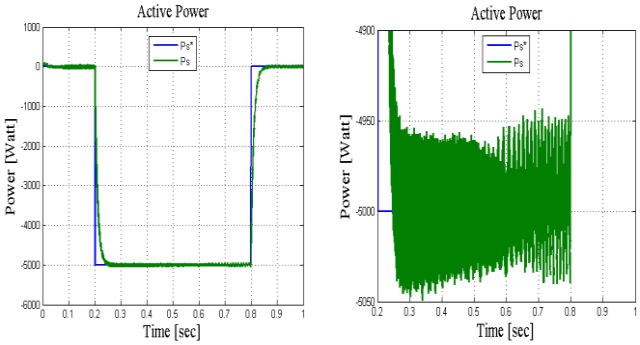

Fig.10. Active power graphics of DFIG with indirect vector control with loop power controlled by FSMC.

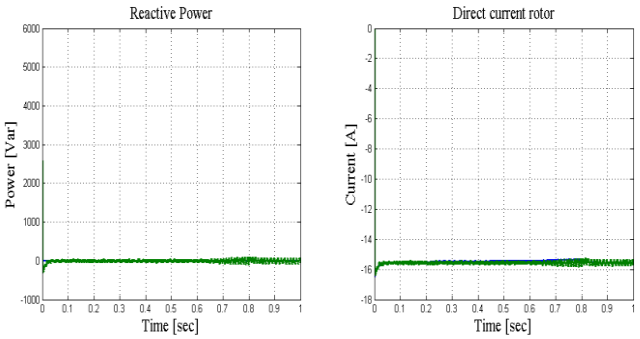

Fig.11. Power & currents graphics.

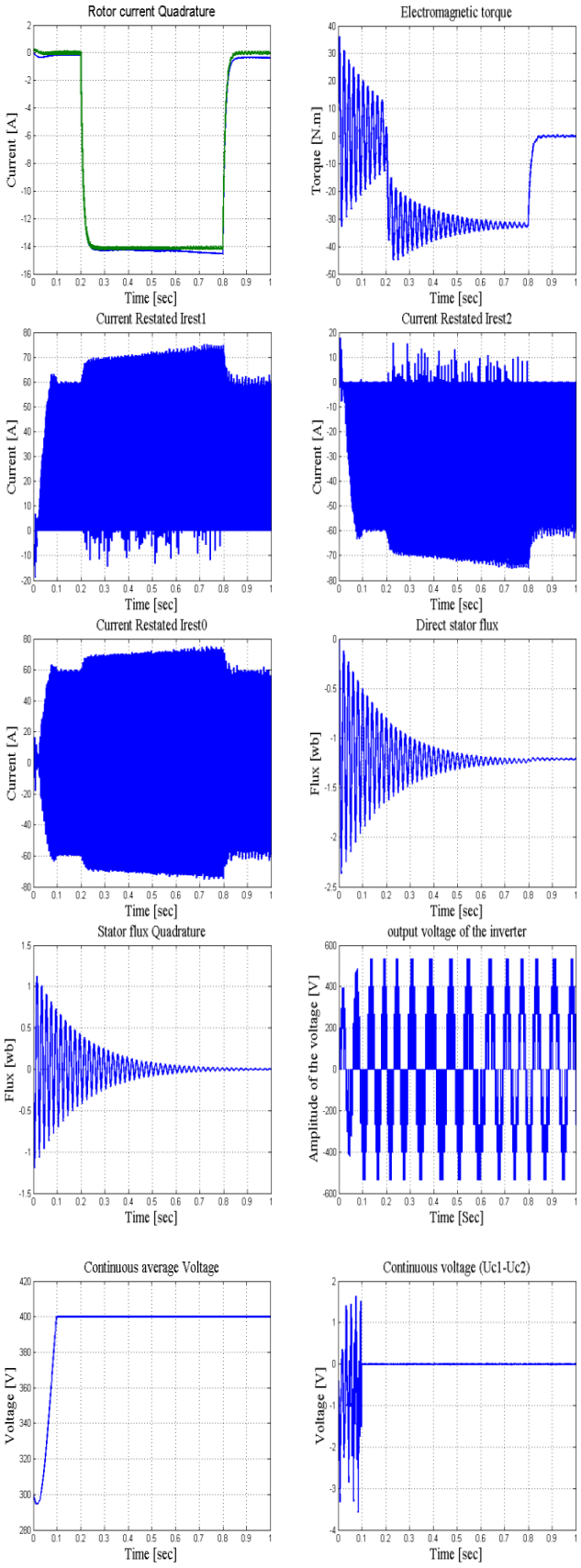

Fig.12. Current, voltage, flux, torque variations of the system.

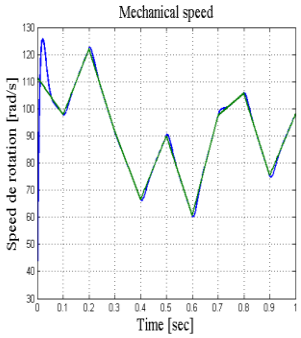

Fig.13. Behavior of the powers of DFIG with indirect vector control with loop power controlled by FSMC.

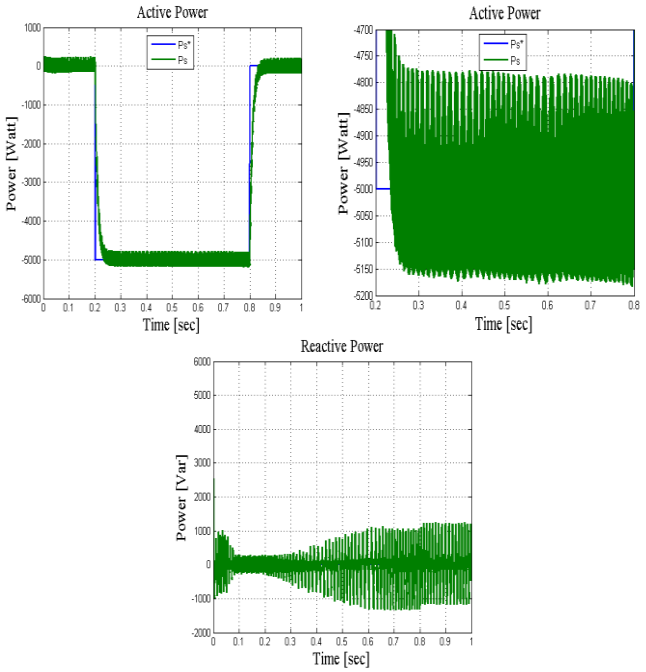

Fig.14. Active and reactive power variations of the system.

The simulation results show different curves are obtained by controlling the active and reactive power generated at the stator of the DFIG. This control technique allows you to decouple the expressions of active and reactive power of the generator or in the flux and torque.

According to the results, we find that the indirect control with loop power controller using SMC or FSMC have good decoupling control of active and reactive power at the stator. After a transitional period, the parameters perfectly follow their reference.

The reactive power is zero and it is a condition of operation of the DFIG for a unity power factor.

As we reported earlier that the disadvantage of the SMC is the ripples. To reduce it, we combined this control with fuzzy logic to build a new structure called FSMC, which allows reducing the chattering phenomena of over 75% in our study.

We can see that the stator flux follows the following reference axis (d) with almost zero quadrature components, which means that the decoupling of the machine is successful.

It is clear that the quadrature component of the rotor current *Irq* control the electromagnetic torque so the active power. The direct component of the rotor current, and thus control the flow of reactive power transmitted between the stator and the network. This is found in the changes in direct and quadrature components of rotor currents, which are the images of active and reactive powers.

Note that the electromagnetic torque reacts spontaneously when there is a demand for active power, reactive power independently

We observe that the current *Irest*1 presents a look opposite to that of *Irest*2. This is necessary for the current *Irest*0 has a zero mean value. As can be seen, the current *Irest*0 is substantially zero mean value.

Note that the two DC voltages well below their reference and we also find that the difference between the two voltages is practically zero after a transient 0.1s which mean a better stability of the midpoint.

X. CONCLUSION

This study has allowed us to study the modeling of a chain of wind conversion based on DFIG consists of a rectifier control by the PWM technique, and a DC bus, all connected to the network via a PWM inverter and a filter.

We studied the indirect vector control loop power DFIG which allows a decoupling between the flux and torque.

The control is provided by two orders SMC and FSMC for which we found the performance of the latter relative to the SMC perspective chattering.

REFERENCES

[1] M. Adjoudj et al, "Sliding mode control of a doubly fed induction generator for wind turbines", conversion systems. Rev. Roum. Sci. Techn. – Électrotechn. et Énerg., Vol.56, No.1, 2011, pp.15-24.

[2] R. Manavalan, C.S. Kumar, "Analysis of Hybrid Renewable Energy System using NPC Inverter", Research Inventy: International Journal of Engineering and Science, Vol.2, No.7, March 2013, pp. 26-30.

[3] G. Abad J. Lopez, M.A. Rodrıguez, L. Marroyo, G. Iwanski, "Doubly fed induction machine: modeling and control for wind energy generation", IEEE press Series on Power Engineering, Aug 2011.

[4] F. Poitiers, M. Machmoum, R.L. Doeuff and M.E. Zaim, "Control of a doubly-fed induction generator for wind energy conversion system", Australasian Universities Power Engineering Conference AUPEC 2009, Australia.

[5] M. Hilal, Y. Errami, M. Benchagra and M. Maaroufi "Fuzzy Power Control For Doubly Fed Induction Generator Based Wind Farm," Journal of Theoretical and Applied Information Technology, 30th September 2012, Vol. 43 No.2, pp.321-330.

[6] F. Valenciaga, C.A. Evangelista "Sliding active and reactive power control of a wind energy conversion system", IET Control Theory and Applications, Vol.4, No.11, 2010, pp.2479-2490.

[7] R. Palm, "Sliding mode fuzzy control," Fuzzy Systems, IEEE conference proceeding, Vol.2, 2002, pp. 1393-1398.

[8] S. Arezki, M. Boudour, "Contribution to the improvement of the performances of a chain of conversion of energy fed by a double source", 2nd International Conference on Advances in Energy Engineering (ICAEE 2011), December 2011, Bangkok , Thailand.

[9] F. Piltan, N. Sulaiman, S. Roosta, A. Gavahian, S. Soltani, "Artificial Chattering Free on-line Fuzzy Sliding Mode Algorithm for Uncertain System: Applied in Robot Manipulator, International Journal of Engineering, Vol.5, No.5, 2011, pp.360-379.

[10] L. Xu and P. Cartwright, "Direct Active and Reactive Power Control of DFIG for Wind Energy Generator", IEEE Transactions on Energy Conversion, Vol.21, No.3, September 2006, pp. 750–758.

BIOGRAPHIES

Belabbas Belkacem was born in Tiaret in Algeria in 1986. In 2009 he received the qualification status in electrical engineering at the University of Ibn Khaldoun Tiaret, Algeria, and in 2012 he was awarded the Magister degree in electrical engineering from the University of Ibn Khaldoun Tiaret-Algeria-. Participate in some international conferences in Algeria. His research focuses on the integration and management of renewable energy into the grid.

BAJECE
Balkan Journal of Electrical & Computer Engineering
An International Peer Reviewed Refereed indexed and Open Access Journal

ISSN: 2147- 284X
Vol: 1
No: 2
Year: September 2013

CONTENTS

G. Gricius, D. Drungilas, J. Guseinovaitė, K. Grigaitis, A.A. Bielskis; Modeling of the Cloud Interconnected Human Friendly Multi-Agent Based Sustainable Power Controller,……**49-55**

T. Slavov, L. Mollov, J. Kralev, P. Petkov; Real-time Robust Control Using Digital Signal Processor,……**56-63**

S. Shojaeian, H. Akrami; Estimating Optimal Wind and Storage Capacity to Avoid Conventional Power Plants Expansion Using Monte Carlo Method;……**64-70**

G. Yanik, E. Isen; Quasi-Resonant Full-Wave Zero-Current Switching Buck Converter Design, Simulation and Application, ……**71-77**

E. Nechadi, M.N. Harmas; Power System Stabilizer Based on Global Fuzzy Sliding Mode Control, ……**78-84**

D. Dzhonova-Atanasova, A. Georgiev, R. Popov; Challenges of Marine Power in the Balkan Region,……**85-92**

B. Belabbas, T. Allaoui, M. Tadjine; Hybrid Fuzzy sliding mode performance control applied to a DFIG system for the production and integrated wind energy into a power grid based three-level converters, ……**93-101**

BALKAN JOURNAL OF ELECTRICAL & COMPUTER ENGINEERING

(An International Peer Reviewed, Refereed, indexed and Open Access Journal**)**

Contact
www.bajece.com
e-mail: editor@bajece.com
bajece@bajece.com

Phone: +90 288 214 05 14
Fax: +90 288 214 05 16

Kirklareli University,
Engineering Faculty,
Department of Electrical & Electronics Engineering,
39020, Kirklareli-Turkey.